

PDF hosted at the Radboud Repository of the Radboud University Nijmegen

The following full text is a publisher's version.

For additional information about this publication click this link.

<http://repository.ubn.ru.nl/handle/2066/127111>

Please be advised that this information was generated on 2017-03-10 and may be subject to change.

**STRATEGIES TO ACCELERATE
THE DEGRADATION OF INJECTABLE
CALCIUM PHOSPHATE-BASED
COMPOSITE MATERIALS FOR
BONE REGENERATION**

Kemal SARIİBRAHİMOĞLU

Colofon

The research presented in this thesis was financially supported by KNAW, China-Netherlands Programme Strategic Alliances (PSA).

Thesis Radboud University Medical Center, with summary in English and Dutch.

Strategies to accelerate the degradation of injectable calcium phosphate-based composite materials for bone regeneration

Kemal Sariibrahimoğlu, Nijmegen, 2014
All rights reserved.

ISBN: 978-90-8891-851-3

Layout: Kemal Sariibrahimoğlu
Cover design: Proefschriftmaken.nl || Uitgeverij BOXPress
Printed by: Proefschriftmaken.nl || Uitgeverij BOXPress
Published by: Uitgeverij BOXPress, 's-Hertogenbosch

**STRATEGIES TO ACCELERATE
THE DEGRADATION OF INJECTABLE
CALCIUM PHOSPHATE-BASED
COMPOSITE MATERIALS FOR
BONE REGENERATION**

PROEFSCHRIFT

ter verkrijging van de graad van doctor
aan de Radboud Universiteit Nijmegen
op gezag van de rector magnificus prof. mr. S.C.J.J. Kortmann,
volgens besluit van het college van decanen
in het openbaar te verdedigen op woensdag 7 mei 2014
om 16:30 uur precies

door

Kemal Sariibrahimoğlu

geboren op 22 maart 1982
te Istanbul (Turkije)

Promotor

Prof. dr. J. A. Jansen

Copromotoren

Dr. J. G. C. Wolke

Dr. S. C. G. Leeuwenburgh

Manuscriptcommissie

Prof. dr. N. H. J. Creugers

Dr. R. de Gelder

Dr. P. Habibovic (Universiteit Twente)

Paranimfen

Dr. Arnold Nijhuis

Alexey Klymov

**STRATEGIES TO ACCELERATE
THE DEGRADATION OF INJECTABLE
CALCIUM PHOSPHATE-BASED
COMPOSITE MATERIALS FOR
BONE REGENERATION**

DOCTORAL THESIS

to obtain the degree of doctor
from Radboud University Nijmegen
on the authority of the Rector Magnificus prof. dr. S.C.J.J. Kortmann,
according to the decision of the Council of Deans
to be defended in public on Wednesday May 7, 2014
at 16:30 hours

by

Kemal Sarıbrahimoğlu

Born on March 22, 1982
in Istanbul (Turkey)

Supervisor

Prof. dr. J. A. Jansen

Co-supervisors

Dr. J. G. C. Wolke

Dr. S. C. G. Leeuwenburgh

Doctoral Thesis Committee

Prof. dr. N. H. J. Creugers

Dr. R. de Gelder

Dr. P. Habibovic (University of Twente)

Paranymphs

Dr. Arnold Nijhuis

Alexey Klymov

CONTENTS

CHAPTER 1 | Page 9

General introduction

CHAPTER 2 | Page 19

Calcium phosphate-based bone substitute materials

CHAPTER 3 | Page 61

Effect of calcium carbonate on hardening, physicochemical properties and in vitro degradation of injectable calcium phosphate cements

CHAPTER 4 | Page 85

Injectable biphasic calcium phosphate cements as a potential bone substitute

CHAPTER 5 | Page 109

Influence of the pore generator on the evolution of the mechanical properties and the porosity and interconnectivity of a calcium phosphate cement

CHAPTER 6 | Page 139

Tuning the degradation rate of calcium phosphate cements by incorporating mixtures of polylactic-co-glycolic acid microspheres and glucono-delta-lactone microparticles

CHAPTER 7 | Page 171

Controlled release of platinum-bisphosphonate complexes from injectable calcium phosphate cements for treatment of bone tumors

CHAPTER 8 | Page 187

English summary, Dutch summary, closing remarks and future perspectives

CHAPTER 9 | Page 203

Acknowledgements, curriculum vitae, list of publications

Chapter 1

GENERAL INTRODUCTION

Kemal Saribrahimoglu, Sander C.G. Leeuwenburgh, Joop G.C. Wolke,
John A. Jansen

1. Introduction

Bone exhibits an outstanding regenerative capacity during fracture healing owing to the well-orchestrated action of bone-forming osteoblasts and bone-resorbing osteoclasts. However, there are critical clinical conditions where bone regeneration is required in large quantity, such as large bone defects created by trauma, tumor resection or skeletal abnormalities¹. These conditions require a bone substitute that fills the defect and facilitates tissue regeneration. Various materials have been used to treat such bone defects including autografts, allografts and alloplasts^{2,3}. Clinically the most reliable graft material is an autologous bone harvested from the iliac crest or fibula^{4,6}. Nevertheless, due to the postoperative morbidity in terms of infection, pain, availability and additional surgery/cost, alternative treatment techniques are necessary. The use of synthetic bone substitutes is an effective alternative approach to regenerate bone tissue⁷⁻⁹.

2. Synthetic bone substitutes

Over the past decades, engineered synthetic biomaterials have changed the lives of billions of patients with musculoskeletal disorders¹⁰. The ideal synthetic bone substitute needs to fulfill a number of criteria, including biocompatibility, biodegradability and easy clinical handling properties¹¹⁻¹³. The majority of synthetic bone substitutes consist of calcium phosphate ceramics which have a chemical composition similar to the mineral phase in teeth and bone. Various types of calcium phosphate ceramics are commonly used in wide variety of medical applications, including hydroxyapatite (HA), tricalcium phosphates (α - or β -TCP) and biphasic ceramics consisting of both apatite and TCP. These latter ceramics possess a long clinical history as synthetic bone substitutes due to their osteoconductivity and biocompatibility^{5,10}.

CaP ceramics are clinically used as monolithic granules, blocks, cements etc. or as dispersed phase in ductile and flexible polymeric matrices to overcome typical drawbacks of ceramic materials such as their inherent brittleness. Polyurethane scaffolds have been researched extensively since they can be injectable, flexible and biodegradable which render them

suitable for bone regeneration. Calcium phosphate nanoparticles can be mixed into these ductile and flexible polymers to combine the beneficial properties of both material classes¹⁴⁻¹⁶.

3. Calcium phosphate cements

From a clinical point of view, injectable calcium phosphate cements (CPCs) offer several advantages over pre-shaped calcium phosphate ceramics. CPCs are composed of a mixture of one or more calcium orthophosphates, which upon mixing with a liquid phase, form a paste that is able to set and harden after implantation. The setting process proceeds through a dissolution and reprecipitation reaction where entanglement of newly formed calcium phosphate nanocrystals is responsible for the hardening. Unlike CaP granules or blocks, CPC pastes are able to adapt to the shape of the bone defect during operation and rapidly integrate with the surrounding bone tissue. Based on the end-product formed after complete hardening, CPCs can be classified into apatitic and brushite cements¹⁷⁻²¹.

3.1. Degradation of apatitic CPCs

Brushite cement has a lower mechanical strength but a faster biodegradability than apatite cements²². Apatitic CPCs are biocompatible and osteoconductive, but their degradation rate is generally very slow. This degradation process depends on various factors such as the chemical composition of the precursor compounds, nano- and macroporosity, presence of impurities and crystal size²³⁻²⁶.

To enhance the degradation of CPCs, various strategies have been performed. One approach involves the incorporation of cationic and anionic substitutions such as carbonate (CO_3^{2-}), magnesium (Mg^{2+}), and strontium (Sr^{2+}). These ions occupy the lattice site of hydroxyapatite mineral and thereby affect lattice dimensions, crystallinity and solubility of the apatite structure²⁷⁻³⁰. Another approach is the incorporation of porogens into CPC to render apatitic CPCs degradable. Porosity can be formed by different techniques including CO_2 foaming from sodium bicarbonate during cement setting³¹, addition of salt and sugar crystals such as mannitol³², sodium

chloride³³, and polymers such as poly(d,l-lactic-co-glycolic acid) (PLGA). Due to its tailorable degradation properties, PLGA polymers have been the material of choice for several clinical applications. The degradation rates of these polymers can be tailored from weeks to months by altering the chemical composition (such as the ratio between lactic and glycolic acid and molecular weight of the PLGA)³⁴⁻³⁷.

Besides the use of CPCs as bone filler, CPCs can also be used as carriers for local and controlled delivery of drugs³⁸. For these applications, several aspects need to be considered regarding the controlled release of drugs from CPC, including the effect of the incorporated drugs on cement setting, the effect of dosing and cement properties on the release kinetics and the bioactivity of the released drugs.

4. Objectives of this study

The main objective of this thesis was to modify the degradation rate of otherwise poorly degradable apatitic CPCs and polymer-nanocomposites to facilitate replacement by bone tissue. To this end, various strategies were explored which focused on modification of either the ceramic phase or organic additives of injectable calcium phosphate-based biomaterials to obtain insight into the following phenomena:

- The influence of the incorporation of calcium carbonate on the in vitro degradation rate of apatitic CPC (Chapter 3)
- The influence of incorporating a secondary β -tricalcium phosphate (β -TCP) phase in hardened apatitic CPCs on the in vitro degradation rate of biphasic CPCs (Chapter 4)
- The influence of incorporating PLGA microsphere porogens on the porosity and mechanical properties of CPC (Chapter 5)
- The influence of incorporating PLGA microspheres and glucono-delta-lactone (GDL) microparticles on the in vitro and in vivo degradation rate of CPC (Chapter 6)

- The influence of incorporating PLGA microspheres on the release kinetics of chemotherapeutic platinum-bisphosphonate (Pt-BP) complexes from CPC (Chapter 7)

References

1. Dimitriou R., Jones E., McGonagle D., Giannoudis P.V. Bone regeneration: current concepts and future directions. *BMC Med* 2011;9:1-10.
2. Sariibrahimoglu K., Leeuwenburgh S.C.G., Wolke J.G.C., Yubao L., Jansen J.A. ed. Fisher J.P., Mikos A.G., Bronzino J.D., Peterson D.R. Fundamentals in Tissue Engineering: Calcium phosphates, book chapter in handbook of “Tissue Engineering: Principles and Practices”, pg 3-1/3-21, CRC press, US, 2012.
3. Barrère F., Mahmood T.A., de Groot K., van Blitterswijk C.A. Advanced biomaterials for skeletal tissue regeneration: Instructive and smart functions. *Mater Sci Eng R* 2008;59:38-71.
4. Habibovic P., de Groot K. Osteoinductive biomaterials-properties and relevance in bone repair. *J Tissue Eng Regen Med* 2007;1:25-32.
5. Kruyt M.C., Delawi D., Habibovic P., Oner F.C., van Blitterswijk C.A., Dhert W.J.A. Relevance of bone graft viability in a goat transverse process model. *J Orthop Res* 2009;27:1055-1059.
6. Ahlmann E., Patzakis M., Roidis N., Shepherd L., Holtom P. Comparison of anterior and posterior iliac crest bone grafts in terms of harvest-site morbidity and functional outcomes. *J Bone Joint Surg* 2002;84:716-20.
7. Silber J.S., Anderson D.G., Daffner S.D, Brislin B.T., Leland J.M., Hilibrand A.S., Vaccaro A.R., Albert T.J. Donor site morbidity after anterior iliac crest bone harvest for single-level anterior cervical discectomy and fusion. *Spine* 2003;28:134-139.
8. Schwartz C.E., Martha J.F., Kowalski P., Wang D.A., Bode R., Li L., Kim H.D. Prospective evaluation of chronic pain associated with posterior autologous iliac crest bone graft harvest and its effect on

- postoperative outcome. *Health and Quality of Life Outcomes* 2009;7:49.
9. Whitehouse M.R., Dacombe P., Webb J.C.J., Blom A.W. Impaction grafting of the acetabulum with ceramic bone graft substitute mixed with femoral head allograft: High survivorship in 43 patients with a median follow-up of 7 years. *Acta Orthop* 2013;84:365-370.
 10. Ruhé P.Q., Wolke G.C.J., Spauwen P.H.M., Jansen A.J. Calcium phosphate ceramics for bone tissue engineering. In: Bronzino JD, editor. *Biomedical Engineering Handbook, section Tissue Engineering*. Connecticut: CRC press; 2005.
 11. Salinas A.J., Vallet-Regí M. Bioactive ceramics: from bone grafts to tissue engineering. *RSC Adv* 2013;3:16-31.
 12. Hench L.L., Polak J.M. Third-Generation biomedical materials. *Science* 2002;295:1014-1017.
 13. Frayssinet P., Trouillet J.L., Rouquet N., Azimus E., Autefage A. Osseointegration of macroporous calcium phosphate ceramics having a different chemical composition. *Biomaterials* 1993;14:423-429.
 14. Guelcher S.A., Patel V., Gallagher K.M., Connolly S., Didier J.E., Doctor J.S., Hollinger J.O. Synthesis and in vitro biocompatibility of injectable polyurethane foam scaffolds. *Tissue Eng Part A* 2006;12:1247-1259.
 15. Matheson L.A., Santerre J.P., Labow R.S. Changes in macrophage function and morphology due to biomedical polyurethane surfaces undergoing biodegradation, *J Cell Physiol* 2004;199:8-19.
 16. Howard G.T. Biodegradation of polyurethane: a review. *Int Biodeterior Biodegrad* 2002; 49:245-252.
 17. Fukase Y., Eanes E.D., Takagi S., Chow L.C., Brown W.E. Setting reactions and compressive strengths of calcium phosphate cements. *J Dent Res* 1990;69:1852-1856.
 18. Khairoun I., Boltong M.G., Driessens F.C.M., Planell J.A. Some factors controlling the injectability of calcium phosphate bone cements. *J Mater Sci Mater Med* 1998;9:425-428.

19. Ginebra M.P., Fernández E., Driessens F.C.M., Planell J.A. Modeling of the hydrolysis of α -tricalcium phosphate. *J Am Ceram Soc* 1999;82:2808-2812.
20. Chow C.L. Next generation calcium phosphate-based biomaterials. *J Dent Mater* 2009;28:1-10
21. Ginebra M.P., Driessens F.C.M., Planell J.A. Effect of the particle size on the micro and nanostructural features of a calcium phosphate cement: a kinetic analysis. *Biomaterials* 2004;25:3453-3462.
22. Theiss F., Apelt D., Brand B., Kutter A., Zlinszky K., Bohner M., Matter S., Frei C., Auer J.A., von Rechenberg B. Biocompatibility and resorption of a brushite calcium phosphate cement. *Biomaterials* 2005;26:4383-4394.
23. LeGeros R.Z. Biodegradation and bioresorption of calcium phosphate ceramics. *Clinic Mater* 1993;14:65-88.
24. Bohner M. Calcium orthophosphates in medicine: from ceramics to calcium phosphate cements. *Injury, Int J Care Injured* 2000;31:37-47.
25. Meyer J.L., Fowler B.O. Lattice defects in nonstoichiometric calcium hydroxylapatites. A chemical approach. *Inorg Chem* 1982;21:3029-3035.
26. Wang L., Nancollas H.G. Calcium orthophosphates: crystallization and dissolution. *Chem Rev* 2008;108:4628-4669.
27. Kolk A., Handschel J., Drescher W., Rothamel D., Kloss F., Blessmann M., Heiland M., Wolff K.D., Smeets R. Current trends and future perspectives of bone substitute materials – from space holders to innovative biomaterials. *J Cranio Maxill Surg* 2012;40:706-718.
28. Landi E., Tampieri A., Celotti G., Sprio S., Sandri M., Logroscino G. Sr-substituted hydroxyapatites for osteoporotic bone replacement. *Acta Biomater* 2007;3:961-969.
29. Boanini E., Gazzano M., Bigi A. Ionic substitutions in calcium phosphates synthesized at low temperature. *Acta Biomater* 2010;6:1882-1894.

30. Li Z.Y., Lam W.M., Yang C., Xu B., Ni G.X., Abbah S.A., Cheung K.M., Lu W.W. Chemical composition, crystal size and lattice structural changes after incorporation of strontium into biomimetic apatite. *Biomaterials* 2007;28:1452-1460.
31. Klijn R.J., van den Beucken J.J.P., Lanao F.R.P., Veldhuis G., Leeuwenburgh S.C.G., Wolke J.G., Meijer G.J., Jansen J.A. Three different strategies to obtain porous calcium phosphate cements: comparison of performance in a rat skull bone augmentation model. *Tissue Eng Part A* 2012;18:1171-1182.
32. Tang M., Weir M.D., Xu H.H.K. Mannitol-containing macroporous calcium phosphate cement encapsulating human umbilical cord stem cells. *J Tissue Eng Regen Med* 2012;6:214-224.
33. Wei J., Jia J., Wu F., Wei S., Zhou H., Zhang H., Shin J.W., Liu C. Hierarchically microporous and macroporous scaffold of magnesium–calcium phosphate for bone tissue regeneration. *Biomaterials* 2010;31:1260-1269.
34. Lanao F.R.P., Sariibrahimoglu K., Wang H., Wolke G.C.J., Jansen A.J., Leeuwenburgh S.C.G. Accelerated calcium phosphate cement degradation due to incorporation of glucono delta-lactone microparticles. *Tissue Eng Part A* 2013;20:378-388.
35. Habraken J.M.W., Liao H.B., Zhang Z., Wolke G.C.J., Grijpma D.W., Mikos A.G., Feijen J., Jansen J.A. In vivo degradation of calcium phosphate cement incorporated into biodegradable microspheres. *Acta Biomater* 2010;6:2200-2211.
36. Xue Z., Zhang H., Jin A., Ye J., Ren L., Ao J., Feng W., Lan X. Correlation between degradation and compressive strength of an injectable macroporous calcium phosphate cement. *J Alloys and Compd* 2012;520:220-225.
37. Lanao F.R.P., Leeuwenburgh S.C.G., Wolke G.J., Jansen J.A. Bone response to fast-degrading, injectable calcium phosphate cements containing PLGA microparticles. *Biomaterials* 2011;32:8839-8847.
38. Ginebra M.P., Canal C., Espanol M., Pastorino D., Montufar E.B. Calcium phosphate cements as drug delivery materials. *Adv Drug Deliv Rev* 2012;64:1090-1110

Chapter 2

CALCIUM PHOSPHATE-BASED BONE SUBSTITUTE MATERIALS

Kemal Saribrahimoglu, Joop G.C. Wolke, Sander C.G. Leeuwenburgh,
John A. Jansen

1. Introduction

Tissue engineering is a combination of materials engineering and biology and involves the application of materials to induce tissue regeneration¹. The overall goal of tissue engineering is to manipulate cellular interaction with synthetic advanced materials for the treatment of structurally degenerated organs in the human body. In view of this, various types of scaffold materials have already been developed to cure musculoskeletal disorders. Engineering materials that can be used for bone tissue engineering are metals, polymers and ceramics. Both metals and polymers are used since decennia to replace bone defects in the body, but they are usually separated from the adjacent bone by a non-physiological capsule causing a mismatch in functional properties between bone tissue and artificial implant. Frequently, the implantation of these materials is also accompanied by wound infection, mobility and resorption of the adjacent bone². An approach to overcome this problem is to use calcium phosphate (CaP) based ceramic materials.

The main interest in calcium phosphate materials for bone regeneration relates to the fact that the inorganic phase of bone mainly consists of CaP (70%). CaP ceramics are considered to be bioactive, which implies that they possess the capacity to form a strong chemical bond with adjacent bone^{3, 4}. Despite the fact that CaP ceramics generally exhibit favorable properties for bone tissue engineering, the biological response depends strongly on their physicochemical properties, which will be discussed in the following paragraph.

2. Physicochemical properties of calcium phosphate compounds

Many attempts have been made to synthesize calcium phosphate ceramics with optimal properties for bone reconstruction. An overview of these different calcium phosphate compounds and their Ca/P ratios are given in Table 1. The thermodynamic stabilities in aqueous solution as a function of pH are also cited.

Table 1: Abbreviations of the CaP compounds with corresponding formulas and Ca/P ratios.

Ca/P	Formula	Abbreviation	Name	Remarks
0.50	$\text{Ca}(\text{H}_2\text{PO}_4)\cdot\text{H}_2\text{O}$	MCPM	Monocalcium phosphate monohydrate	stability: < pH 2
1.00	$\text{CaHPO}_4\cdot 2\text{H}_2\text{O}$	DCPD	Dicalcium phosphate dihydrate	stability: $2 < \text{pH} < 4$
1.00	CaHPO_4	DCPA	Dicalcium phosphate anhydrous (monetite)	stability: $2 < \text{pH} < 4$
1.33	$\text{Ca}_8(\text{HPO}_4)_2(\text{PO}_4)_4\cdot 5\text{H}_2\text{O}$	OCP	Octacalcium phosphate	stability: $6.5 < \text{pH} < 8$
1.50	$\text{Ca}_3(\text{PO}_4)_2\cdot x\text{H}_2\text{O}$	ACP	Amorphous calcium phosphate	stability: $4 < \text{pH} < 8$
1.50	$\text{Ca}_9(\text{HPO}_4)(\text{PO}_4)_5\cdot\text{OH}$	CDHA (ns-HA)	Calcium deficient hydroxyapatite	stability: $5 < \text{pH} < 10$
1.50	$\text{Ca}_3(\text{PO}_4)_2$	α -TCP	Alpha-Tricalcium phosphate	stability: $6 < \text{pH} < 8$, more stable than DCPD but less than CDHA
1.50	$\text{Ca}_3(\text{PO}_4)_2$	β -TCP	Beta-Tricalcium phosphate	stability: $6 < \text{pH} < 8$, more stable than α -TCP
1.67	$\text{Ca}_{10}(\text{PO}_4)_6(\text{OH})_2$	s-HA	Stoichiometric hydroxyapatite	stability: $4 < \text{pH}$
2.00	$\text{Ca}_4(\text{PO}_4)_2\text{O}$	TTCP	Tetracalcium phosphate	less stable than CDHA, DCPD or OCP in water at pH 7.4

2.1. Dicalcium phosphate

Two different crystalline dicalcium phosphates (DCP) are known at ambient conditions: (i) brushite (dicalcium phosphate dehydrate, $\text{CaHPO}_4\cdot 2\text{H}_2\text{O}$, DCPD) and (ii) monetite (dicalcium phosphate anhydrous,

CaHPO₄, DCPA). The hydrated DCPD has a monoclinic (*Ia*) structure. OH⁻ molecules in the unit cell occupy an interlayer between Ca²⁺ and PO₄³⁻ chains, which are arranged parallel to each other⁵. Absence of OH⁻ molecules in the structure is referred to as monetite (DCPA). DCPA has a triclinic structure with a Ca/P ratio of 1.5⁶. DCPA can be prepared by the precipitation reaction of Ca(OH)₂ or CaCO₃ slurry with H₃PO₄ solution at a pH of 3.5 around 90°C or by evaporation of a Ca(NO₃)₂·4H₂O and NH₄H₂PO₄ mixture in water at room temperature^{7,8}.

At all pH values, DCPA is less soluble than the DCPD structure^{6,9}, but both types of DCP's are stable at a pH lower than 4.2 (Table 1). Under biological conditions, DCPA is thermodynamically more stable than DCPD¹⁰. Both phases have been proposed as a precursor in bone mineralization.

DCPA and DCPD are widely used as an initial precursor component of self-setting CaP bone cements^{11, 12}. It is reported that cells are able to rapidly resorb DCP ceramics¹³. However, this structure is metastable under physiological conditions and transforms towards a more stable apatitic structure⁶. Many attempts have been made to maintain its structure under conditions where the apatite formation is favored thermodynamically. It is reported that the presence of magnesium ions strongly reduces the transformation rate¹⁴. Absorbance of magnesium ions into DCP crystal nuclei prevents crystallization and gradually decreases the mechanical properties¹⁰. However, maximally 0.3 wt. % Mg²⁺ can be replaced with Ca²⁺ atomic sites⁶.

2.2. Tricalcium phosphate

Two polymorphous forms of tricalcium phosphates (TCPs) are beta-tricalcium phosphate (β-TCP) and alpha-tricalcium phosphate (α-TCP). α-TCP is stable between 1120-1470°C and β-TCP is stable below 1120°C¹⁵. β-TCP crystallizes into the R3c rhombohedral space group¹⁶. The structure is less stable than apatite under physiological conditions. β-TCP is more soluble than HA, which is formed by sintering at high temperatures¹⁷.

Thermodynamically, the most stable structure of β -TCP is whitlockite, where 15% calcium ion vacancies can be occupied by magnesium ions ($\text{Ca}_9(\text{Mg})(\text{PO}_4)6(\text{PO}_3\text{OH})$). Substitution with Mg^{2+} ions decreases its solubility to a lower extent. Moreover, Mg^{2+} plays an important role in the control of the degradation as well as osteoinductivity of β -TCP ceramics^{18, 19}.

α -TCP crystallizes into the monoclinic ($\text{P}2_1/\text{a}$) space group⁶. The major difference with β -TCP is its strong degree of lattice misfit and the presence of atomic vacancies, which creates a higher internal energy. Thus, the solubility and the biodegradability of α -TCP is higher than β -TCP ceramics²⁰. Therefore, the main application area of α -TCP is as constituent of CaP cements, because α -TCP powders easily hydrolyze towards stable hydroxyapatite phases under physiological conditions²¹.

α -TCP can also be sintered as a dense or porous ceramic. The main drawback of this ceramic form is its high reactivity owing to its high solubility²². In an attempt to counteract excessive degradation, α -TCP/ β -TCP biphasic porous ceramics have been produced. The degradation rate of biphasic α -TCP/ β -TCP ceramics was reported to be more effective for bone regeneration than α -TCP or β -TCP alone²³.

2.3. Tetracalcium phosphate

Tetracalcium phosphate ($\text{Ca}_4(\text{PO}_4)_2$, TTCP) crystallizes into the monoclinic unit cell. TTCP is prepared by heating an equimolar mixture of DCPA and CaCO_3 at higher temperatures ($>1300^\circ\text{C}$)²⁴.

Generally, TTCP is highly basic and its Ca/P ratio is higher than stoichiometric apatite. The main application of TTCP is as constituent of self-setting calcium phosphate cement²⁴. It can be combined with other calcium phosphate cement compounds with lower Ca/P ratios^{15, 25}. More acidic DCP is frequently used to dissolve TTCP with TTCP/DCP molar ratios of 1:1, 1:2, 1:3²⁶. Under physiological conditions, it is easily hydrolyzed towards large rod-like or plate-like hydroxyapatite crystals (CDHA or s-HA)²⁴. The solubility of the final compound increases with the

use of low TTCP/DCP ratios. Consequently, fast bioresorbable calcium phosphate cements can be prepared with low TTCP/DCP ratios^{25, 26}.

2.4. Octacalcium phosphate

Synthetic octacalcium phosphate (OCP) materials are crystallized into the triclinic structure (P1)¹⁵. OCP ($\text{Ca}_8(\text{HPO}_4)_2(\text{PO}_4)_4 \cdot 5\text{H}_2\text{O}$) has a Ca/P ratio of 1.33. Its unit cell consists of calcium phosphate apatitic layers with hydrated interlayers²⁷. OCP contains less water molecules than DCPD, which explains its lower solubility⁶. Weakly bonded water molecules near the center of hydrated layer allow incorporation of other ions^{27, 28}. OCP is instable in physiological conditions and it tends to convert into the hydroxyapatite structure²⁹.

2.5. Apatites

The CaP phase as present in the inorganic mineral component of calcified tissue is referred to as apatite³⁰. The general formula of synthetic CaP apatite is $\text{Ca}_5(\text{PO}_4)_3\text{X}$. When the X position is occupied by OH^- groups, the apatite is referred to as hydroxyapatite (HA). Hydroxyapatites can be grouped into two categories: (i) stoichiometric apatite (s-HA) or (ii) non-stoichiometric apatite (calcium deficient hydroxyapatite, CDHA)⁶.

Stoichiometric apatite has a hexagonal structure (P63/m) with a Ca/P ratio of 1.67³¹. Sintered s-HA has generally large crystallite sizes and thus a low solubility. As a result, the biodegradation rate of s-HA is generally low³².

Non-stoichiometric apatite (CDHA) has a formula of $\text{Ca}_{10-x}(\text{OH})_{2-x}(\text{HPO}_4)_x(\text{PO}_4)_{6-x}$ ($0 < x \leq 1$). The lack of Ca^{2+} and OH^- ions in non-stoichiometric apatite creates atomic vacancies, which increase the susceptibility to acidic dissolution³¹. As a consequence, they are structurally and physically more reactive than s-HA.

Chemical analysis of biological apatites, on the other hand, indicated that bone apatite structure also contains trace elements such as Mg, Na, Si, Cl and F (Table 2).

Table 2. Chemical and crystallographic characteristics of biologic apatites.

Composition, wt. %	Bone	Dentin	Enamel
Calcium ^a	36.6	40.3	37.6
Phosphorus ^a	17.1	18.6	18.3
Sodium ^b	1.0	0.6	0.5
Magnesium ^b	0.7	1.2	0.4
Potassium ^b	0.07	0.07	0.05
Carbonate ^b	7.4	5.6	3.5
Fluoride ^c	0.03	0.06	0.01
Chloride ^{ad}	0.33	0.01	0.30
Ca/P ^a	1.65	1.67	1.59
Lattice Parameters ($\pm 0.003 \text{ \AA}$)			
a-axis (\AA)	9.41 ^c	9.42 ^c	9.44 ^e
c-axis (\AA)	6.89 ^c	6.88 ^c	6.87 ^e

^a ref: 6 The composition is relative to the ash content of whole dentin (73 wt %) and enamel (96%). Bone is from bovine cortical bone (taken as 73 wt % of fat-free dry bone). ^b ref: 14, ^c ref: 33, ^d ref: 34, ^e ref: 35

2.5.1. Fluorapatite

The ionic radii of the OH⁻ lattice positions as located in the apatite structure, allow for substitution by fluoride ions (FAP: Ca₁₀(PO₄)₆(OH)_{2-x}F_x)³⁶. Incorporation of fluoride ions into the apatite structure results into stabilization of the lattice and correspondingly a decreased solubility³⁷. Clinical studies on dental caries have revealed that fluoride inhibits acidic etching³⁶. FAP's resistance to acid etching is higher than all other calcium phosphate compounds³⁸.

2.5.2. Carbonated apatite

As shown in Table 2, bone mineral contains a high amount of carbonate. Biological apatites as present in human bone can therefore be referred to as carbonated apatite (CHA). Carbonate in biological apatites primarily substitutes for phosphate groups (B-type substitution). This type of substitution in synthetic CO₃-Aps can be obtained by synthesis at lower temperatures (60-100°C)³⁹. On the other hand, when the reaction is performed at high temperatures (800-1000°C) for several hours in dry CO₂,

the substitution preferentially takes place on OH⁻ molecular sites (A-type substitution)⁶.

Both A-type and B-type carbonated apatite structure are chemically unstable yielding a hydroxyapatite structure that is more reactive than synthetic hydroxyapatite under physiological conditions⁴⁰.

2.5.3. Silicon-substituted apatite

Silicon-substituted calcium phosphates have received much attention because of their supposed positive effect on bone healing⁴¹. Apatites having 1.5-4.6 wt% of Si incorporated into the lattice have been suggested to display improved bone formation^{14, 42}. The incorporation of Si in HA is suggested to enhance its bioactivity by increasing the number of defect sites, which are responsible for partial dissolution of the apatite structure⁴³. Moreover, released Si ions are claimed to stimulate cellular activity by affecting the adsorption of proteins onto silicon-substituted apatites⁴². Nevertheless, final evidence for the supposed effect of silicon substitution has not been found in animal studies⁴⁴.

3. CaP Blocks/Granules

The calcium phosphate compounds as mentioned in the previous chapter have been primarily fabricated in the form of blocks/granules. They have been used in dental and orthopedic applications^{45, 46}. The majority of calcium phosphate blocks/granules are chemically based on HA, β -TCP and biphasic calcium phosphates (HA/ β -TCP, BCP). Commercially available CaP blocks/granules as being currently marketed are listed in Table 3.

Table 3. Commercially available calcium phosphate blocks/granules substitutes.

Company	Commercially available product	Available forms	Macroporosity (μm)	Resorption	Comp. Strenght (MPa)	Target Area	Ref.
Biomet OsteoBiologics, US	ProOsteon 500R	CHA - Blocks	500	9-18 months	6	Distal radius for internal- external fixation, cervical fusion, oral and maxillofacial surgery, orthognathic applications, posttraumatic metaphyseal defects	47, 48, 49
	Endobon	HA -Blocks -Granules	100-1.500	> 5 years	2.5-16	Blocks: Tibial plateau fractures, pelvis and femur, acetabulum, pseudarthrosis defects Granules: bone cysts in hand, feet, knee, and spine	50, 51
	ProOsteon 200R	CHA -Granules	200	6-13 months	10	Anterior/posterior iliac crest corticocancellous bone graft	52, 53
DePuy Spine US	Conduit	β -TCP -Granules	1-600	64% 6-7 months	-	Femoral neck fractures, vertebral body compression fractures	54

CeraVer, France	Cerapatite	HA -Granules	100-400	Several years	40-45	-	55
	Calciresorb	β -TCP -Granules	100-400 500-1000	-	40-45 -	Sinus augmentation	56
FH Orthopedics, France	Eurocer 400	BCP 55%HA/45% β - TCP -Granules	300-500	6-12 months	No mech. resistance	Femoral systems, metaphyseal fractures	57, 58
	Eurocer 200+	BCP 65%/ 35% β -TCP -Blocks	150-300	>15 months	10	Femoral systems, arthrodeses, ankle fractures	57
Medtronic, US	BCP	BCP 60%HA/40% β - TCP -Granules	200-500	-	1-2	Iliac crest	58

Table 3. Continued

Company	Commercially available product	Available forms	Macroporosity (μ m)	Resorption	Comp. Strength (MPa)	Target Area	Ref
Sybron Implant Solutions, Germany	Bioresorb	β -TCP -Granules	200-500 500- 1000 1000-2000 1400-3200	2 years - - -	15 - - -	Osteochondritis, mandibular cysts, ankle-foot fracture, calcaneus cystic lipoma, acetabular revision, tumoral Cavities	59, 60

Wright Medical Technology, U.S.	Cellplex TCP	BCP α -TCP/ β -TCP/HA -Granules	-	62% 8 weeks	1.4	Metadiaphyseal fracture of tibia	61
Mitsubishi Materials Corp. Japan	Bonfil	HA -Blocks -Granules	90-200	> 160 weeks	Blocks: 15 granules: 2-3	Distal radius for internal, external fixation, hip arthroplasty, ilium, dental applications	62, 63
Sumitomo Osaka Cement Co. Japan	Bonceram	HA -Blocks -Granules	50-300	-	44-68.6	Spinal surgery: cervical laminoplasty	64, 65
Pentax Corp. Japan	Apaceram	HA -Dense granules -Porous granules	100-400	> 20 months	Dense: 210 Porous: 66 (40%)	Maxillofacial reconstruction: buccal, inferior mandibular, and posterior margins.	66, 67, 68
Olympus Terumo Biomaterials, Japan	Osferion	β -TCP -Granules	100-500	24 weeks	2	Acetabulum, distal femur, proximal femur	63
Curasan, CryoLife and Spinal Con., Germany	Cerosorb	β -TCP -Blocks -Granules	50- 2000	80-90% within 12 months	-	Sinus floor augmentation, periodontal applications	69

3.1. Production methods

CaP blocks/granulate powder can be fabricated by precipitation, sol-gel and hydrothermal synthesis^{70, 71}. The precipitation route is a widely used technique to obtain CaP powders. In this method, powders are prepared by the reaction of diammonium hydrogen phosphate with calcium nitrate⁷² or orthophosphoric acid with calcium hydroxide (lime: Ca(OH)₂) at pH 10^{73, 74}. Parameters such as stirring rate and temperature have an influence on chemical composition, crystallinity, morphology, size, shape and specific surface area⁷³. The sol-gel method involves the calcination of ammonium, urea and calcium nitrate tetrahydrate solution to produce s-HA powders (Ca/P=1.67)⁷⁵. During hydrothermal processing; monetite, brushite or ACP compounds can be used to obtain more homogeneous and 30-50 nm in length needle-like HA particles under steam pressure at high temperature⁷⁶. The processing of powders into block-form can be done by solid-state high temperature sintering (<1500°C) and hot isostatic pressing (10-300 MPa)⁷⁰. The sintering temperatures depend on the powder characteristics. For instance, sintering of β-TCP powders at high temperature (>1250°C) leads to the composition transformation towards the α-TCP form, which slows down the sintering process. Therefore, this process is usually performed under water vapor in order to be able to increase the temperature while preserving the crystal phase⁷¹. The sintering process under water vapor increases the crystallite size, removes impurities and facilitates the production of dense blocks.

Another limitation related to high temperature sintering is excessive grain growth, high density, loss of porosity and correspondingly low specific surface area^{77, 78}. For example, densification of HA above 700°C decreases the specific area from 50-200 m²/g to 1 m²/g. In contrast, the specific area of bone is around 80 m²/g⁷⁹⁻⁸².

In order to improve the biological success of CaP ceramics, interconnected macroporous calcium phosphate blocks or granules have been developed. Macroporosity within the ceramic increases the success of the implant by enabling vascularisation and bone ingrowth throughout the ceramic material. Macroporosity in CaP ceramics can be introduced by polymeric

substances or production of gas bubbles (CO₂). Although macroporosity enhances the resorption and cellular interaction, the reduced mechanical resistance of the material does not allow its use in load-bearing applications⁸³.

3.2. Structure-property relationships

3.2.1. Mechanical properties

The stiffness of a biomaterial should be comparable to that of cortical and trabecular bone to support loading at the fracture site⁸⁴. Therefore, bone substitutes have to be designed in order to withstand long-term or short-term compressive and bending forces. The main drawback of calcium phosphates materials is their brittleness and poor strength, limiting their use as implants in loaded situations.

Porous calcium phosphates are attractive for a wide variety of applications. However, deterioration of mechanical properties is the main disadvantage of these structures. It is reported that high macroporosity (>40%) induces bone growth, but decreases the elastic modulus and compressive strength more than ten-fold^{85, 86}. Therefore, a remarkable increase in mechanical properties and biological performance can be achieved by controlling the preparation conditions.

3.2.2. Bioresorption

Bioresorption is a biological erosion process by which a material is resorbed and replaced by tissue over a period of time. Bioresorption of calcium phosphate ceramics is divided into two main categories; (i) active resorption, and (ii) passive resorption^{4, 87, 88}.

Passive resorption is a solution-mediated process (extracellular liquid of the body) and predominantly initiates at potential stress accumulated regions in the structure. Porosities, grain boundaries, dislocations, cracks, irregularities, substitution ion sites and atomic vacancies are known to be potential dissolution sites in ceramic apatites because of their higher sensitivity to acidic etching^{89, 90}.

Active resorption takes place by osteoclasts. Upon implantation of CaP ceramics, the activity of the osteoclasts determines the dissolution and remodeling characteristics of the CaP ceramic.

Remodeling of the CaP material is strongly influenced by the presence of porosity. Microporosity ($<10\mu\text{m}$) allows the influx of body liquids. The material serves than as a nutrition provider for osteoprogenitor cells. Macroporosity ($>100\mu\text{m}$) enables the penetration of fibrovascular tissue and the development of mature osteons^{91,92}. It is reported that the ideal pore size for CaP ceramics is between 100-400 μm in order to act as a convenient template for rapid bone growth⁹³. Interconnections between pores are also favorable for nourishment and colonization of the material with blood vessels.

3.2.3. Biological properties

3.2.3.1. In vivo animal studies

The bone healing capacity of various calcium phosphate ceramics has been tested in different animal models (Figure 1). Calcium phosphate biomaterials with various amounts of HA and TCP (BCP) blocks were reported to have high bone forming capacity²¹.

Compared to high temperature sintered β -TCP, α -TCP and HA ceramics that showed low amount of bone formation in a dog implantation study due to an unbalanced passive resorption⁹³, high biodegradability and bone regeneration was observed for low temperature sintered (1150°C) BCP ceramics (80/20, 60/40 wt% HA/ β -TCP) in goat and sheep experiments^{94,95}. In another study, the optimum bone formation rate of six different CaP ceramic implants (HA/ β -TCP: 100/0, 76/24, 63/37, 56/44, 20/80) was determined in a femoral gap defect as created in rats. More bone formation within 12 weeks was determined in the BCP group, which consisted of 56/44 wt% and 20/80 wt% HA/ β -TCP. The high amount of bone formation in the BCP group was attributed to a low activity of osteoclast induced by Ca^{2+} release⁹⁶.

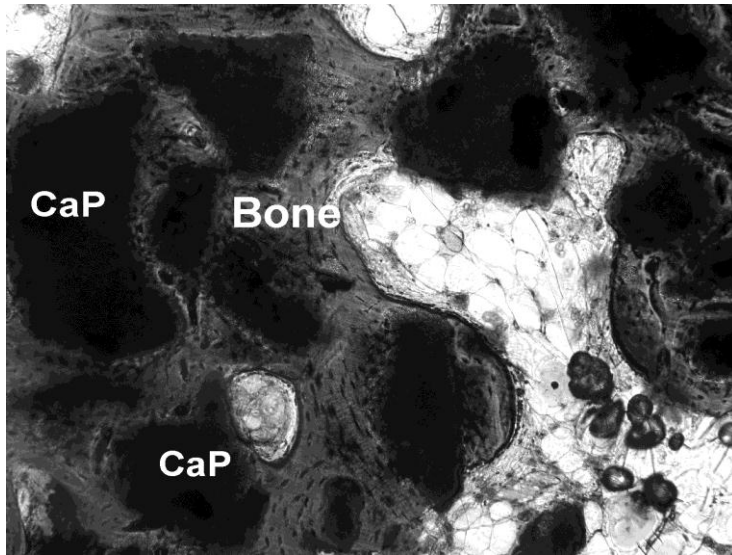


Figure 1. Micrographs showing the tissue response of CaP granules after 12 weeks of implantation in sheep tibia. A close contact between the newly formed bone and the CaP granules supporting the osteoconductive properties of the CaP ceramic materials.

3.2.3.2. Clinical applications

3.2.3.2.1. Hydroxyapatite

HA granules can be used as filler of bone defects and blocks can be used to prevent e.g. dorsal displacement of the distal fragments in orthopedic fractures (Figure 2). However, many clinical results demonstrated a lower quantity of bone growth on HA granules when used in human craniofacial and maxillofacial bone defects in long term follow up studies⁹⁷⁻⁹⁹.

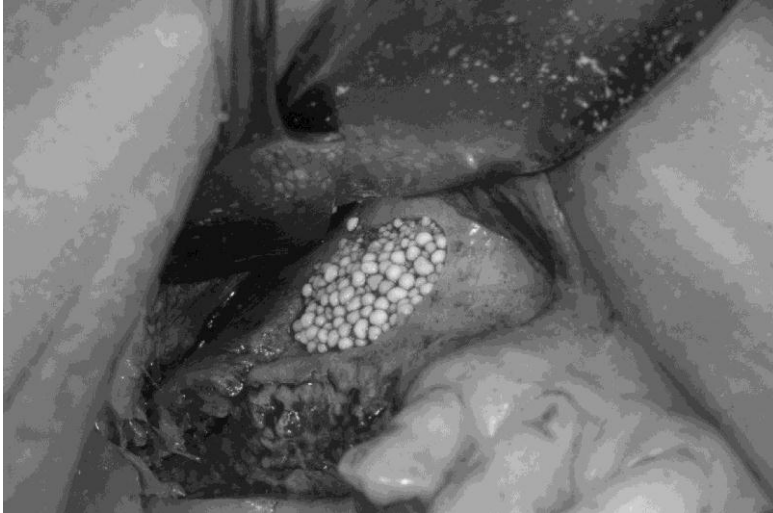


Figure 2. Placement of hydroxyapatite granules into pockets created between the soft tissues and the alveolar bone.

The main problem with the granules is their migration in the defect site and the unpredictable bone growth. On the other hand, hydroxyapatite blocks overcome these problems by producing a stable augmentation. HA blocks can successfully support teeth and bone segments in their replaced positions and they are convenient materials for alveolar ridge augmentation procedures^{2, 100}. Histological studies showed good bony healing and early host bone attachment with no evidence of any foreign body reaction. However, it is difficult to shape the solid-dense hydroxyapatite blocks during surgery. This may result into implant migration through the cavity¹⁰¹.

3.2.3.2.2. Coral-derived Apatites

In an attempt to enhance the osteoconductivity and osteoinductivity of apatites, thermochemically treated marine coral apatites (CaCO_3 , Porites, Goniopora) have been developed. When corals are treated with ammonium phosphate solution under hydrothermal conditions at pH 7 for 3 days, their structure is converted into resorbable osteoconductive coralline hydroxyapatite^{102, 103}.

Currently, the most commonly used commercial coral-derived carbonated apatite blocks/granules are Biocoral[®], ProOsteon[®]500 and Interpore[®]200 (ProOsteon[®]200). They have been reported to be bioresorbable and osteoinductive¹⁰⁴. They can be used for alveolar ridge augmentation, periodontal, and orthognathic reconstructions¹⁰⁵. It is reported that when coralline blocks are used for the repair of lumbar discogenic pain surgery in 40 patients with an anterior lumbar interbody fusion (ALIF) technique, a success rate of 82.5% with a fusion rate of 92.5% can be achieved in patients. Histological analysis after 24 months confirmed conclusive evidence of bone ingrowth⁴⁸. Another histological study showed a 93.5% implant success rate when coralline apatite granules were used in the posterior maxilla and mandible for the placement of dental implants during a 3-8 year follow-up period in 21 patients¹⁰⁶.

3.2.3.2.3. β -Tricalcium phosphate

Biodegradable CaP materials are used to replace a defect sites with newly formed bone. In many bone reconstruction surgeries, bioresorbable β -TCP blocks/granules attract more attention for tissue engineering applications because of their osteoinductivity. Although β -TCP has almost the same chemical composition ($\text{Ca}_3(\text{PO}_4)_2$) as HA, the crystallographic difference strongly influences its dissolution and resorption activity.

β -TCP granules such as ConduitTM, RTR[®] or Osferion[®] alone, possess a fast resorption rate and superior osteoconductivity^{54, 63, 107}. In vivo studies have revealed that β -TCP resorption depending on passive erosion due to its reactivity at biologic conditions¹⁰⁸.

3.2.3.2.4. Biphasic calcium phosphate

As implants made of dense pure HA are maintained in the defect area for many years because of their thermodynamic stability and β -TCP implants can degrade too fast before bone formation can occur, the soluble HA/TCP (BCP) composite calcium biomaterials have been developed for biomedical applications. Notably, the use of two calcium phosphate phases has gained

in importance due to its high bone growth rate at physiological conditions¹⁰⁹.

Clinical application of BCPs is shown in a study of Mailac *et. al.*¹¹⁰, who used 21% microporous and 49% macroporous (macropores: >300 μ m) 60/40 wt% HA/TCP granules in a sinus lift augmentation procedure in human. After 6 months of implantation, 53% of the granules were resorbed and almost completely replaced by newly formed bone. Vascularization and hematopoietic cells around the residual HA material confirmed the high osteoconduction properties of BCP granules. Besides their biological activity, a broad pore size range production stimulates infiltration of large osteoclast and small leukocytes, which enhance cellular interactions and bone regeneration⁹⁴.

The bioactivity of BCPs is also ascribed to the HA/ β -TCP ratio. When 50/50 wt% BCP granules (pore size: 90-100 μ m) were used in the anterior maxilla, gradual resorption and new bone substitution is observed with no evidence of inflammatory response¹¹¹. High bone remodeling of low HA/ β -TCP ratio occurs by (i) partial dissolution of β -TCP, (ii) carbonated hydroxyapatite transformation associated with an organic matrix, (iii) mineralization of the collagen fibrils, and (iv) a rapid remodeling process¹¹².

Although the bone repairing ceramics based on HA or β -TCP become more and more applied, biphasic structure grafts provide a significant alternative to autogenous bone for orthopedic and dental applications.

4. Calcium phosphate cements

In contrast to premade CaP blocks or granules, which are difficult to handle from a clinical point of view, self-setting CaP cements (CPC) have been developed. These materials are injectable, which allows for optimal defect filling.

Injectable calcium phosphate cements for the use as a bone graft were first described by Chow and Brown in 1985. Their cement is based on at least two sparingly soluble CaP mixtures that are precipitated apatite crystals in an aqueous environment. Under physiological conditions, the end product is

an apatite structure, which is remarkably biocompatible¹¹³. So far, a large number of CaP cements have been developed as a potential grafting material for use in orthopedics and dentistry (Table 4). For each formulation, in vivo tests have been performed to prove the success of calcium phosphate cements. Cements having identical chemical compositions display large differences in physicochemical and biological properties due to several factors such as the presence of impurities, the particle size distribution and correspondingly specific surface area resulting into differences in solubility of the precursor phases^{114, 115}.

4.1. Setting of cement

Calcium phosphate cements are formulated as a solid-liquid mixture. The general principle of mixing more than one calcium phosphate compound is to balance the precipitation reaction of CaP compounds with respect to solubility.

Dry calcium phosphate sources may include: $\text{Ca}_3(\text{PO}_4)_2$ (TCP), CaHPO_4 (DCP), $\text{Ca}_4(\text{PO}_4)_2\text{O}$ (TTCP), $\text{Ca}_3(\text{PO}_4)_2\text{H}_2\text{O}$ (ACP). Alternatively, calcium sources include: CaCO_3 (calcite), CaO (calcium oxide), $\text{Ca}(\text{OH})_2$ (calcium hydroxide), while phosphate sources can be: H_3PO_4 (phosphoric acid), Na_2HPO_4 (disodium hydrophosphate) or NaH_2PO_4 (sodium dihydrphosphate)¹¹⁶. When mixed in aqueous solvents that often contain buffers based on e.g. phosphate or acetate, these dry powders convert into a self-setting paste that can be injected into bone cavities and subsequently harden within 10-20 minutes (Figure 3).

Table 4. List of commercially available calcium phosphate cements.

Company	Cement Type	Components	Solution Mixture	End Product	Compressive Strength (MPa)
Teknimed	Cementek®	α -TCP TTCP Ca(OH)_2	$\text{H}_2\text{O} + \text{Ca(OH)}_2,$ H_3PO_4	HA Ca/P=1.64	20
Biomed	Calcibon®	α -TCP (61%) DCPA (26%) CaCO_3 (10%) pHA (3%)	$\text{H}_2\text{O} + \text{Na}_2\text{HPO}_4$	Carbonated apatite (CHA)	60-70
	Mimix™	α -TCP TTCP $\text{C}_6\text{H}_5\text{O}_7\text{Na}_3 \cdot 2\text{H}_2\text{O}$	$\text{H}_2\text{O} + \text{C}_6\text{H}_8\text{O}_7$	HA	22
ETEX	Biobon®	ACP(50%) DCPD (50%)	H_2O	HA Ca/P= 1.45	12
Stryker-Leibinger	BoneSource®	TTCP (73%) DCPD (27%)	$\text{H}_2\text{O} + \text{Na}_2\text{HPO}_4$ + NaH_2PO_4	HA Ca/P=1.67	36
Synthes-Norian	Norian®SRS	α -TCP (85%) CaCO_3 (12%) MCPM (3%)	$\text{H}_2\text{O} +$ Na_2HPO_4	Brushite Ca/P=1.67	28-55
	chronOST™	β -TCP (42%) MCPM (21%) $\text{MgHPO}_4 \cdot 3\text{H}_2\text{O}$ (5%)	$\text{H}_2\text{O} +$ Sodium hyaluronate (0.5%)	Brushite	3
Mitsubishi Materials	Biopex®	α -TCP (75%) TTCP (18%) DCPD (5%) HA (2%)	$\text{H}_2\text{O},$ sodium succinate (12%), sodium chondroitin sulphate	HA	80



Figure 3. Injection of calcium phosphate cement from syringe.

The setting behavior of the paste is an important property that strongly affects its clinical performance. The setting time should not be too fast or too long because it can only be shaped before it hardens, whereas the wound area can only be closed after hardening. Generally, the final setting time of the cement should be below 15 min. for optimal clinical handling¹¹⁷. In order to accelerate the setting time of the paste, Na_2HPO_4 ($\text{pH}>7$) and/or NaH_2PO_4 ($\text{pH}<6$) liquid additives can be used¹¹⁸. These additives not only modify the pH of the medium for dissolution reaction, but also supply PO_4^{3-} sources to accelerate the precipitation reaction⁹.

The liquid/powder ratio (L/P) is an important aspect of the cement that affects the workability and the injectability of the paste. Generally, low L/P ratios cause flowable and viscous pastes, while liquid deprivation reduces the injectability of the paste. On the other hand, excess aqueous solution is often associated with the phenomenon of filter-pressing, which implies that the liquid flows faster than the ceramic particles⁸⁰. Although liquid films surrounding the particles keep the particles separated, improve the fluidity and allow injection by minimally invasive techniques, the final setting time of the cement increases due to delayed crystallization, which causes a

weaker structure due to a high micro and nanoporosity in the final cement^{119, 120}.

The cohesion is the ability of the paste to maintain its shape upon contact with body liquid. Washout of the cement may result in inflammatory reactions at the defect site. Small particle sizes, low L/P ratios or addition of gelling agents (0.2-2% sodium alginate, 0.4-1.5% chitosan, 2-4% hydroxypropylmethyl (HPMC) or carboxymethyl cellulose (CMC)) can be used to prevent disintegration of the paste¹²¹⁻¹²³.

The evolution of the crystal structure is governed by the dissolution/precipitation, crystallization and crystal growth mechanism (Figure 4). In relatively high supersaturations, an amorphous calcium phosphate (ACP) is the phase that forms first.

Incorporation of carbonate and other impurities occurs during irreversible hydrolysis reactions of ceramic precursors towards precipitation of HA. These ions decrease the transformation rate and crystal size of precipitated HA¹²⁴.

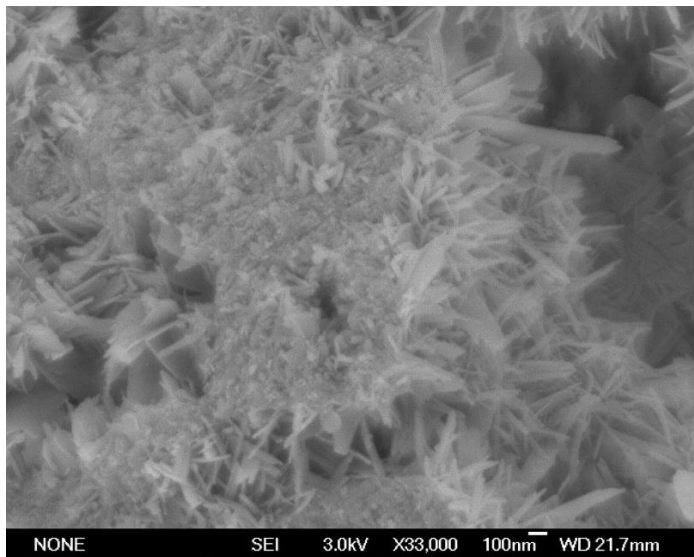


Figure 4. SEM pictures of the acicular microcrystalline hydroxyapatite structure.

4.2. Structure-property relationships

4.2.1. Mechanical properties

A critical limitation for long-term performance of CPCs is their relatively low mechanical strength. Because of the self-setting reaction and the absence of high sintering temperatures, compressive strengths of CaP cements are up to 10 times lower than sintered calcium phosphate compounds¹²⁵. However, the compressive strength of CPCs is still comparable to that of cortical bone (88-164 MPa)¹²⁶.

Calcium phosphate cements exhibit a high amount of nano- and microporosity. Porosity that develops between entangled crystals is the main reason for the weak mechanical structure of cements. For example, a decrease in microporosity from 50% to 31% in the end product of TTCP/DCPA cements increased the wet compressive strength from 4 to 37 MPa, respectively¹²⁷. Additionally, an addition of 10 wt% silica or titanium oxide in TTCP/DCPA cements significantly increased the compressive strength (80-100 MPa) due to the more dense structure¹²⁸. On the other hand, for α -TCP cement, which sets into CDHA as end product, a compressive strength of 40MPa was obtained by using fine particles of about 2-3 μm to obtain a structure with a low porosity²¹.

4.2.2. Bioresorption

Calcium phosphate cements consisting of α -TCP/DCP, TTCP/DCP or β -TCP/MCPM (Monocalcium phosphate monohydrate) powders set into highly osteoconductive and osteoinductive HA, CDHA or DCPD final products (Table 4)¹²⁹⁻¹³¹. Their resorption rate and bone formation rate has been reported to be higher than sintered HA based ceramics¹³². Due to the low density of the final HA structure, these cements can be resorbed by osteoclasts¹³³. Moreover, because of the uniform distribution of the paste throughout the bone defect, new bone formation can occur more rapidly and uniformly in the entire defect area due to calcium release into the surrounding medium by active and passive resorption of the cement¹³⁴.

4.2.3. Biological properties

4.2.3.1. In vivo animal studies

Calcium phosphate cements have been proven to be effective as bone substitutes because of their high biocompatibility and osteoconductive structure (Figure 5).

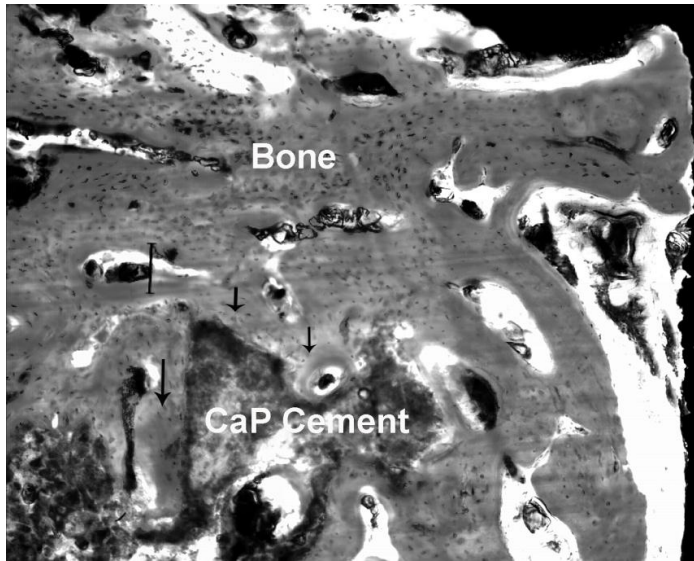


Figure 5. Low magnification photomicrograph of a transversal section of the CaP cement after 24 weeks of sinus implantation in goat model. Parts of the cement mass is resorbed and followed by bone ingrowth (arrowheads). A close contact between the newly formed bone and the CaP cement, (end product: CDHA, Ca/P: 1.54) supporting the osteoconductive properties of the cement (original magnification 2.5X, bar = 400 μ m).

Several histological and histomorphometrical examinations confirmed the excellent bone biocompatibility, osteoconductivity and bone healing capacity of apatite and brushite cements in various animal models^{130, 133, 135}. Apatite cements have been reported to be able to enhance osteoblast and osteoclast activity and increased mesenchymal cell differentiation when implanted in rabbits and goats^{131, 136}. Upon implantation, fully osseointegration of the apatitic cement to the rim of the acetabulum in 22 sheep was also reported¹³⁷. For brushite cements, on the other hand, the

resorption occurred through body liquid dissolution with cement disintegration, which is accompanied with new bone formation when implanted in sheep femur defects for a period of 8 weeks¹³⁵. However, the osteoinduction rate for brushite cements is higher when vascular endothelial growth factor and platelet derived growth factors (VEGF/PDGF) are loaded into this material¹³⁸.

4.2.3.2. Clinical applications

Various bone cement materials are currently being commercialized for various clinical indications. The most important are discussed below.

The first commercially available injectable cement, Norian Skeletal Repair System (SRS), (Norian/Synthes USA, Paoli, PA), was marketed in the 1990s¹³⁹. Norian Skeletal is a calcium phosphate cement consisting of MCPM, α -TCP and CaCO_3 , while the liquid phase contains phosphate source. Within 10 minutes, the cement begins to crystallize into carbonated apatite with a molar calcium-phosphate ratio of 1.67. The hardening reaction is almost completed after 12 hours. The final compressive strength equals 55 MPa which is higher than cancellous bone¹⁴⁰. The end product of the cement setting reaction is biocompatible, osteoconductive and stimulates osteogenesis¹⁴¹. The cement is approved for more general orthopedic use in tibial and femoral metaphyseal bone defects and displaced tibial plateau fractures¹⁴². Bioresorption of SRS in cancellous bone defect is completed as early as 16 weeks after implantation¹⁴⁰. Long-term follow up (1 year) with Norian cements in cranial defects and bony deformities showed that the main complications were related to sterile seroma and infection due to cement fragmentation. However, problems related to infections could be solved with antibiotic therapy. The complication rate was observed to increase in patients who received more than 25 g of Norian¹³.

BoneSource® (Stryker-Howmedica-Osteonics, Rutherford, NJ) is another calcium phosphate cement, which consist of TTCP and DCPD with a powder-liquid ratio of 4:1. Hardening of the paste is reached between 10-15 minutes resulting into complete conversion towards HA (Ca/P: 1.65-1.67)

as an end product²⁴. BoneSource® has been approved for use in metaphyseal fractures. High success rates are reported for craniofacial defects for time periods between 24 months to 6 years¹⁴³. Effectiveness and healing of metaphyseal bone voids, translabyrinthine, middle cranial fossa and suboccipital craniectomy have also been reported, but long-term stability of final product is the main disadvantage of this cement type when high amounts of the cement are used at the defect site^{144, 145, 146}.

5. Conclusion

The osteoconductivity and in some cases osteoinductivity of calcium phosphate ceramics render these materials highly suitable as scaffold material for the engineering of bone tissue. Still, the biological performance of these ceramics in terms of biodegradation and the amount of new bone formation is strongly dependent on their physicochemical properties, which stresses the fact that proper characterization of CaP scaffolds is of utmost importance. Although calcium phosphate based blocks/granules have been safely and effectively used in a wide range of orthopedic and dental applications, recent evidence indicates that self-hardening cements can be as effective as sintered CaP granules to regenerate bone tissue. In combination with their superior clinical handling, it can be concluded that CaP cements with controlled injectability, porosity and degradation can become the preferred material of choice for hard tissue engineering applications.

References

1. Langer R., Vacanti J.P. Tissue engineering. *Science* 1993;260:920-926.
2. Frame J.W. Hydroxyapatite as a biomaterial for alveolar ridge augmentation. *Int J Oral Max Surg* 1987;16:642-655.
3. Daculsi G., LeGeros R.Z., Heughebaert M., Barbieux I. Formation of carbonate-apatite crystals after implantation of calcium phosphate ceramics. *Calcified Tissue Int* 1990;46:20-27.

4. Frayssinet P., Trouillet J.L., Rouquet N., Azimus E., Autefage A. Osseointegration of macroporous calcium phosphate ceramics having a different chemical composition. *Biomaterials* 1993;14:423-429.
5. Wang L., Nancollas H.G. Calcium orthophosphates: Crystallization and dissolution. *Chemical Rev* 2008;108:4628-4669.
6. Elliott J.C. Structure and chemistry of the apatites and other calcium orthophosphates. Amsterdam: Elsevier Science, 1994.
7. Louati B., Hlel F., Guidara K., Gargouri M. Analysis of the effects of thermal treatments on CaHPO_4 by ^{31}P NMR spectroscopy. *J Alloy Compd* 2005;394:13-18
8. Tas A.C. Monetite Synthesis in ethanol at room temperature. *J Am Ceramic Soc* 2009;92:2907-2912.
9. Fernandez E., Gil F.J., Ginebra M.P., Driessens F.C.M., Planell J.A., Best S.M. Calcium phosphate bone cements for clinical applications, part 1: Solution chemistry. *J Mater Sci - Mater Med* 1999;10:169-176.
10. Lilley K.J., Gbureck U., Knowles J.C., Farrar D.F., Barralet J.E. Cement from magnesium substituted hydroxyapatite. *J Mater Sci - Mater Med* 2005;16: 455-460.
11. Barrere F., van Blitterswijk C.A., de Groot K. Bone Regeneration: Molecular and cellular interactions with calcium phosphate ceramics. *Int J Nanomed* 2006;1:317-332.
12. Hofmann M.P., Mohammed A.R., Perrie Y., Gbureck U., Barralet J.E. High-strength resorbable brushite bone cement with controlled drug-releasing capabilities. *Acta Biomater* 2009;5:43-49.
13. Gilardino S.M., Cabiling S.D., Bartlett P.S. Long-term follow-up experience with carbonated calcium phosphate cement (Norian) for cranioplasty in children and adults. *Plastic Recons Surg* 2009;123:983-994.
14. Boanini E., Gazzano M., Bigi A. Ionic substitution in calcium phosphates syntheses at low temperature. *Acta Biomater* 2010;6:1882-1894.

15. Mathew M., Takagi S. Structures of biological minerals in dental research. *J Res Natl Inst Stan* 2001;106:1035-1044.
16. Yashima M., Sakai A., Kamiyama T., Hoshikawa A. Crystal structure analysis of b-tricalcium phosphate ($\text{Ca}_3(\text{PO}_4)_2$) by neutron powder diffraction. *J Solid State Chem* 2003;175:272-277.
17. Yang H., Thompson I., Yang S., Chi X., Evans J., Cook R. Dissolution characteristics of extrusion freeformed hydroxyapatite-tricalcium phosphate scaffolds. *J Mater Sci - Mater Med* 2008;19:3345-3353.
18. Qi G., Zhang S., Khor K.A., Lye S.W., Zeng X., Weng W., Liu C., Venkatraman S.S., Ma L.L. Osteoblastic cell response on magnesium-incorporated apatite coatings. *Appl Surf Sci* 2008;255:304-307.
19. Pina S., Olhero S.M., Gheduzzi S., Miles A.Q., Ferreira J.M.F. Influence of setting liquid composition and liquid-to-powder ratio on properties of Mg-substituted calcium phosphate cement. *Acta Biomater* 2009;5:1233-1240.
20. Mathew M., Schroeder L.W., Dickens B., Brown W.E. The crystal structure of $\text{Ca}_3(\text{PO}_4)_2$. *Acta Cryst* 1977;B33:1325-1333.
21. Ginebra M.P., Driessens F.C.M., Planell J.A. Effect of the particle size on the micro and nanostructural features of calcium phosphate cement: A kinetic analysis. *Biomaterials* 2004;25:3453-3462.
22. Yuan H., Yang Z., Li Y., Zhang X., de Bruijn J.D., de Groot K. Osteoinduction by calcium phosphate biomaterials. *J Mater Sci - Mater Med* 1998;9:723-726.
23. Kamitakahara M. Behavior of ceramic biomaterials derived from tricalcium phosphate in physiological condition. *J Biomater Appl* 2008;23:197-112
24. Fukase Y., Eanes E.D., Takagi S., Chow L.C., Brown WE. Setting reactions and compressive strenghts of calcium phosphate cements. *J Dent Res R* 1990;69:1852-1856.

25. Chow C.L., Takagi S. A natural bone cement—A laboratory novelty led to the development of revolutionary new biomaterials. *J Res Natl Inst Stan* 2001;106:1029-1033.
26. Hirayama S., Takagi S., Marcovic M., Chow C.L. Properties of calcium phosphate cements with different tetracalcium phosphate and dicalcium phosphate anhydrous molar ratios. *J Res Natl Inst Stan* 2008;113:311-320.
27. Brown E.W. Octacalcium phosphate and hydroxyapatite: Crystal structure of octacalcium phosphate. *Nature* 1962;196:1048-1050.
28. Johnsson M.S., Nancollas G.H. The role of brushite and octacalcium phosphate in apatite formation. *Crit Rev Oral Biol Med* 1992;3:61-82.
29. Suzuki O. Octacalcium phosphate: Osteoconductivity and crystal chemistry. *Acta Biomater* 2010;6:3379-3387.
30. Biltz R.M., Pellegrino E.D. The composition of recrystallized bone mineral. *J Dent Res* 1983;62:1190-1195.
31. Yubao L., Xingdong Z., de Groot K. Hydrolysis and phase transition of alpha-tricalcium phosphate. *Biomaterials* 1996;18:737-741.
32. Driessens F.C.M., Boltong M.G., Zapatero M.I., Verbeeck R.M.H., Bonfield W., Bermudez O., Fernandez E., Ginebra M.P., Planell J.A. In vivo behaviour of three calcium phosphate cements and magnesium phosphate cement. *J Mater Sci - Mater Med* 1995;6:272-278.
33. Dorozhkin S.V. Calcium orthophosphates in nature, biology and medicine. *Materials* 2009;2:399-398.
34. Handschin R.G., Stern W.B. X-ray diffraction studies on the lattice perfection of human bone apatite (Crista Iliaca). *Bone* 1995;16:S355-363.
35. Elliott J.C., Holcomb D.W., Young R.A. Infrared determination of the degree of substitution of hydroxyl by carbonate ions in human enamel. *Calcified Tissue Int* 1985;37:372-375.

36. Lin J., Raghavan S., Fuerstenau D.W. The adsorption of fluoride ions by hydroxyapatite from aqueous solution. *Colloid Surface* 1981;3:357-370.
37. Little F.M., Rowley J. Studies on the carbon dioxide component of human enamel III. The effect of neutral and acid fluoride. *J Dent Res* 1961;40:915-920.
38. Budz J.A., Lore M., Nancollas G.H. Hydroxyapatite and carbonated apatite as models for the dissolution behavior of human dental enamel. *Adv J Dent Res* 1987;1:314-321.
39. LeGeros R.Z. Effect of carbonate on the lattice parameters of apatite. *Nature* 1965;4982:403-404.
40. Habibovic P., Juhl V.M., Clyens S., Martinetti R., Dolcini L., Theilgaard N., van Blitterswijk C.A. Comparison of two apatite ceramics in vivo. *Acta Biomater* 2010;6:2219-2226.
41. Bohner M. Physical and chemical aspects of calcium phosphates used in spinal surgery. *Eur Spine J* 2001;10:114-121.
42. Gasqueres G., Bonhomme C., Maquet J., Babonneau F., Hayakawa S., Kanaya T., Osaka A. Revisiting silicate substituted hydroxyapatite by solid-state NMR. *Magn Reson Chem* 2007;46:342-346.
43. Regi V.M., Arcos D. Silicon substituted hydroxyapatites: A method to upgrade calcium phosphate based implants. *J Mater Chem* 2005;15:1509-1516.
44. Bohner M. Silicon-substituted calcium phosphates - A critical view. *Biomaterials* 2009;30:6403-6406.
45. Bucholz R.W., Carlton A., Holmes R. Interporous hydroxyapatite as a bone graft substitute in tibial plateau fractures. *Clin Orthop Relat Res* 1989;240: 53-62.
46. Navarro M., Michiardi A., Castano O., Planell J.A. Biomaterials in orthopedics. *J R Soc Interface* 2008;5:1137-1158.
47. Wolfe S.W. Augmentation of distal radius fracture fixation with coralline HA bone graft substitutes. *J Hand Surg* 1999;24A:816-827.

48. Thalgott J.S., Giuffre J.M., Fritts K., Timlin M., Klezl Z. Instrumented poster lateral lumbar fusion using coralline hydroxyapatite with or without demineralized bone matrix, as an adjunct to autologous bone. *The Spine J* 2001;1:131-137.
49. Korovessis P., Koureas G., Zacharatos S., Papazisis Z., Lambiris E. Correlative radiological, self-assessment and clinical analysis of evolution in instrumented dorsal and lateral fusion for degenerative lumbar spine disease. Autograph versus coralline hydroxyapatite. *Eur Spine J* 2005;14:630-638.
50. Gierse H., Donath K. Reactions and complications after the implantation of Endobon including morphological examination of explants. *Arch Orthop Trauma Surg* 1999;119:349-355.
51. Baer W., Schaller P., Carl H.D. Spongy hydroxyapatite in hand surgery- A five year follow up. *J Hand Surg* 2002;27B:101-103.
52. Shord E.C. Coralline bone graft substitutes. *Orthop Clin N Am* 1999;30:599-613.
53. Stubbsa D., Deakina M., Sheatha P.C., Bruceb W., Debesc J., Gillies R.M., Walsh W.R. In vivo evaluation of resorbable bone graft substitutes in a rabbit tibia defect mode. *Biomaterials* 2004;25:5037-5044.
54. Bodde E.W.H., Wolke G.C.J., Kowalski R.S.Z., Jansen J.A. Bone regeneration of porous β -tricalcium phosphate (conduit-tcp) and of biphasic calcium phosphate ceramic (biosel) in trabecular defects in sheep. *J Biomed Mater Res Part A* 2007;82A:711-722.
55. Henno S., Lambotte J.C., Glez D., Guigand M., Lancien G., Cathelineau G. Characterization and quantification of angiogenesis in β -tricalcium phosphate implants by immunohistochemistry and transmission electron microscopy. *Biomaterials* 2003;24:3173-3181.
56. Gruber R.M., Ludwig A., Merten H.A., Achilles M., Poehling S., Schliephake H. Sinus floor augmentation with recombinant human growth and differentiation factor-5 (rhGDF-5): A histological and histomorphometric study in the goettingen miniature pig. *Clin Oral Implan Res* 2008;19:522-529.

57. Schwartz C., Liss P., Jacquemaire B., Lecestre P., Frayssinet P. Biphasic synthetic bone substitute use in orthopaedic and trauma surgery: Clinical, radiological and histological results. *J Mater Sci - Mater Med* 1999;10:821-825.
58. Schwartz C., Bordei R. Biphasic phospho-calcium ceramics used as bone substitutes are efficient in the management of severe acetabula bone loss in revision total hip arthroplasties. *Eur J Orthop Surg Traumatol* 2005;15:191-196.
59. Galois L., Mainard D., Pfeffer F., Traversari R., Delagoutte J.P. Use of β -tricalcium phosphate in foot and ankle surgery: A report of 20 cases. *J Foot Ankle Surg* 2001;7:217-227.
60. Knežević G., Rinčić M., Knežević D. Radiological evaluation of the healing of bone defects filled with tricalcium phosphate (bioresorb) after cystectomy of the mandible. *Acta Stomatol* 2007;41:66-73.
61. Fredericks D.C., Bobst J.A., Petersen E.B., Nepola J.V., Dennis J.E., Caplan A.I., Burgess A.V., Overby R.J., Schulz O.H. Cellular interactions and bone healing responses to a novel porous tricalcium phosphate bone graft material. *Orthopedics* 2004;27:167-173.
62. Yaszemski M.J., Trantolo D.J., Lewandrowski K.U., Hasirci V., Altobelli D.E., Donald L.W. *Biomaterials in orthopedics*. New York: Northeastern Univ. Press, 2004.
63. Ogose A., Kondo N., Umezū H., Hotta T., Kawashima H., Tokunaga K., Ito T., Kudo N., Hoshino M., Gu W., Endo N. Histological assessment in grafts of highly purified beta-tricalcium phosphate (OSferion) in human bones. *Biomaterials* 2006;27:1542-1549.
64. Kokubun S., Kashimoto O., Tanaka Y. Histological verification of bone bonding and ingrowth into porous hydroxyapatite porous process spacer for cervical aminoplasty. *The Tohoku J Exp Med* 1994;173:337-344.
65. Yoshikawa H., Tamai N., Murase T., Myoui A. Interconnected porous hydroxyapatite ceramics for bone tissue engineering. *J R Soc Interface* 2009;6:341-348.

66. Li D.J., Ohsa K., Li K., Ye Q., Nobuto Y., Tenshin S., Yamamoto T.T. Long-term observation of subcutaneous tissue reaction to synthetic auditory ossicle (Apaceram®) in rats. *J Laryngol Otol* 1997;111:702-706.
67. Saijo H., Chung I., Igawa K., Mori Y., Chikazu D., Ino M., Takato T. Clinical application of artificial bone in the maxillofacial region. *J Artif Organs* 2008;11:171-176.
68. Yamasaki N., Hirao M., Nanno K., Sugiyasu K., Tamai N., Hashimoto N., Yoshikawa H., Myoui A. A comparative assessment of synthetic ceramic bone substitutes with different composition and microstructure in rabbit femoral condyle model. *J Biomed Mater Res Part B: Appl Biomater* 2009;91:788-798.
69. Horch H.H., Sader R., Pautke C., Neff A., Deppe H., Kolk A. Synthetic, pure-phase beta-tricalcium phosphate ceramic granules (Cerasorb) for bone regeneration in the reconstructive surgery of the jaws. *Int J Oral Maxillofac Surg* 2006;35:708-713.
70. Orlovskii P.V., Komlev V.S., Barinov S.M. Hydroxyapatite and hydroxyapatite based ceramics. *Inorganic Mater* 2002;38:1159-1172.
71. Tanaja Y., Yamashita K. Fabrication processes for bioceramics. *Bioceramics and their clinical applications*, ed. T. Kokubo. pg. 30-40. Boca Raton: Woodhead Publishing in Materials, CRC Press, 2008.
72. Zhang S., Gonsalves K.E. Preparation and characterization of thermally stable nanohydroxyapatite. *J Mater Sci - Mater Med* 1997;8:25-28.
73. Bernard L., Freche M., Lacout J.L., Biscans B. Preparation of hydroxyapatite by neutralization at low temperature-influence of purity of raw material. *Adv Powder Technol* 1999;103:19-25.
74. Kweh S.W.K., Khor K.A., Cheang P. The production and characterization of hydroxyapatite (HA) powders. *J Mater Process Technol* 1999;89-90:373-377.

75. Sopyan I., Singh R., Hamdi M. Synthesis of nano sized hydroxyapatite powder using sol-gel technique and its conversion to dense and porous bodies. *Indian J Chem* 2008;47A:1626-1631.
76. Mahabole M.P., Aiyer R.C., Ramakrishna C.V., Sreedhar B., Khairnar R.S. Synthesis, characterization and gas sensing property of hydroxyapatite ceramic. *Bull Mater Sci* 2005;28:535-545.
77. Komlev V.S., Barinov S.M. Porous Hydroxyapatite Ceramics of Bimodal Pore Size Distribution. *J Mater Sci - Mater Med* 2002;13:295-299.
78. Hsu H.Y., Turner G.I., Miles W.A. Fabrication and mechanical testing of porous calcium phosphate bio-ceramic granules. *J Mater Sci - Mater Med* 2007;18:1931-1937.
79. Muralithran G., Ramesh S. The effects of sintering temperature on the properties of hydroxyapatite. *Ceram Int* 2000;26:221-230.
80. Bohner M., Barroud G., Gasser B. Critical aspects in the use of injectable calcium phosphates in spinal surgery. *Biomaterials* 2010;31:4609-4611.
81. Bailliez S., Nzihou A. The kinetics of surface area reduction during isothermal sintering of hydroxyapatite adsorbent. *Chem Eng J* 2004;98:141-152.
82. Kasten P., Luginbuhl R., van Griensven M., Barkhausen T., Krettek C., Bohner M., Bosch U. Comparison of human bone marrow stromal cells seeded on calcium-deficient hydroxyapatite, β -tricalcium phosphate and demineralized bone matrix. *Biomaterials* 2003;24:2593-2603.
83. Habraken W.J., Wolke J.G.C., Jansen J.A. Ceramic composites as matrices and scaffolds for drug delivery in tissue engineering. *Adv Drug Deliv Rev* 2007;59:234-248.
84. Nilsson M. Injectable calcium sulphate and calcium phosphate bone substitutes. PhD thesis: Lund University, 2003.
85. Zheltonoga L.A., Gabriwlov I.P. Characteristics of crack growth in sintered materials *Powder Metall Met C+* 1979;18:744-748.

86. Chevalier E., Chulia D., Pouget C., Viana M. Fabrication of porous substrates: A review of processes using pore forming agents in the biomaterial field. *J Pharm Sci* 2008;97:1135-1154.
87. Blokhuis T.J., Termaat M.F., den Boer F.C., Patka P., Bakker F.C., Haarman H.J. Properties of Calcium Phosphate Ceramics in Relation to Their In Vivo Behavior. *J Trauma* 2000;48:179-186.
88. Ooms E.M., Wolke J.G.C., van de Heuvel R., Jeschke B., Jansen J.A. Histological evaluation of the bone response to calcium phosphate cement implanted in cortical bone. *Biomaterials* 2003;24:989-1000.
89. Koerten H.K., van der Meulen J. Degradation of calcium phosphate ceramics. *J Biomed Mater Res Part A* 1999;44:78-86.
90. Ambard J.A., Museninghoff L. Calcium phosphate cement: Reviews of mechanical and biological properties. *J Prosthodont* 2006;15:321-328.
91. Afonso A., Santos J.D., Vasconcelos M., Branco R., Cavalheiro J. Granules of osteoapatite and glass-reinforced hydroxyapatite implanted in rabbit tibiae. *J Mater Sci - Mater Med* 1996;7:507-510.
92. Smith I.A., McCabe L.R., Baumann M.J. MC3T3-E1 osteoblast attachment and proliferation on porous hydroxyapatite scaffolds fabricated with nano-phase powder. *Int J Nanomedicine* 2006;1:189-94.
93. Yuan H., Yang Z., de Bruijn J.D., de Groot K., Zhang X. Material-dependent bone induction by calcium phosphate ceramics: A 2.5-year study in dog. *Biomaterials* 2001;22:2617-2623.
94. Le Nihouanna D., Daculsi G., Saffarzadeh A., Gauthier O., Delplace S., Pilet P., Layrolle P. Ectopic bone formation by microporous calcium phosphate ceramic particles in sheep muscles. *Bone* 2005;36:1086-1093
95. Wilson C.E., Kruyt M.C., de Bruijn J.D., van Blitterswijk C.A., Oner C.F., Verbout A.J., Dhert W.J.A. A new in vivo screening model for posterior spinal bone formation: Comparison of ten calcium phosphate ceramic material treatments. *Biomaterials* 2006;27:302-314.

96. Livingston T.L., Gordon S., Archambault M., Kadiyala S., McIntosh K., Smith A., Peter SJ. Mesenchymal stem cells combined with biphasic calcium phosphate ceramics promote bone regeneration *J Mater Sci - Mater Med* 2003;14:211-218.
97. Sakano H., Koshino T., Takeuchi R., Sakai N., Saito T. Treatment of the unstable distal radius fracture with external fixation and a hydroxyapatite spacer. *J Hand Surg* 2001;26:923-930.
98. Fortunato G., Marini E., Valdinucci F., Bonucci E. Long-term results of hydroxyapatite-fibrin sealant implantation in plastic and reconstructive craniofacial surgery. *J Cranio Maxill Surg* 1997;25:124-135.
99. Bonucci E., Marini E., Valdinucci F., Fortunato G. Osteogenic response to hydroxyapatite-fibrin implants in maxillofacial bone defects. *Eur J Oral Sci* 2007;105:557-561.
100. Frame J.W., Brady C.L. The versatility of hydroxyapatite blocks in maxillofacial surgery. *Brit J Oral Max Surg* 1987;25:452-464.
101. Quayle A.A., Marouf H., Holland I. Alveolar ridge augmentation using a new design of inflatable tissue expander: Surgical technique and preliminary results. *Brit J Oral Max Surg* 1990;28:375-382.
102. Sivakumar M., Kumar T.S., Shanta K.L., Rao K.P. Development of hydroxyapatite derived from Indian coral. *Biomaterials* 1996;17:1709-1714.
103. Zaffe D. Some considerations on biomaterials and bone. *Micron* 2005;36:583-592.
104. Damien E., Revell P.A. Coralline hydroxyapatite bone graft substitute: A review of experimental studies and biomedical applications. *J Appl Biomater Biom* 2004;2:65-73.
105. White E., Shors E. Biomaterial aspects of Interpore-200 porous hydroxyapatite. *Dent Clin N Am* 1986;30:49-67.
106. Sandor G.K.B., Kainulainen V.T., Queiroz J.O., Carmichael R.P., Oikarinen K.S. Preservation of ridge dimensions following grafting with coral granules of 48 post-traumatic and post-extraction dento-alveolar defects. *Dent Traumatol* 2003;19:221-227.

107. Dong J., Uemura T., Shirasaki Y.T. Promotion of bone formation using highly pure porous b-TCP combined with bone marrow-derived osteoprogenitor cells. *Biomaterials* 2002;23:4493-4502.
108. Kotani S., Fujita Y., Kitsugi T., Nakamura T., Yamamuro T., Ohtsuki C., Kukubo T. Bone bonding mechanism of beta-tricalcium phosphate. *J Biomed Mater Res* 1991;1:1303-1315.
109. Chena T.M., Shihb C., Linc F.T., Lin F.H. Reconstruction of calvarial bone defects using an osteoconductive material and post-implantation hyperbaric oxygen treatment. *Mater Sci Eng C* 2004;24:855-860.
110. Mailac N., Daculsi G. Bone ingrowth for sinus lift augmentation with micro macroporous biphasic calcium human cases evaluation using micro-CT and histomorphometry. *Key Eng Mater* 2008;361:1347-1350.
111. Piattelli A., Scarano A., Mangano C. Clinical and histologic aspects of biphasic calcium phosphate (bcp) ceramic used in connection with implant placement. *Biomaterials* 1996;17:1767-1770.
112. Daculsi G. Biphasic calcium phosphate concept applied to artificial bone, implant coating and injectable bone substitute. *Biomaterials* 1996;19:1473-1478.
113. Brown W.E., Chow L.C. Dental restorative cement paste. 1985; US Patent: 4,518,430.
114. Fernandez E., Gil F.J., Ginebra M.P., Driessens F.C.M., Planell J.A., Best S.M. Production and characterization of new calcium phosphate bone cements in the CaHPO₄-TCP system: pH, workability and setting times. *J Mater Sci - Mater Med* 1999;10:223-230.
115. Vanderschot P., Muylaert D., Schepers E. CaP-cement as a bone substitute in defect areas: An animal study. *Injury Extra* 2007;38:102-103.
116. Constantz B.R., Delaney D., Yetkinler D. Rapid setting calcium phosphate cements. 2007, US Patents: 7,252,841 B2.

117. Kairoun I., Boltong M.G., Driessens F.C.M., Planell J.A. Effect of calcium carbonate on the compliance of apatitic calcium phosphate bone cement. *Biomaterials* 1997;18:1535-1539.
118. Fernandez E., Boltong M.G., Ginebra M.P., Bermudez O., Driessens F.C.M., Planell J.A. Common ion effect on some calcium phosphate cements. *Clinic Mater* 1994;16:99-103.
119. Lanao F.R.P., Leeuwenburgh S.C.G., Wolke J.G., Jansen J.A. Bone response to fast degrading injectable calcium phosphate cements containing PLGA microparticles. *Biomaterials* 2011;32:8839-8847.
120. Espanol M., Perez R.A., Montufar E.B., Marichal C., Sacco A., Ginebra M.P. Intrinsic porosity of calcium phosphate cements and its significance for drug delivery and tissue engineering applications. *Acta Biomater* 2009;5:2752-2762.
121. Takechi M., Miyamoto Y., Ishikawa K., Yuasa M., Nagayama M., Kon M., Asaoka K. Non-decay type fast-setting calcium phosphate cement using chitosan. *J Mater Sci - Mater Med* 1996;7:317-322.
122. Cherng A., Takagi S., Chow L.C. Effects of hydroxypropyl methylcellulose and other gelling agents on the handling properties of calcium phosphate cement. *J Biomed Mater Res Part A* 1997;35:273-277.
123. Ishikawa K., Miyamoto M., Takechi M., Toh T., Kon M., Nagayama M., Asaoka K. Non-decay type fast-setting calcium phosphate cement: Hydroxyapatite putty containing an increased amount of sodium alginate. *J Biomed Mater Res Part A* 1997;36:393-399.
124. LeGeros R.Z. Calcium phosphate-based osteoinductive materials. *Chem Rev* 2008;108:4742-4753.
125. Komath M., Varma H.K. Development of fully injectable calcium phosphate cement for orthopedic and dental applications. *Bull Mater Sci* 2003;26:415-422.
126. Nissan B.B., Choi A.H., Cordingley R. Alumina ceramics. *Bioceramics and their clinical applications*, ed.T. Kokubo, pg. 223-242. Boca Raton: Woodhead Publishing, CRC Press, 2008.

127. Barralet J.E., Gaunt T., Wright A.J., Gibson I.R., Knowles J.C. Effect of porosity reduction by compaction on compressive strength and microstructure of calcium phosphate cement. *J Biomed Mater Res Part A* 2002;63:1-9.
128. Gbureck U., Spatz K., Thull R. Improvement of mechanical properties of self setting calcium phosphate bone cements mixed with different metal oxides. *Materialwissenschaft und Werkstofftechnik* 2003;34:1036-1040.
129. Ohura K., Bohner M., Hardouin P., Lemaitre J., Pasquier G., Flautre B. Resorption of, and bone formation from, new beta-tricalcium phosphate-monocalcium phosphate cements: an in vivo study. *J Biomed Mater Res Part A* 1996;30:193-200.
130. Lew D., Farrell B., Bardach J., Keller J. Repair of craniofacial defects with hydroxyapatite cement. *J Oral Maxillofac Surg* 1997;55:1441-1449.
131. Ooms E.M., Wolke J.G.C., van der Waerden J.P.C.M., Jansen J.A. Trabecular bone response to injectable calcium phosphate (Ca-P) cement. *J Biomed Mater Res Part A* 2002;61:9-18.
132. Fujikawa K., Sugawara A., Murai S., Nishiyama M., Takagi S., Chow C.L. Histopathological reaction of calcium phosphate cement in periodontal bone defect. *Dent Mater J* 1995;14:45-57.
133. Sugawara A., Fujikawa K., Takagi S., Chow L.C. Histological analysis of calcium phosphate bone grafts for surgically created periodontal bone defects in dogs. *Dent Mater J* 2008;27:787-794.
134. Sugawara A., Kusama K., Nishimura S., Nishiyama M., Moro I., Kudo I., Takagi S., Chow C.L. Histopathological reactions to calcium phosphate cement for bone filling. *Dent Mater J* 1993;12:691-698.
135. Theiss F., Apelt D., Brand B., Kutter A., Zlinszky K., Bohner M., Matter S., Frei C., Auer J.A, von Rechenberg B. Biocompatibility and resorption of a brushite calcium phosphate cement. *Biomaterials* 2005;26:4383-4394.
136. Camiré C.L., Saint-Jean S.J., Mochales C., Nevsten P., Wang J.S., Lidgren L., McCarthy I., Ginebra M.P. Material characterization

- and in vivo behavior of silicon substituted alpha-tricalcium phosphate cement. *J Mater Sci - Mater Med* 2006;76B:424-431.
137. Timperley A.J., Nusem I., Wilson K., Whitehouse S.L., Buma P., Crawford R.W. A modified cementing technique using BoneSource to augment fixation of the acetabulum in a sheep model. *Acta Orthop* 2010;81:503-507.
 138. De la Riva B., Sánchez E., Hernández A., Reyes R., Tamimi F., López-Cabarcos E., Delgado A., Évora C. Local controlled release of VEGF and PDGF from a combined brushite-chitosan system enhances bone regeneration. *J Control Release* 2010;143:45-52.
 139. Ilan D.I., Ladd A.L. Bone Graft Substitutes. *Oper Techn Plast Rec Surg* 2003;9:151-160.
 140. Constantz B.R., Ison I.C., Fulmer M.T., Smith S.T., van Wagoner M., Ross J., Goldstein S.A., Jupiter J.B., Rosenthal D.I. Skeletal repair by in situ formation of the mineral phase of bone. *Science* 1995;267:1796-1799.
 141. Manzotti A., Confalonieri N., Pullen C. Grafting of tibial bone defects in knee replacement using norian skeletal repair system. *Arch Orthop Trauma Surg* 2006;126:594-598.
 142. Frankenburg E.P., Goldstein S.A., Bauer T.W., Harris S.A., Poser R.D. Biomechanical and histological evaluation of a calcium phosphate cement. *J Bone Joint Surg* 1998;80:1112-1124.
 143. Friedman C.D., Costantino P.D., Takagi S., Chow L.C. BoneSourceTM hydroxyapatite cement: A novel biomaterial for craniofacial skeletal tissue engineering and reconstruction. *J Biomed Mater Res B: Appl Biomater* 1998;43:428-432.
 144. Kneton J.F., Friedman C.D., Costantino P.D. Indications for hydroxyapatite cement reconstruction in lateral skull base surgery. *Am J Otolaryngol* 1995;16:465-469.
 145. Kveton J.F., Friedman C.D., Piepmeier J.M., Costantino P.D. Reconstruction of suboccipital craniectomy defects with hydroxyapatite cement: A preliminary report. *Laryngoscope* 1995;105:156-159.

146. Dickson K.F., Friedman J., Buchholz J.G., Flandry F.D. The use of bone source hydroxyapatite cement for traumatic metaphyseal bone void filling. *J Trauma* 2002;53:1103-1108.



Chapter 3

**EFFECT OF CALCIUM CARBONATE ON HARDENING,
PYSICOCHEMICAL PROPERTIES AND IN
VITRO DEGRADATION OF INJECTABLE
CALCIUM PHOSPHATE CEMENTS**

Kemal Sariibrahimoğlu, Sander C.G. Leeuwenburgh, Joop G.C. Wolke,
Li Yubao, John A. Jansen

1. Introduction

Health problems related to bone defects as caused by diseases or trauma have led to an increased interest in synthetic graft materials. Man-made calcium phosphate (CaP) ceramics have been widely used as bone substitutes because of their non-toxicity, excellent biocompatibility and osteoconductivity^{1, 2}. In contrast to CaP blocks or granules, which are difficult to handle from a clinical point of view, injectable self-setting CPC was shown to be more effective for optimal defect filling, thereby reducing postoperative complications for patients³.

One of the most effective self-hardening CPCs, consisting of alpha-tricalcium phosphate [$\text{Ca}_3(\text{PO}_4)_2$, α -TCP] and monetite [CaHPO_4 , DCPA] as main precursor phases, was first described by Driessens et al.⁴. The cement is based on two sparingly soluble acidic-basic CaP mixtures that dissolve and reprecipitate in an aqueous environment in hydroxyapatite crystals. Under physiological conditions, the end-product of the precipitation reaction is a calcium-deficient hydroxyapatite phase ($\text{Ca}_9(\text{HPO}_4)(\text{PO}_4)_5(\text{OH})$, CDHA), which is chemically similar to the mineral phase in bone⁵. In addition to the hydrolysis reaction of α -TCP, calcite and monetite are known to react towards apatite, thereby providing an additional source for precipitation of nanosized apatite crystals⁶. However, the slow degradation rate with limited bone ingrowth at osseous sites is the major disadvantage of the cement^{7, 8}. Recently, our group showed that α -TCP based cement (85% α -TCP, 10% CaHPO_4 , 5% pHA) containing polymeric microspheres were hardly degradable upon implantation in cranial defects in rats and femoral condylar defects in rabbits even after 12 weeks of implantation^{8, 9}.

Contrary to synthetic hydroxyapatite, biological apatites are carbonated apatites (dahllite, CHA), which differ from hydroxyapatite in terms of crystallinity and resorbability¹⁰⁻¹². The amount of carbonate varies from 3-6 wt% in enamel^{13, 14} to 3-10 wt% in bone tissue^{15, 16}. LeGeros et al.¹⁷ first showed the correlation between carbonate substitution and the sensitivity of apatites to acidic etching. When CO_3^{2-} was part of the apatite lattice, PO_4^{3-}

and/or OH⁻ ions were markedly disturbed from their lattice positions, the solubility of the apatites was increased¹⁸⁻²⁰.

Khairoun et al.^{21, 22} investigated the influence of calcite on cement setting characteristics. These studies, however, did not vary the amount of calcite but studied only two single amount of calcite, while the effect of calcite particle size was not investigated either. Since the dissolution kinetics of CaCO₃ in neutral or weak acids is critical, the dissolution rate can be manipulated by the particle size of the CaCO₃. Although, it is known that prolonged milling of the particles leads to increased specific surface area and reactivity of the solid particles²³, the impact of particle size of CaCO₃ on the setting characteristics of apatite cement has not been studied systematically before.

CO₃²⁻ can be introduced into CPC from CaCO₃ as a precursor phase. So far, only two commercially carbonate apatite cements, Calcibon[®] and Norian SRS[®], using CaCO₃ as a source of CO₃²⁻, have been developed as a bone substitute for use in dentistry and orthopedics^{24, 25}. These cements were shown to be safe and effective for bone regeneration^{2, 25}. Still, the effect of CaCO₃ particle characteristics (CaCO₃ amount and CaCO₃ particle size) on the injectability, setting and degradation of apatitic CPC has not been systematically studied. Therefore, the aim of this investigation was to study the effect of CaCO₃ content (0–4–8–12 wt%) and its particle size (coarse and fine) on the setting characteristics, physicochemical properties and accelerated in vitro degradation behavior of apatitic CPCs.

2. Materials and methods

2.1. Calcium phosphate precursor phases and milling

The cement powder mixture consisted of commercially available α -tricalcium phosphate (α -TCP; CAM Implants BV, Leiden, the Netherlands), dicalcium phosphate anhydrous (DCPA, analytical grade; J.T. Baker Chemical Co., Phillipsburg, USA), precipitated hydroxyapatite (pHA; Biomet Merck, Darmstadt, Germany) and calcite (CaCO₃; Sigma-Aldrich Chemical Co., St. Louis, MO). Dry grinding experiments were performed using a laboratory ball mill at 500 rpm in order to control the

particle size of the reactants. The particle size distribution of the various CaP precursor phases (α -TCP: $9.7 \pm 2.0 \mu\text{m}$, pHA: $4.5 \pm 1.9 \mu\text{m}$, DCPA: $5.0 \pm 1.9 \mu\text{m}$) was determined by using Mastersizer-2000 ultrasonic particle size equipment (Malvern Inst. Ltd., U.K). Two calcite powders with different particle sizes were studied. Calcite particles with mean diameters of $12 \pm 3.0 \mu\text{m}$ (coarse) and $2.5 \pm 1.0 \mu\text{m}$ (fine) were obtained by a milling time of 30 min and 240 min, respectively, as measured using Mastersizer-2000.

2.2. Preparation of cements

Synthesis parameters of the various experimental groups are summarized in Table 1. The reference composition used in this study contained 85 wt% α -TCP since this cement was shown to be safe and osteoconductive in several in vivo studies from our group^{8,9}. In order to accommodate for the addition of 4–8–12 wt% CaCO_3 , the amount of α -TCP was reduced to 75 wt%.

Table 1. Weight proportions of the CPC reactants.

	Cement Type	α -TCP	CaCO_3	DCPA	HA
Weight proportions (wt.%)	12% CaCO_3	75	12	10	3
	8% CaCO_3	75	8	14	3
	4% CaCO_3	75	4	18	3
	0% CaCO_3	85	0	10	5

Cement pastes were obtained by the homogeneous mixing of precursor powders with a 2% Na_2HPO_4 (Merck, Germany) solution at a liquid-to-powder ratio (L/P) of 0.35 ml/g. Briefly, 1 g of powder was placed in an exit-closed 2 ml syringe (orifice diameter 1.7 mm). Then, 0.35 ml of the 2% Na_2HPO_4 (0.2 M) solution was added to the powder and the piston was placed back into the syringe. The syringe was placed in a mixing apparatus (Silamat® Vivadent, Liechtenstein) and mixed for 20 seconds²⁶. After mixing, a paste was obtained and injected into Teflon® molds of 4.5 mm in diameter by 9 mm in height to obtain cylindrical samples. The samples in

the mold were left to set at 37 °C. Cylinders of cement were removed from the mold and immersed in Ringer`s solution at 37 °C to allow hardening.

2.3. Setting characteristics

Injectability time of the samples was measured by using a tensile bench (858 MiniBionix2[®], MTS Corp., USA). After mixing of the cement/liquid for 20 seconds, the syringe, with an orifice diameter of 1.7 mm, was fitted vertically in a fixture and put under the plates of a tensile bench set in compression mode. Compression force was applied to the syringe at a constant velocity of 20 mm.min⁻¹ up to a final force of 100 N²⁷⁻²⁹. Two parameters were measured: (1) the applied force was recorded as a function of the plunger travel time, (2) the injectability time (defined as the period of time necessary to a force of 100 N). All tests were performed in triplicate (n = 3).

The initial and final setting times of the various cement pastes were assessed using Gillmore needles according to ASTM C266³⁰. A bronze block, containing 6 holes (6 mm in diameter, 12 mm in height), was used as a mold. The mold was placed in a water bath at body temperature (37 °C). Samples of each formulation were mixed and injected into the mold. The Gillmore needles were carefully lowered onto the surface of the freshly shaped cement paste and kept there for 3 seconds. The setting time was recorded when penetration was not observed anymore (n = 3).

2.4. pH measurements and calcium release during cement setting

Variations in solution chemistry during the setting reaction were recorded in Milli-Q^{31, 32}. 1 g of CPC paste was injected into 30 ml of deionized water and incubated at 37 °C in a water bath on a shaker table (60 rpm) for 9 weeks. Sample medium was collected and refreshed every week. For each time point, solution pH and calcium content were measured using a pH electrode (Orion, Sigma-Aldrich[®]) and the ortho-cresolphthalein complexone (OCPC, Sigma-Aldrich[®]) assay, respectively.

2.5. Physicochemical and mechanical characterization of cements

Phase identifications of set cements in powder were performed by using XRD (Philips, Cu-K α , 45 kV, 30 mA). Data were collected in the 2θ range of 25° - 38° with a step size of 0.05° and a counting time of 20 seconds at each step. X-ray diffraction patterns of the (002) reflections were used to evaluate the crystallite sizes and lattice constants of the hexagonal apatite phase. The crystallite size was determined from the broadening of the diffraction peaks using the Scherrer equation³³. Apatite unit-cell dimensions of the c-axis were calculated from the (002) reflection using the formula as described elsewhere³³.

Fourier transform infrared spectroscopy (FTIR, Perkin-Elmer, Fremont, CA, USA) was used to characterize the molecular structure of the set cements.

The morphology of the set cements was evaluated by scanning electron microscopy (SEM, JEOL 6301, JAPAN). Prior to SEM examination, all samples were mounted on aluminum stubs using carbon tape and sputter coated with gold-palladium.

The compressive strength of the samples were measured by using a mechanical testing bench (858 MiniBionixII®, MTS, USA) at a cross-head speed of $1 \text{ mm}\cdot\text{min}^{-1}$. Samples were tested after 3 weeks of immersion in Ringer's solution at 37°C . The solution was renewed every week ($n = 3$).

2.6. Accelerated *in vitro* degradation test

In vitro degradation kinetics of CPCs was evaluated under accelerated conditions in acidic solutions over the course of 8 hours³⁴. Prior to testing, injected samples were cured in phosphate buffer saline (PBS) for 48 hours at 37°C . After curing, samples were removed from the bath, dried in air and weighed. Each disc was immersed in sealable glass bottles containing 13 mL of 0.14 M NaCl and 0.01 M HCl (pH 2) at 37°C . Every hour, the samples were carefully transferred to new vials with fresh medium. The cumulative amount of calcium in solution was calculated using the ortho-cresolphthalein complexone (OCPC, Sigma-Aldrich®) assay as the amount

of calcium dissolved from samples in eight hours. Total weight loss of the samples were detected after drying in air for two days (n= 3).

2.7 Statistics

All measurements were statistically evaluated using GraphPad Instat[®] software (GraphPad Software Inc., San Diego, CA, USA) using one-way analysis of variance (ANOVA) with Tukey multiple comparison post test. Data were presented as mean \pm standard deviation.

3. Results

3.1. Setting characteristics

The shortest injectability time was observed for the calcite free combination (Figure 1A, Figure 1B). The injectability time of the cement pastes increased with increasing CaCO₃ content. Additionally, the injectability time of the CPC paste increased when using fine calcite particles instead of coarse particles. Inclusion of 12% CaCO₃ increased the injectability time required to reach 100 N from 69 ± 1 s (0% CaCO₃) to 78 ± 1 s and 85 ± 1 s for coarse and fine CaCO₃ powder, respectively.

Similar effects were observed for the initial and final setting times as measured using Gillmore needles (Figure 2). Setting times increased with increasing CaCO₃ content and decreasing CaCO₃ particle size.

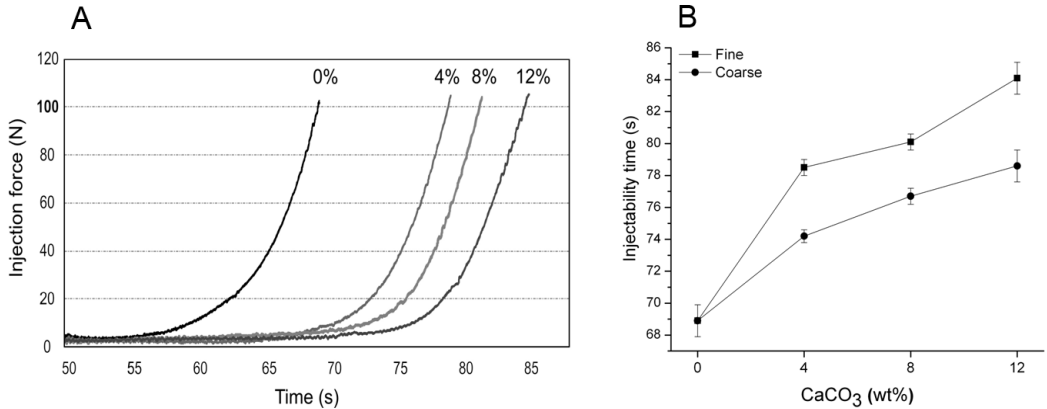


Figure 1. Injectability properties of the cements. [A] Injection force vs. time after the start of CPC paste mixing (fine CaCO₃), and [B] injectability time as a function of CaCO₃ content and particle size (fine vs. coarse).

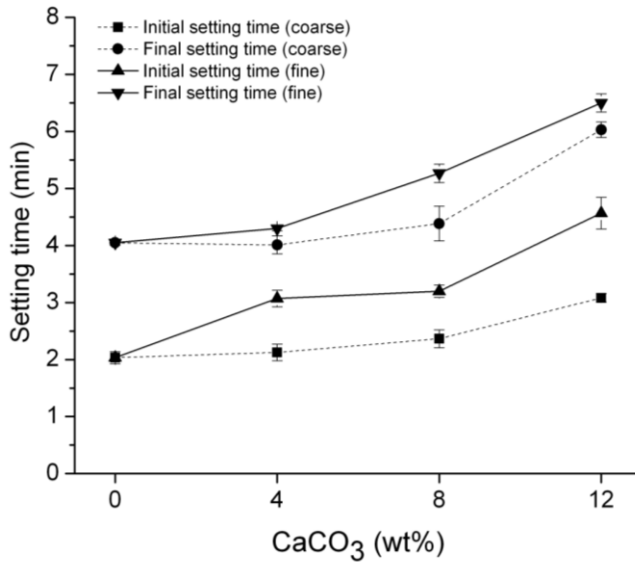


Figure 2. Setting times of the cements as a function of CaCO₃ content.

3.2. Variations of pH and calcium release during setting

The cumulative calcium release during setting of the cements for total 9 weeks is depicted in Figure 3. It was observed that all types of cement

released considerable amounts of calcium. The highest amount of calcium release was observed in calcite-free and 4% coarse CaCO_3 -containing cement paste. Total calcium release decreased with increasing CaCO_3 content. For all calcite-containing cement types, the use of fine CaCO_3 particle size exhibited less cumulative release of calcium.

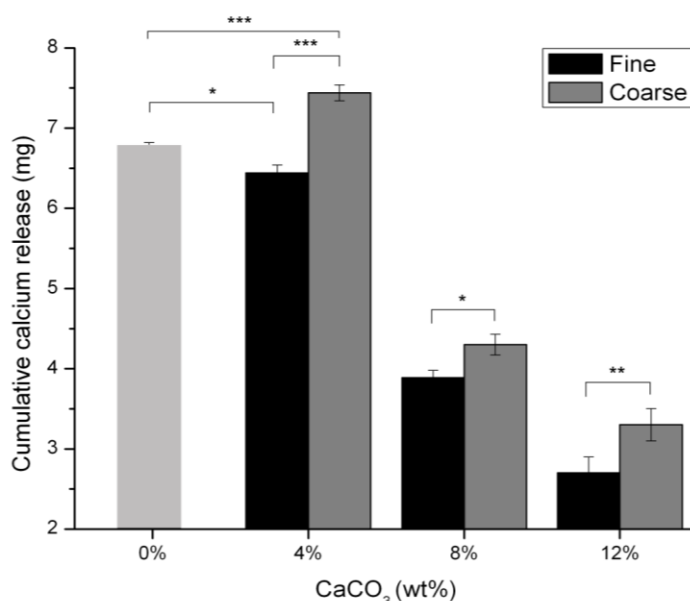


Figure 3. Cumulative calcium release after 9 weeks of reaction in deionized water for coarse and fine particles.

The corresponding solution pH variations of the CPCs from setting to a period of 9 weeks are shown in Figure 4. In the first week, a fast pH decrease from 9.5-9 to 6.2-7.5 was recorded for all cements. Thereafter, the pH value was maintained around pH 7.5 for cements containing 12% CaCO_3 , whereas a slower pH decrease from 6.2-7.2 to 5.7-6.2 was observed for 0-8% CaCO_3 -containing cements.

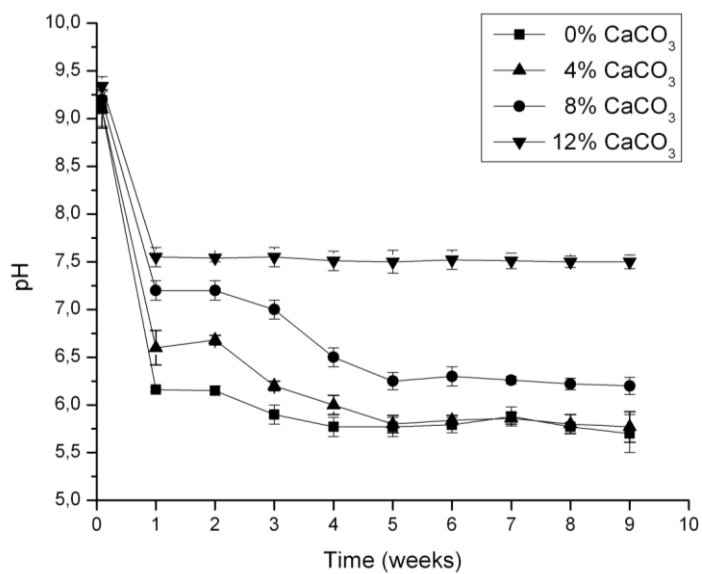


Figure 4. Variations in pH of the medium as a function of time.

3.3. Physicochemical and mechanical analyses

The IR spectra of all samples are shown in Figure 5A and Figure 5B. The main characteristic band of PO_4^{3-} stretching/absorption vibrations which are typical for the HA structure was around 1021 cm^{-1} and 559 cm^{-1} , and a HPO_4^{3-} vibration band (ν_5) was located at around 860 cm^{-1} ³⁵.

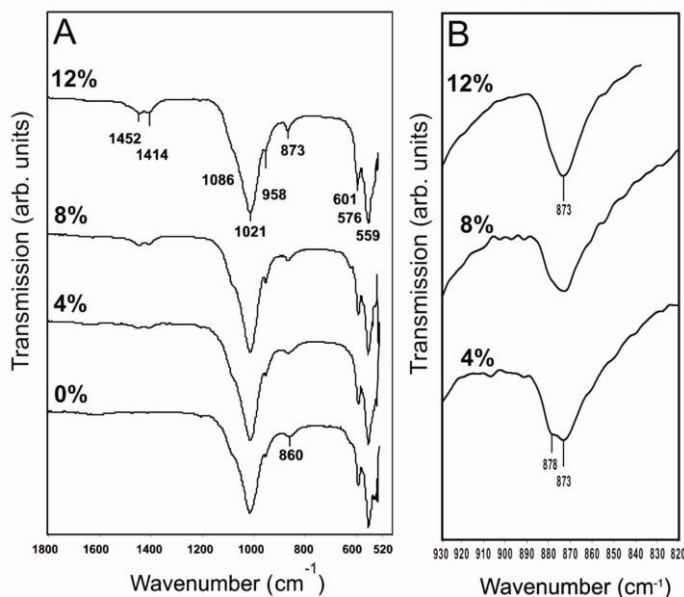


Figure 5. The FTIR spectrum of the calcite-free and fine particle size CaCO₃-incorporated cements after immersion in Ringers solution for 3 weeks. Wavenumber interval between [A] 1800-520 cm⁻¹, [B] 930-820 cm⁻¹.

Calcite-containing samples showed the main adsorption band characteristic of CO₃²⁻ present in the apatite structure, indicating the formation of carbonated apatite. Three absorption bands could be observed at 1452, 1414 and 873 cm⁻¹, corresponding to B-type carbonate-for-phosphate substitution (Figure 5A)³⁶. A-type carbonate-for-hydroxyl absorptions at 878 cm⁻¹ decreased in intensity with increasing carbonate content, whereas B-type carbonate-for-phosphate absorptions at 1414 and 1452 cm⁻¹ increased in intensity with increasing carbonate amount, suggesting that most of the carbonate ions substituted for phosphate groups (Figure 5B)^{37, 38}. No obvious differences were observed between fine and coarse calcite-containing cement groups.

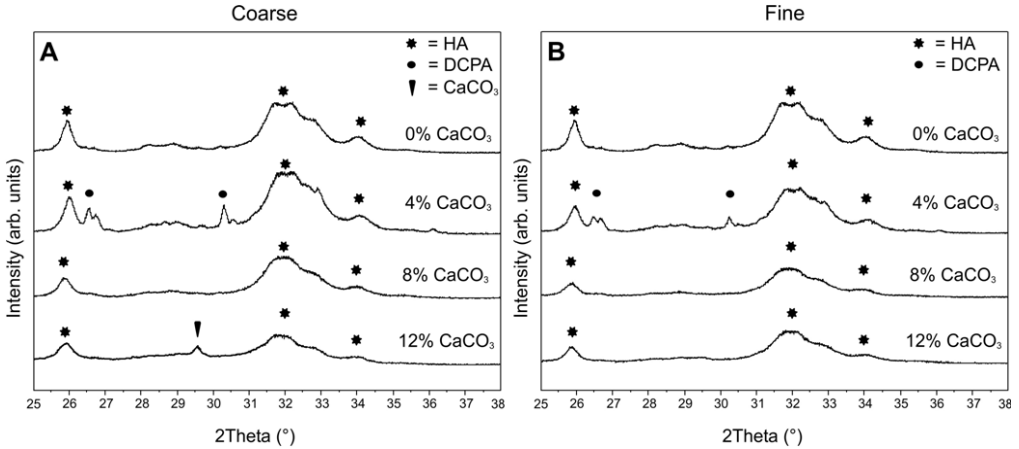


Figure 6. X-ray diffraction patterns of the CPCs after immersion in Ringers solution for 3 weeks. [A] Coarse particle size, [B] fine particle size CaCO₃-incorporated cements.

Figure 6A shows the XRD patterns of the structures after hardening at 37 °C for 3 weeks in Ringer`s solution. For all types of cements, initial α -TCP peaks were not detectable after incubation. The typical HA characteristic peaks at $2\theta = 31.7^\circ$ (112) and 25.9° (002) were identified. As the highest amount of DCPA was used in cement formulations containing 4 % CaCO₃, reflections corresponding to DCPA remnants were observed at $2\theta = 26.5^\circ$ and $2\theta = 30.3^\circ$ while these peaks were absent for cement formulations containing less DCPA as precursor phase. Unreacted CaCO₃ was detected at $2\theta = 29.4^\circ$ only for incorporation of 12% CaCO₃. However, CaCO₃ peaks were not detected as a separate phase when fine CaCO₃ particles were used even at high CaCO₃ content of 12% (Figure 6B). Table 2 indicates a systematic decrease of the crystal size and mechanical strength of the hardened cements with increasing CaCO₃ content. Compared to coarse CaCO₃ particle size, XRD peaks became a little broader for cements made of fine CaCO₃. Additionally, the c-axis dimensions of the apatite phase increased with increasing CaCO₃ content (Table 2).

Table 2. 2theta position, unit-cell dimensions, crystallite size and compressive strength of the hardened cements.

Abbreviation	2theta (°)	Unit-cell dimensions (c-axis, Å)	Crystal Size (nm)	Compressive strength (MPa)
0% CaCO ₃	25.93	6.88	41±1	24±3
4% CaCO ₃ (C)	25.92	6.89	36±2	20±1
4% CaCO ₃ (F)	25.89	6.89	32±1	18±2
8% CaCO ₃ (C)	25.89	6.89	28±1	19±2
8% CaCO ₃ (F)	25.84	6.90	25±1	16±2
12% CaCO ₃ (C)	25.84	6.90	26±1	17±2
12% CaCO ₃ (F)	25.87	6.90	26±1	15±2

Scanning electron micrographs of the prepared cements are shown in Figure 7. The images clearly show that the calcite-free samples are composed of large needle-like crystals. With increasing CaCO₃ content, the morphology of the samples changes from needle-like to plate-like.

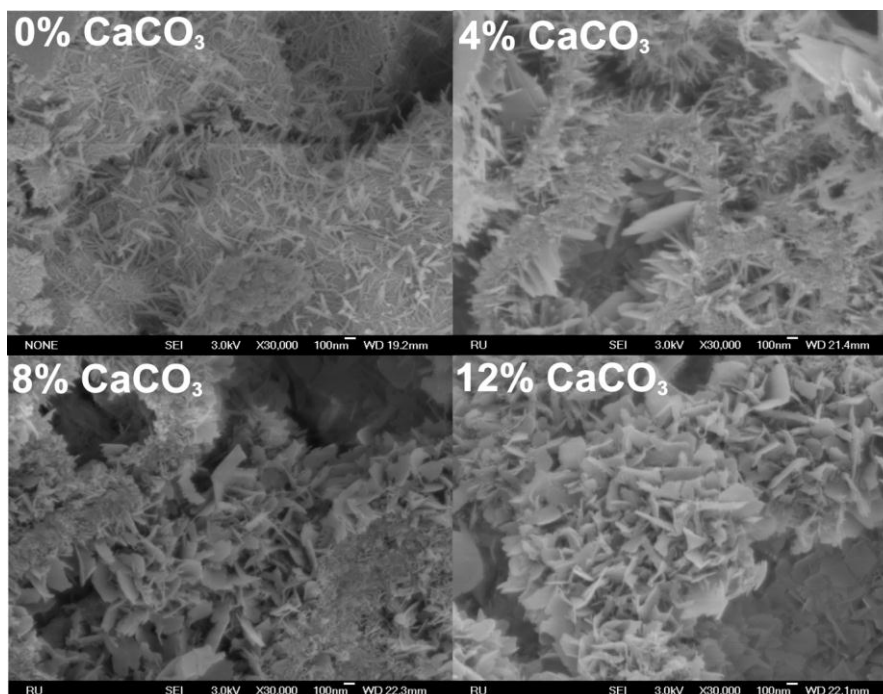


Figure 7. Scanning electron micrographs of calcite-free and fine particle size CaCO₃-incorporated cements. Micrographs show representative structures at a magnification of 30K.

3.4. Degradability and calcium release experiments

Figure 8A and Figure 8B show the weight loss and calcium release of the cements after soaking in HCl/NaCl solution for 8 hours. It is apparent that the degradation rate of the cements and the calcium release from the cements increased with increasing CaCO_3 content, whereas no effect of CaCO_3 particle size on degradation was detected ($p > 0.05$).

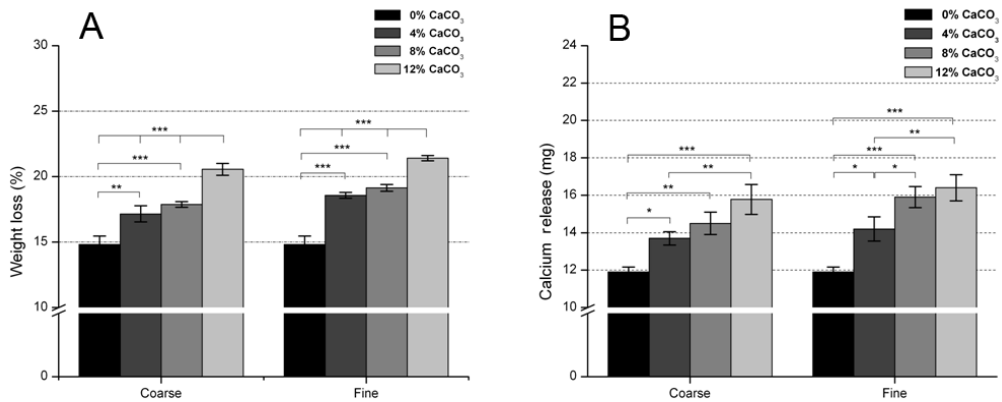


Figure 8. Accelerated in vitro degradation tests of the CPCs after soaking in HCl/NaCl solution (pH 2) at 37°C. [A] Weight loss, and [B] calcium release as a function of CaCO_3 particle size.

4. Discussion

The aim of this study was to evaluate the effect of CaCO_3 content (0-4-8-12 wt%) and CaCO_3 particle size ($12 \pm 3.0 \mu\text{m}$ (coarse), $2.5 \pm 1.0 \mu\text{m}$ (fine)) on setting characteristics, physicochemical properties and degradation of CPCs under accelerated in vitro conditions.

The characterization of the injectability time of CPCs is of interest in view of the control over the handling of the CPC paste^{39, 40}. The pattern observed from Figure 1A, B showed that the addition of CaCO_3 to the cement resulted in an increased injectability time. This is caused by the fact that CaCO_3 particles decrease the viscosity and increase the fluidity of the paste.

Similarly, Combes et al.⁴⁰ also observed a shear-thinning effect of CaCO₃ paste using rheometry for a CaCO₃ self-setting cement.

Differences in injectability time were also observed between the coarse and fine CaCO₃-containing cement pastes. CPCs made of CaCO₃ with a fine particle size were characterized by an increased flowability of the paste resulting from reduced filter-pressing⁴¹⁻⁴³.

In case of calcite-free cement, fast hydrolysis of the reactants into poorly crystalline hydroxyapatite occurred. During HA formation, the dissolution/precipitation of the soluble α -TCP and DCPA compounds are responsible for the supersaturation of the solution with Ca²⁺ and PO₄³⁻ and a pH drop of the medium^{44, 45}. The cumulative calcium release results show that Ca²⁺ release decreases with increasing calcite content and decreasing particle size. Increasing the calcite content was accompanied by decreasing the monetite content, which explains the higher cumulative calcium release for formulations of lower calcite content since monetite is the most soluble precursor phase in the cement powder mixture. Regarding the particle size, it can be concluded that smaller calcite particles were able to consume calcium released from monetite at a faster rate than coarse particles of lower specific surface area. Moreover, acid production was buffered by basic carbonate groups from the calcite particles leading to a less pronounced decrease in pH. Since low pH of the setting reaction was the reason for dissolution-precipitation, buffered CO₃²⁻ ions in medium reduced Ca²⁺ concentration by decreasing the solubility of the basic α -TCP. These results are in line with recent observations of Brown et al.⁴⁶ and Durucan et al.⁴⁷, who studied the hydrolysis reaction of CO₃-containing α -TCP and TTCP blends by using calorimetry in water at 37 °C. The lower heat outputs of the curves and X-ray analyses confirmed that carbonate ions considerably delayed early dissolution of CaP precursors and suppressed precipitation of HA.

LeGeros et al.⁴⁸ showed that CO₃²⁻ can coprecipitate into the apatite lattice and disturb the apatite forming process. Consequently, in the current study, CO₃²⁻ absorption into the apatite lattice inhibited HA precipitation. The physicochemical analyses of the calcite-containing cements suggested that

some PO_4^{3-} ions in the apatite crystal structure were displaced by CO_3^{2-} and OH^- ions, resulting into a poorly crystalline A-B-type carbonated apatite structure. LeGeros et al.⁴⁹ and Fernandez et al.⁵⁰ reported that CO_3^{2-} located at active crystal sites of the sintered CaP ceramics resulted in reduced growth rate of the crystals. Thus, the uptake of the CO_3^{2-} ions into apatite PO_4^{3-} sites in CPCs substantially reduced the crystallite size. In fact, because of the differences in occupation sites between CO_3^{2-} and PO_4^{3-} ions, the replacement is followed by changes in morphology and unit-cell dimensions. Additionally, with increasing carbonate content, the mechanical strength of the cement formulations decreased, which was attributed to the higher (nano)porosity of the carbonated cements (Figure 7). However, CaCO_3 could be incorporated up to 8% for coarse and 12% for fine CaCO_3 particle size, suggesting that the maximum amount of CaCO_3 uptake in apatitic CPCs varies from 8% to 12% depending on the particle size of CaCO_3 .

Biodegradable CPCs that are gradually replaced by hard tissue are preferred in bone reconstruction surgery because they improve the post-operative implant success rate by eliminating heterogeneous stress distribution, fatigue failure, and long-term wear while allowing for complete bone regeneration^{51, 52}. Both the correlation between the dissolution in acellular in vitro conditions and cell-mediated biodegradation in vivo are related to dissolution of CaP under acidic conditions. Thus, the factors affecting dissolution properties of CaP ceramics in vitro under acidic conditions were similar to those affecting bioresorption/biodegradation of the ceramics in a biological environment^{53, 54}. The comparative dissolution properties in acidic medium demonstrated that CaCO_3 -free apatite exhibited the lowest dissolution rate. Incorporation of CaCO_3 into CPC was associated with about 30-40% more in vitro degradation. It can be suggested that the CO_3^{2-} absorption into the apatite lattice led to a higher solubility rate and thus to a considerably increased amount of weight loss and Ca^{2+} release for the CaCO_3 -containing CPCs. To date, most of the studies on carbonate apatite focused on the dissolution characteristics of wet-chemically precipitated and sintered carbonated apatite ceramics for in vitro and in vivo

applications^{17-20, 54-56}. Comparison of the current results with those of previous studies indicates that similar dissolution trends occur for CaCO₃-containing CPCs and sintered carbonated apatites. Although prolonged milling of the calcite particles can induce phase transformations (from crystalline to amorphous) that affect the solubility of the final apatite phase⁵⁷, prolonged milling of CaCO₃ particles did not alter the degradability of calcite-containing cement composition.

5. Conclusion

The influence of the amount and particle size of calcite on the setting behavior, physicochemical characteristics and degradability of injectable apatitic calcium phosphate cements has been studied systematically. The results demonstrated that the injectability and setting time of these cements could be varied by changing the particle size of the calcite phase. Upon introduction of calcite into the cement, carbonate anions were introduced into the apatite lattice that reduced the growth rate of hydroxyapatite crystals, resulting into decrease crystallite sizes and a change in shape from needles (without calcite) to smaller plate (for calcite-containing cements). Compressive strength decreased with increasing CaCO₃ content in the mixture. The maximum amount of calcite that could be incorporated into the apatite matrix was about 8-12% depending on the particle size of calcite. Degradation tests under accelerated in vitro conditions revealed that dissolution rates of the cements increased with increasing calcite amount.

References

1. Ginebra M.P., Traykova T., Planell J.A. Calcium phosphate cements as bone drug delivery systems: a review. *J Control Release* 2006;113:102-110.
2. Ooms E.M., Wolke J.G.C., van der Waerden J.P.C.M., Jansen J.A. Trabecular bone response to injectable calcium phosphate cement. *J Biomed Mater Res A* 2002;61:9-18.
3. Constantino P.D., Chaplin J.M., Wolpoe M.E., Catalano P.J., Sen C., Bederson J.B., Govindaraj S. Applications of fast-setting

- hydroxyapatite cement: cranioplasty. *Otolaryngol Head Neck Surg* 2000;123:409-412.
4. Driessens F.C.M., Boltong M.G., Bermudez O., Planell J.A. Formulation and setting times of some calcium orthophosphate cements: a pilot study. *J Mater Sci Mater Med* 1993;4:503-508.
 5. Ginebra M.P, Fernandez E., Driessens F.C.M., Planell J.A. Modeling of the hydrolysis of α -tricalcium phosphate. *J Am Ceram Soc* 1999;82:2808-2812.
 6. LeGeros R.Z. Crystallographic studies on the carbonate substitution in the apatite structure. PhD Thesis. University of London, London, 1967.
 7. Magee W.P., Ajkay N., Freda N., Rosenblum R.S. Use of fast-setting hydroxyapatite cement for secondary craniofacial contouring. *J Plast Reconstruct Surg* 2004;114:289-297.
 8. Liao H., Walboomers X.F., Habraken W.J., Zhang Z., Li Y., Grijpma D.W., Mikos A.G., Wolke J.G., Jansen J.A. Injectable calcium phosphate cement with PLGA, gelatin and PTMC microspheres in a rabbit femoral defect. *Acta Biomater* 2011;7:1753-1759.
 9. van de Watering F.C.J., van den Beucken J.J., Walboomers X.F., Jansen J.A. Calcium phosphate/poly(d,l-lactic-co-glycolic acid) composite bone substitute materials: evaluation of temporal degradation and bone ingrowth in a rat critical-sized cranial defect. *Clin Oral Implants Res* 2012;23:151-159.
 10. Kirschner R.E., Karmacharya J., Ong G., Gordon D.A., Hunenko O., Losee J.E., Gannon F.H., Bartlett S.P. Repair of the immature craniofacial skeleton with a calcium phosphate cement: quantitative assessment of craniofacial growth. *An Plast Surg* 2002;49:33-38.
 11. Biltz R.M., Pellegrino E.D. The composition of recrystallized bone mineral. *J Dent Res* 1983;62:1190-1195.
 12. Bushinsky A.D., Smith S.B., Gavrilov L., Gavrilov L.F., Li J., Setti L.R. Acute acidosis-induced alteration in bone bicarbonate and phosphate. *Am J Physiol - Ren Physiol* 2002;283:f1091-f1097.

13. LeGeros R.Z., Sakae T., Bautista C., Retino M., LeGeros J.P. Magnesium and carbonate in enamel and synthetic apatites. *Adv Dent Res* 1996;10:225-231.
14. Zax S.M., Mayer I., Deutsch D. Carbonate content in developing human and bovine enamel. *J Dent Res* 1991;70:913-916.
15. Knuuttila M., Lappalainen R., Alakuijala P., Lammi S. Statistical evidence for the relation between citrate and carbonate in human cortical bone. *Calcif Tissue Int* 1985;37:363-366.
16. Pellegrino E.D., Blitz R.M. Bone carbonate and the Ca to P molar ratio. *Nature* 1968;219:1261-1262.
17. LeGeros R.Z., Trautz O.R. Apatite crystallites: effects of carbonate on morphology. *Science* 1967; 155:1409-1411.
18. Doi Y., Shibusaki T., Moriwaki Y., Kajimoto T., Iwayama Y. Sintered carbonate apatites as bioresorbable bone substitutes. *J Biomed Mater Res A* 1998;39:603-610.
19. Nelson D.G.A., Featherstone J.D.B., Duncan J.F., Cutress T.W. Paracrystalline disorder of biological and synthetic carbonate-substituted apatites. *J Dent Res* 1982;61:1274-1281.
20. Mayer I., Scblum R., Featherstone J.D.B. Magnesium-containing carbonate apatites. *J Inorg Biochem* 1997;66:1-6.
21. Khairoun I., Boltong M.G., Driessens F.C.M., Planell J.A. Effect of calcium carbonate on the compliance of an apatitic calcium phosphate bone cement. *Biomaterials* 1997;18:1535-1539.
22. Khairoun I., Boltong M.G., Driessens F.C.M., Planell J.A. Effect of calcium carbonate on clinical compliance of apatitic calcium phosphate bone cement. *J Biomed Mater Res* 1997;38:356-360.
23. Rau G.H., Caldeira K. Enhanced carbonate dissolution: a means of sequestering waste CO₃ as ocean bicarbonate. *Energ Convers Manage* 1999;40:1803-1813.
24. Tas A.C. Use of vaterite and calcite in forming calcium phosphate cement scaffolds. In: Brito M, Case E, Kriven WM, editors. *Developments in Porous, Biological and Geopolymer Ceramics:*

- Ceramic Engineering and Science Proceedings. New Jersey: John Wiley & Sons;2009:135-150.
25. Cassidy C., Jupiter J.B., Cohen M., Santi M.D., Fennell C., Leinberry C., Husband J., Ladd A., Seithz W.R., Constanz B. Norian srs cement compared with conventional fixation in distal radial fractures. *J Bone Joint Surg* 2003;85:2127-2137.
 26. Heredia L.M.A., Kamphuis B.G.J., Thune P.C., Oner C.F., Jansen J.A., Walboomers F.X. An injectable calcium phosphate cement for the local delivery of paclitaxel to bone. *Biomaterials* 2011;32:5411-5416.
 27. Khairoun I., Boltong M.G., Driessens F.C.M., Planell J.A. Some factors controlling the injectability of calcium phosphate bone cements. *J Mater Sci Mater Med* 1998;9:425-428.
 28. Habraken W.J.E.M., Wolke J.G.C., Mikos A.G., Jansen J.A. Injectable PLGA microsphere/calcium phosphate cements: physical properties and degradation characteristics. *J Biomater Sci Polym Ed.* 2006;17:1057-1074.
 29. Khairoun I., Magne D., Gauthier O., Bouler J.M., Aguado E., Daculsi G., Weiss P. In vitro characterization and in vivo properties of a carbonated apatite bone cement. *J Biomed Mater Res A* 2002;60:633-642.
 30. Fernandez E., Gil F.J., Ginebra M.P., Driessens F.C.M., Planell J.A., Best S.M. Production and characterization of new calcium phosphate bone cements in the CaHPO_4 -TCP system: pH, workability and setting times. *J Mater Sci Mater Med* 1999;10:223-230.
 31. Fernandez E., Gil F.J., Ginebra M.P., Driessens F.C.M., Planell J.A. Calcium phosphate bone cements for clinical applications part 1: solution chemistry. *J Mater Sci Mater Med* 1999;10:169-176.
 32. Khashaba R.M., Lockwood P.E., Lewis J.B., Messer R.L., Chutkan N.B., Borke L.B. Cytotoxicity, calcium release, and pH changes generated by novel calcium phosphate cement formulations. *J Biomed Mater Res B* 2010;93:297-303.

33. Yao F., LeGeros J.P., LeGeros R.Z. Simultaneous incorporation of carbonate and fluoride in synthetic apatites: Effect on crystallographic and physico-chemical properties. *Acta Biomater* 2009;5:2169-2177.
34. Hankermeyer C.R., Ohashi K.L., Delaney D.C., Ross J., Constantz B.R. Dissolution rates of carbonated hydroxyapatite in hydrochloric acid. *Biomaterials* 2002;23:743-750.
35. Mahabole M., Aiyer R., Ramakrishna C., Sreedhar B., Khairnar R. Synthesis, characterization and gas sensing property of hydroxyapatite ceramic. *Bull Mater Sci* 2005;28:535-545.
36. Rehman I., Bonfield W. Characterization of hydroxyapatite and carbonated apatite by photo acoustic FTIR spectroscopy. *J Mater Sci Mater Med* 1997;8:1-4.
37. Rey C., Collins B., Goehl T., Dickson R., Glimcher M.J. The carbonate environment in bone mineral: A resolution-enhanced fourier transform infrared spectroscopy study. *Calcif Tissue Int* 1989;45:157-164.
38. Combes C., Bareille R., Rey C. Calcium carbonate-calcium phosphate mixed cement compositions for bone reconstruction. *J Biomed Mater Res A* 2006;79:318-328.
39. Miyamoto Y., Ishikawa K., Takechi M., Toh T., Yuasa T., Nagayama M., Suzuki K. Histological and compositional evaluations of three types of calcium phosphate cements when implanted in subcutaneous tissue immediately after mixing. *J Biomed Mater Res A* 1999;48:36-42.
40. Combes C., Tadier S., Galliard S., Fullana G.S., Charvillat C., Rey C., Auzely V.R., El Kissi N. Rheological properties of calcium carbonate self-setting injectable paste. *Acta Biomater* 2010;6:920-927.
41. Burguera F.E., Xu H.K.H., Sun L. Injectable calcium phosphate cement: effects of powder-to-liquid ratio and needle size. *J Biomed Mater Res B* 2008;84:493-502.
42. Bohner M., Baroud G. Injectability of calcium phosphate pastes. *Biomaterials* 2005;26:1553-1563.

43. Bohner M., Barroud G., Gasser B. Critical aspects in the use of injectable calcium phosphates in spinal surgery. *Biomaterials* 2010;31:4609-4611.
44. Fernandez E., Planell J.A. Synthesis of dahhlite through a cement setting reaction. *J Mater Sci Mater Med* 1998;9:789-792.
45. Fernandez E., Ginebra M.P., Boltong M.G., Driessens F.C.M., Planell J.A., Ginebra J., De Maeyer E.A., Verbeeck R.M., Planell J.A. Kinetic study of the setting reaction of a calcium phosphate bone cement. *J Biomed Mater Res A* 1996;32:367-374.
46. Brown P.W., Sturgeon J.L. Effects of carbonate on hydroxyapatite formed from CaHPO_4 and $\text{Ca}_4(\text{PO}_4)_2\text{O}$. *J Mater Sci Mater Med* 2009;20:1787-1794.
47. Durucan C., Brown P.W. Reactivity of α -tricalcium phosphate. *J Mater Sci* 2002;37:963-969.
48. LeGeros R.Z., Kijkowska R., Bautista C., LeGeros J.P. Synergistic effects of magnesium and carbonate on properties of biological and synthetic apatites. *Connect Tissue Res* 1995;33:203-209.
49. LeGeros R.Z., Trautz O.R., Klein E., LeGeros J.P. Two types of carbonate substitution in the apatite structure. *Cell Mol Life Sci* 1969;25:5-7.
50. Fernandez E., Gil F.J., Best S.M., Ginebra M.P., Driessens F.C.M., Planell J.A. Improvement of the mechanical properties of new calcium phosphate bone cements in the CaHPO_4 - $\text{Ca}_3(\text{PO}_4)_2$ system: compressive strength and microstructural development. *J Biomed Mater Res A* 1998;41:560-567.
51. Navarro M., Michiardi A., Castano O., Planell J.A. Biomaterials in orthopaedics. *J R Soc Interface* 2008;5:1137-58.
52. Koerten H.K., van der Meulen J. Degradation of calcium phosphate ceramics. *J Biomed Mater Res A* 1999;44:78-86.
53. Lu J., Descamps M., Dejou J., Koubi G., Hardouin P., Lemaitre J., Proust J.P. The biodegradation mechanism of calcium phosphate biomaterials in bone. *J Biomed Mater Res* 2002;63:408-412.

54. LeGeros R.Z. Biodegradation and bioresorption of calcium phosphate ceramics. *Clin Mater* 1993;14:65-88.
55. Daitou F., Maruta M., Kawachi G., Tsuru K., Matsuya S., Terada Y., Ishikawa K. Fabrication of carbonate apatite block based on internal dissolution-precipitation reaction of dicalcium phosphate and calcium carbonate. *J Dent Mater* 2010;29:303-308.
56. Habibovic P., Juhl M.V., Clyens S., Martinetti R., Dolcini L., Theilgaard N., van Blitterswijk C.A. Comparison of two carbonated apatite ceramics in vivo. *Acta Biomater* 2010;6:2219-2226.
57. Gbureck U., Grolms O., Barralet J.E., Grover L.M., Thull R. Mechanical activation and cement formation of β -tricalcium phosphate. *Biomaterials* 2003;24:4123-4131.



Chapter 4

INJECTABLE BIPHASIC CALCIUM PHOSPHATE CEMENTS AS A POTENTIAL BONE SUBSTITUTE

Kemal Sariibrahimoğlu, Joop G.C. Wolke, Sander C.G. Leeuwenburgh,
Li Yubao, John A. Jansen

1. Introduction

During the last decades, a variety of materials has been used for bone grafting of non-healing defects resulting from injury, trauma or tumor resection. The use of autologous bone is considered to be the gold standard. The most important disadvantages adherent related to autologous bone grafts include i) additional surgery, ii) limited supply, and iii) donor site morbidity. Calcium phosphate (CaP) based materials represent a promising candidate for bone grafting due to their biocompatibility and osteoconductive properties. CaP materials are available in different forms, such as pre-made granules and blocks, which are difficult to handle from a clinical point of view^{1,2}. Injectable self-setting calcium phosphate cements (CPCs) proved to be more effective for optimal defect filling, thereby reducing postoperative complications for patients³. Several cement formulations are currently commercially available and received a CE mark for specific clinical applications. In general, injectable apatitic CPCs are biocompatible and osteoconductive, but their degradation rate is generally very slow. Several approaches can be used to enhance the rate of cement degradation. Incorporation of polymeric microparticles into CPCs was shown to be a feasible approach to facilitate the creation of macropores during the setting process⁴. Many animal studies demonstrated that pores created after degradation of these polymeric microparticles accelerate CPC degradation and bone ingrowth into bone defects^{5, 6}. Another purely ceramic approach towards resorbable apatitic CPCs was based on the fact that the degradation rate of sintered, poorly soluble apatitic ceramics can be accelerated considerably by introducing a secondary phase of a CaP ceramic of higher solubility such as β -tricalcium phosphate (β -TCP). This concept of biphasic CaP ceramics has been investigated and commercialized extensively, but injectable, biphasic CPCs which form apatite and β -TCP from tricalcium phosphate precursors in both α - and β -polymorphs have not been studied in much detail⁷⁻⁹. Jansen *et al.*¹⁰ showed that cements consisting of 85% α -TCP and 15% β -TCP stimulated bone ingrowth in tibia of goats. The β -TCP component was actively resorbed without any foreign reaction in six months. Yet, the degradation rate of the

poorly degradable hydroxyapatite (HA) phase was not sufficient to make the cement degradable¹¹. More recently, novel biphasic CPCs containing dual phase α/β -TCP powder particles were developed by our laboratory and evaluated *in vivo*¹². Biphasic cements did not cause any adverse tissue response, but the rate of bone formation was similar to monophasic apatitic CPC. In this latter study, only one ratio between α/β -TCP was evaluated, while only one time point was selected for *in vivo* evaluation, thereby impeding precise quantification of the degradation behavior of the biphasic BCPCs. Moreover, handling and physicochemical characteristics of this BCP were not studied thoroughly.

Therefore, the purpose of the current study was to develop and characterize BCPCs based on dual phase α/β -TCP particles as powder precursor phase. Dual α/β -TCP powder particles were obtained by thermal treatment method. Subsequently, the physicochemical properties of the heat-treated precursor powders were studied in detail as well as the handling and degradation behavior of the resulting cements.

2. Experimental section

2.1. Calcium phosphate precursor phases

To vary the ratio between α - and β -TCP in the powder precursor phase, commercially available alpha tricalcium phosphate (α -TCP, CAM Implants BV, Leiden, the Netherlands) powder was sintered in a furnace (Lenton UAF 15/10, UK) for 6h at different temperatures ranging from 1000 to 1200°C (5g/batch). The heating rate and the cooling rate were 2.5 °C/min and 5 °C min⁻¹, respectively. X-Ray Diffraction (XRD, PW3710 Philips, The Netherlands) was used to analyze the effect of the thermal treatment on the crystallographic structure of the α -TCP powders. Quantitative analysis of crystal polymorphism (i.e. ratio between α -TCP and β -TCP) was performed by measuring the relative intensity ratio (RIR) of the strongest lines of both polymorphs in comparison to standard mixtures of pure α -TCP and β -TCP¹³.

The dual phase α/β -TCP powders were observed by Transmission Electron Microscopy (JEOL TEM 1010, JEOL Ltd. Tokyo, Japan) for

morphological analyses. Selected area electron diffraction (SAED) was used to determine the phase structure of biphasic particles after heat-treatment. To this end, heat-treated samples were washed with ethanol (3x) followed by embedding into 100% EponTM (Epoxy resins) on a shaker at 37 °C for 4 hours. Sections of 100 µm thickness were prepared using a diamond knife (Diatome) on a microtome (Leica Ultracut SLeica Microsystems GmbH, Germany).

2.2. Preparation of cements

The CPC powder consisted heat-treated or as received α -TCP (CAM Implants BV, Leiden, the Netherlands), dicalcium phosphate anhydrous (DCPA, analytical grade, J.T. Baker Chemical Co., Phillipsburg, USA), precipitated hydroxyapatite (pHA, Biomet Merck, Darmstadt, Germany) and calcite (CaCO₃, Sigma-Aldrich Chemical Co., St. Louis, MO) (see Table 1 for the composition and abbreviations of precursor powders of the various cements). For biphasic CPC, heat-treated, dual phase (α/β -TCP) particles were used instead of the pure α -TCP of the biphasic CPC. CPC and BCPC reactants were ball-milled in according to a previously developed method using a laboratory ball mill for 5.30 h at 500 rpm¹⁴. The particle size distribution of the various CaP precursor phases after milling (α -TCP and α/β -TCP, 8.7 ± 3.0 µm, pHA, 4.5 ± 1.9 µm, DCPA, 5.0 ± 1.9 µm, CaCO₃, 2.5 ± 1.0 µm) was determined by using Mastersizer-2000 ultrasonic particle size equipment (Malvern Inst. Ltd., United Kingdom).

Table 1. Composition of precursor powder phase of CPC and BCPCs.

Abbreviation	α/β -TCP	DCPD	CaCO ₃	pHA
CPC	75/0	18	4	3
BCPC1	56/19	18	4	3
BCPC2	37.5/37.5	18	4	3
BCPC3	19/56	18	4	3
BCPC4	0/75	18	4	3

Cement pastes were obtained by homogeneous mixing of precursor powders with a 2% Na₂HPO₄ (Merck, Germany) solution at a liquid-to-powder ratio (L/P) of 0.35 ml/g. Briefly, 1 g of precursor powder was placed in an exit-closed 2 ml syringe (orifice diameter 1.7 mm). Subsequently, 0.35 ml of the 2% Na₂HPO₄ (0.2 M) solution was added to the powder. The syringe was placed in a mixing apparatus (Silamat® Vivadent, Liechtenstein) and mixed for 20 seconds. After mixing, a paste was obtained and injected into Teflon® molds of 4.5 mm in diameter by 9 mm in height to obtain cylindrical cement samples. The samples in the mold were left to set at 37 °C. Cylinders of cement were removed from the mold and immersed in phosphate buffer saline (PBS) at 37 °C to allow hardening.

2.3. Injectability and setting times

Injectability time of the samples was measured by using a tensile bench (858 MiniBionix2®, MTS Corp., USA). After mixing of the cement/liquid for 20 seconds, the syringe (orifice diameter of 1.7 mm) was fitted vertically in a fixture and mounted under the plates of a tensile bench set in compression mode. Compression force was applied to the syringe at a constant velocity of 20 mm.min⁻¹ up to a final force of 100 N¹⁵. The injectability time (defined as the period of time necessary to reach the final force of 100 N) was recorded as a function of the plunger travel time. All tests were performed in triplicate.

The initial and final setting times of the various cement pastes were assessed using Gillmore needles according to ASTM C266¹⁶. A bronze block (6 mm in diameter, 12 mm in height) was used as a mold. The mold was placed in a water bath at body temperature (37 °C). Samples of each formulation were mixed and injected into the mold, after which the initial and final setting was determined (n = 3).

2.4. Physicochemical and mechanical characterization of cements

Samples were ground in a mortar and used for X-Ray Diffraction analyses (XRD, Panalytical, PW3710 Philips, The Netherlands). The analyses were

performed with a Cu-K α radiation source having a wavelength of 1.5405 Å, a voltage of 40 kV and a current of 30 mA. Patterns were collected for 2 θ values of 25° to 38° with a step size of 0.05° and a counting time of 20 seconds per step. Fourier Transform InfraRed spectroscopy (FTIR, Perkin-Elmer, Fremont, CA, USA) was used to characterize the molecular structure of the set cements. The morphology of the set cements was evaluated by scanning electron microscopy (SEM, JEOL 6301). Prior to SEM examination, all samples were mounted on aluminum stubs using carbon tape and sputter coated with gold-palladium. The compressive strength of the samples was measured by using a mechanical testing bench (858 MiniBionixIIVR, MTS, USA) at a cross-head speed of 1 mm min⁻¹. Samples were tested before and after immersion in PBS (pH 7.4) solution at 37°C. The PBS solution was refreshed every week (n=3).

2.5. *In vitro* degradation test

In vitro degradation of CPCs was evaluated in calcium- and phosphate-free saline solution (0.15 M NaCl aqueous solution, pH 6.4) over the course of 6 weeks^{17, 18}. Injected samples were removed from the mold, dried in air and weighed. Each disc was immersed in glass bottles containing 13 mL of saline solution at 37 °C. Every week, the cement samples were carefully transferred to new bottles containing fresh saline solution. The cumulative total amount of calcium release was calculated using the ortho-cresolphthalein complexone (OCPC, Sigma-Aldrich[®]) assay by determining calcium concentrations in the solution. Total weight loss of the samples were measured after drying in air for two days (n= 6).

2.6. Statistical analysis

All measurements were statistically evaluated using GraphPad InStat[®] software (GraphPad Software Inc., San Diego, CA, USA) using one-way analysis of variance (ANOVA) with Tukey multiple comparison post test.

3. Results

3.1. Physicochemical analyses of precursor powders

The XRD patterns of the heat-treated and non-treated α -TCP powders showed the effect of heat treatment on the (partial) crystal phase transition from α - to β -TCP (Figure 1A). α -TCP revealed a main reflection at 30.9° 2θ , while the presence of β -TCP was confirmed by the main reflection at 31.2° 2θ (ICDD File No. 9-169) (Figure 1A). Based on the measured peak areas of the main α - and β -TCP peaks, the percentage of each respective phase was calculated (Figure 1B, Table 1). Clearly, the amount of β -TCP increased with decreasing sintering temperature.

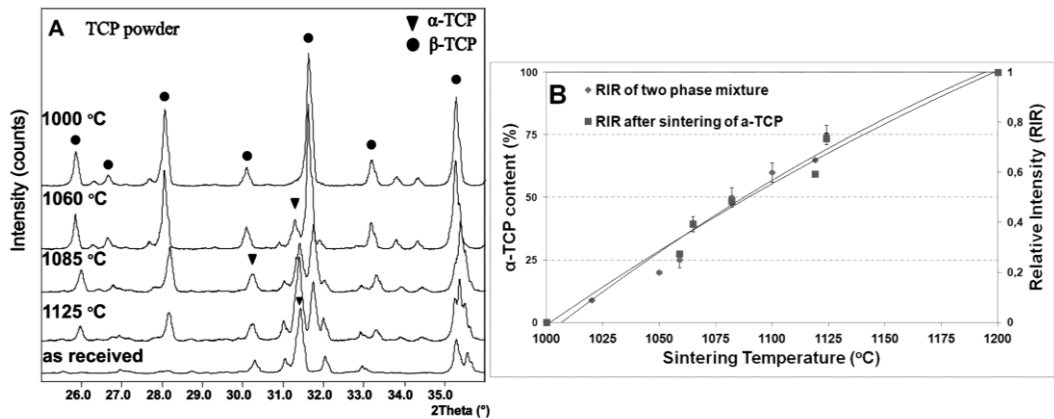


Figure 1. [A] XRD patterns of the α -TCP powder heat-treated at different temperatures for 6 h, [B] α -TCP content as a function of sintering temperature between 1000-1200°C. The standard curve (measured on powder mixtures of α - and β -TCP) is shown as a reference.

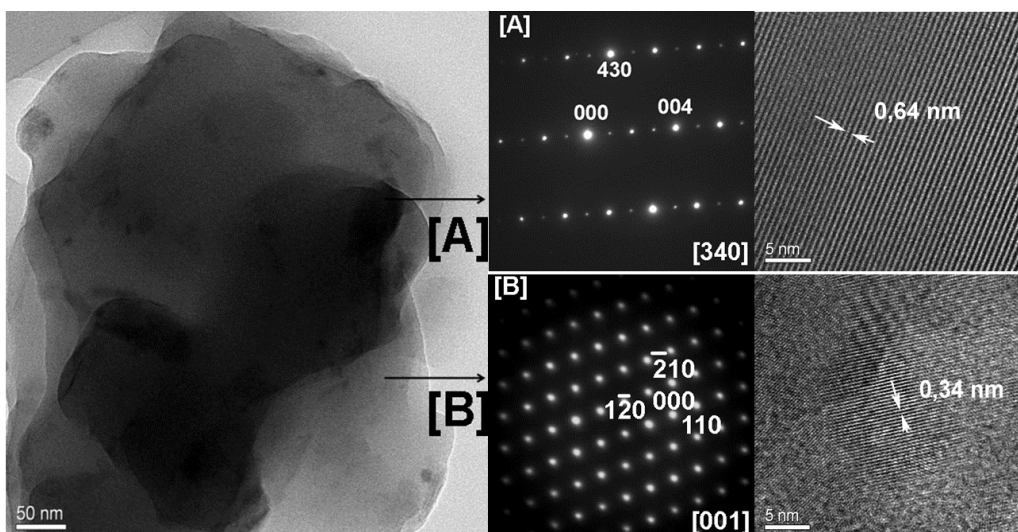


Figure 2. Transmission electron micrograph and SAED pattern of a dual phase α/β -TCP particle; [A] α -TCP, [B] β -TCP.

Characterization using TEM and SAED revealed that the two TCP-polymorphs (α -TCP and β -TCP) were present in single agglomerated particles after heat treatment (Figure 2)^{19, 20}.

3.2. Injectability and setting times

The shortest injection time was observed for the conventional β -TCP-free CPC, while the injectability time of the biphasic BCPCs increased with increasing β -TCP content (Figure 3). Similar effects were observed for the initial and final setting times (Figure 4). The shortest initial setting time (3.0 ± 0.3 min) and final setting time (4.5 ± 0.3 min) were observed for the β -TCP-free CPC paste that contained 75 wt% α -TCP, whereas the slowest final setting time (9.5 ± 1 min) was observed for BCPCs containing 75 wt% β -TCP (BCPC4).

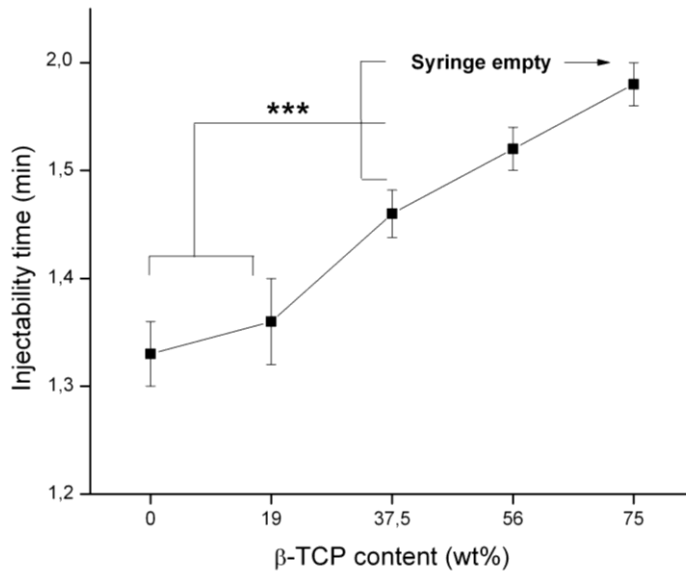


Figure 3. Injectability time of the cements as a function of β -TCP content (***) $P < 0.001$).

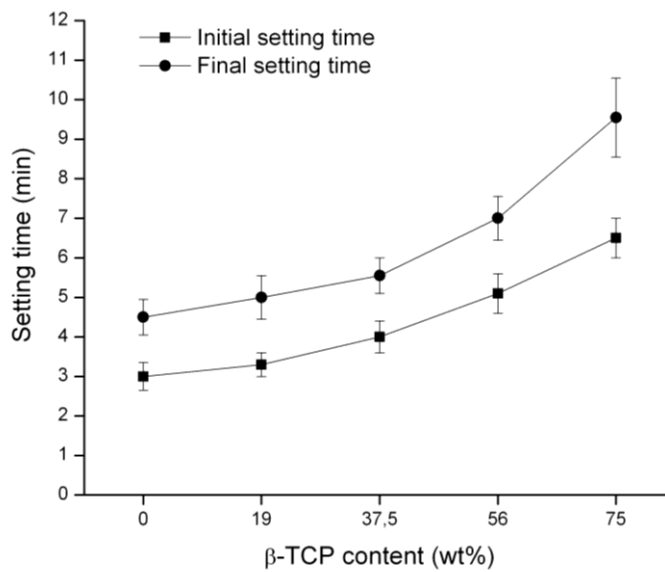


Figure 4. Initial and final setting times of the cements as a function of β -TCP content.

3.3. Physicochemical and mechanical analyses of set cements

The IR spectra of the CPC (75 wt% α -TCP) and BCPC4 (75 wt% β -TCP) after hardening at 37 °C for 6 weeks in PBS were shown in Figure 5. The main PO_4^{3-} absorption bands characteristic for hydroxyapatite were observed at 960 (ν_1), 1022 cm^{-1} (ν_{3c}) cm^{-1} , and 1087 cm^{-1} (ν_{3a}). PO_4^{3-} (ν_1) bands appeared at 944 cm^{-1} and 972 cm^{-1} for β -TCP containing biphasic cements²¹. Besides, absorption bands were observed at 873 cm^{-1} (ν_2), which revealed that carbonate was substituting for phosphate anions (type B substitutions)^{22, 23}.

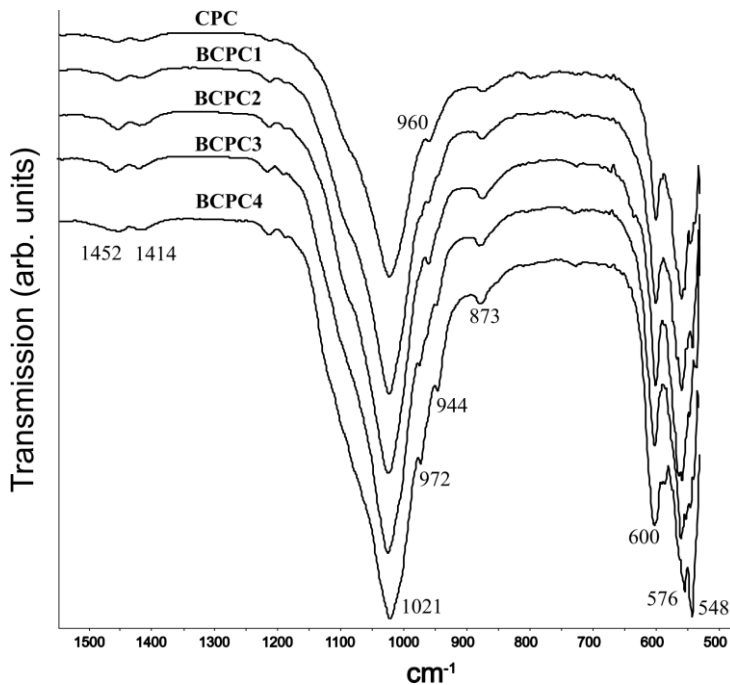


Figure 5. FTIR spectra of CPC and BCPC4 after immersion in PBS for 6 weeks.

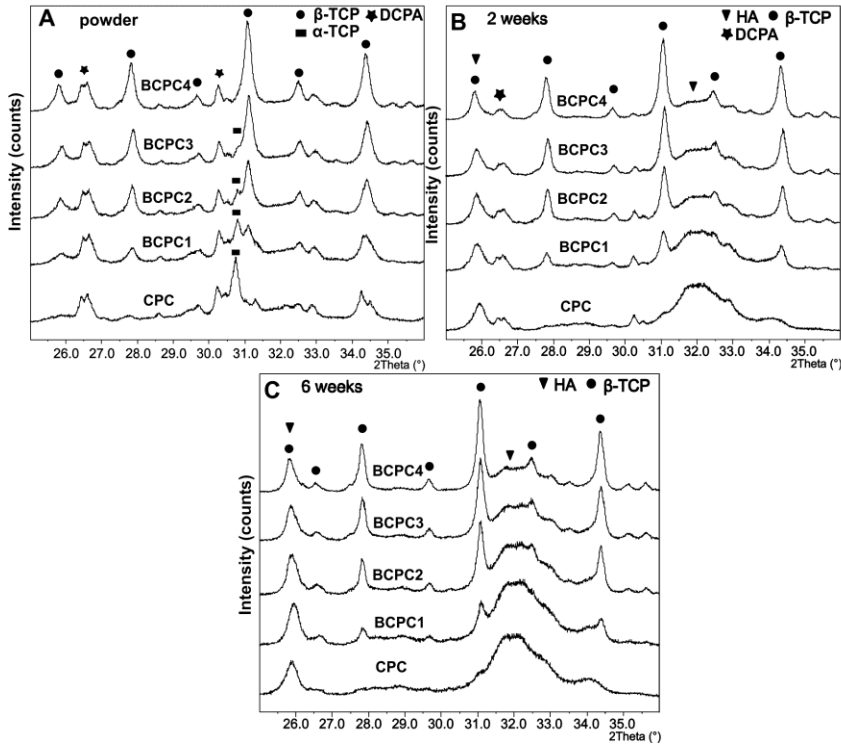


Figure 6. X-Ray Diffraction patterns of the CPC and BCPCs cements; [A] before immersion in PBS, [B] after immersion in PBS solution for 2 weeks and [C] after immersion in PBS for 6 weeks.

Figure 6 shows the XRD patterns of the cements before (Figure 6A) and after hardening for 2 (Figure 6B) and 6 (Figure 6C) weeks in PBS at 37 °C. Figure 6B demonstrated that α -TCP peaks were not detectable anymore after 2 weeks of incubation in PBS. The main reflection lines were located at $2\theta = 25.8^\circ$, 31.9° and 32.9° , which corresponded to (002), (211) and (300) reflections of the apatite structure (ICDD File No. 9-432). In addition, monetite (dicalcium phosphate anhydrous, DCPA) peaks were observed at $2\theta = 26.5^\circ$ and 30.3° (ICDD File No. 9-80). After 6 weeks of incubation (Figure 6C), only β -TCP was observed at $2\theta = 31.3^\circ$ and 34.8° (ICDD File No. 9-169) in addition to a broad reflection peak at $32^\circ 2\theta$ characteristic for hydroxyapatite which decreased in intensity with increasing β -TCP content in the dual α/β -TCP precursor powder.

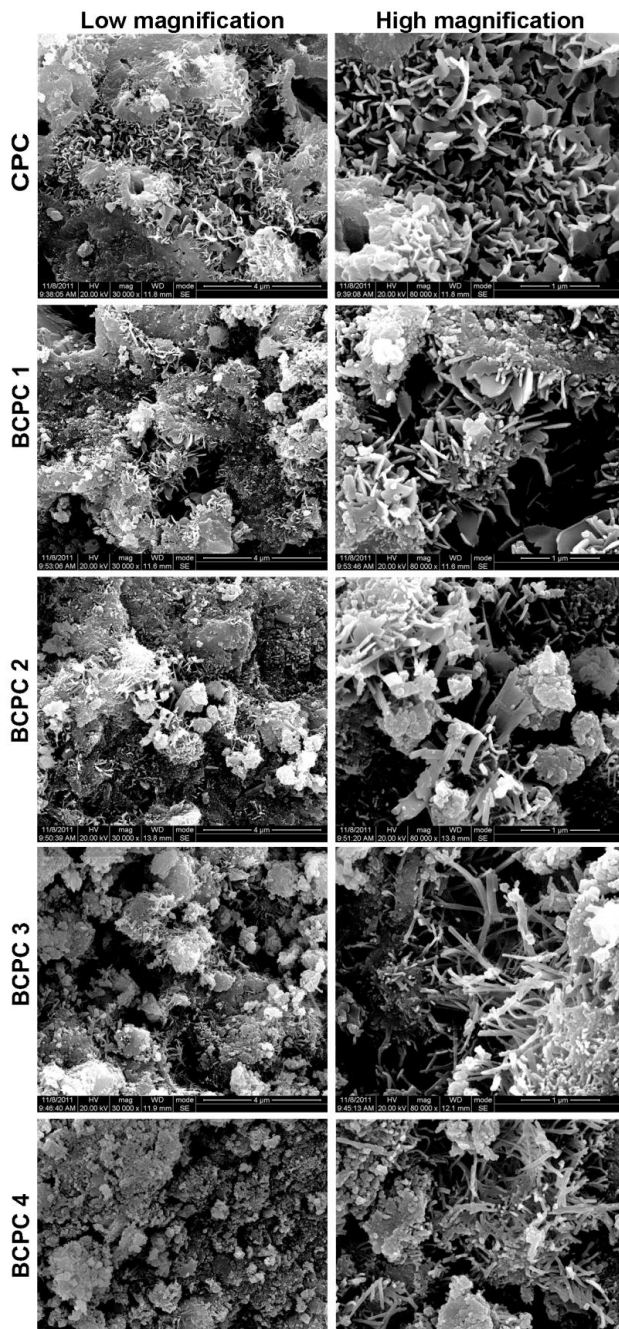


Figure 7. Scanning electron micrographs of monophasic CPC and biphasic BCPCs. Micrographs show representative structures at a magnification of 30K (low magnification, left column) and 80K (high magnification, right column).

Scanning electron micrographs of the prepared cements were shown in Figure 7, which revealed that the morphology of the crystals changed from platelets of low aspect ratio to elongated needles of high aspect ratio with increasing β -TCP content.

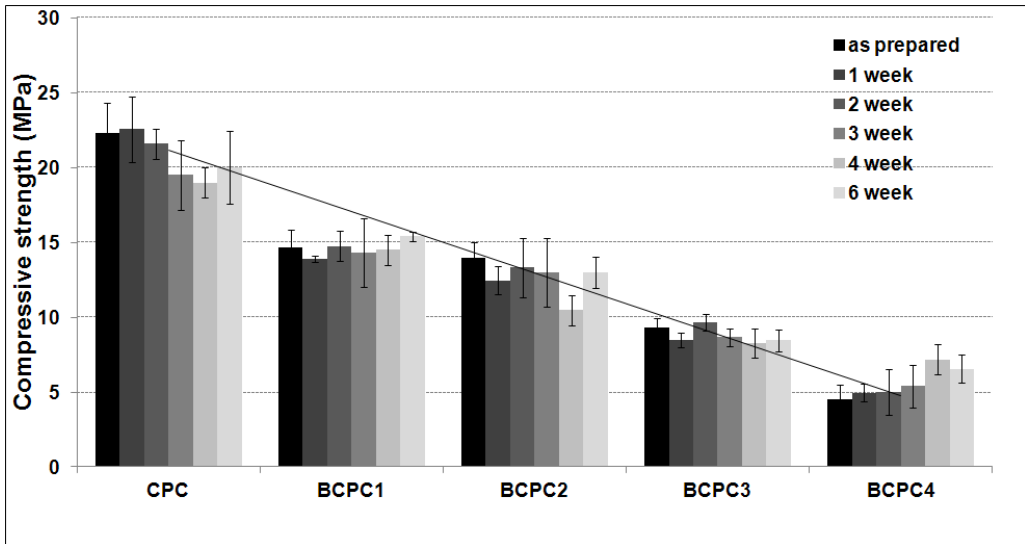


Figure 8. Compressive strength of the CPCs and BCPCs before and after soaking into PBS for various time points.

The compression strength of the samples was given in Figure 8 as a function of the composition and soaking time in PBS. Generally, the mechanical properties of CPCs decreased with increasing β -TCP content, whereas soaking in PBS for up to 6 weeks did not affect the compressive strength of set cements.

3.4. Degradability and calcium release experiments

Figure 9 shows the calcium release and weight loss of the various monophasic and biphasic cements after soaking in saline solution for 6 weeks. Compared to the poor degradability of β -TCP (as characterized by low amounts of calcium release and mass loss), rates of cement degradation doubled for BCPCs that consisted by more than half of β -TCP ($p < 0.05$),

confirming that introduction of considerable amounts of β -TCP resulted into acceleration of the degradation rate of CPCs.

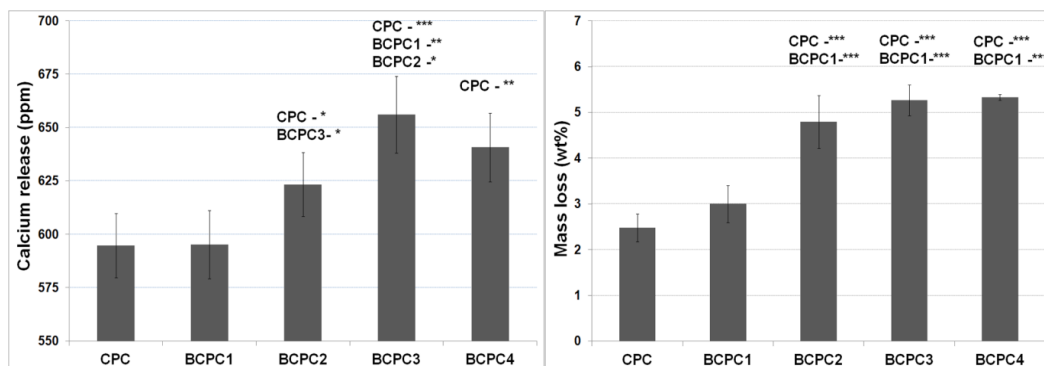


Figure 9 [A] Cumulative calcium release, and [B] mass loss of the CPC and BCPCs after soaking in saline solution (pH 6.4) at 37°C for 6 weeks (* $P < 0.05$, ** $P < 0.01$, *** $P < 0.001$).

4. Discussion

The aim of the current study was to develop resorbable, biphasic calcium phosphate cement (BCPC) and to analyze their physicochemical, mechanical and handling properties in more detail. The mechanical and physical characteristics of the different BCPCs as well as the degradation behavior under accelerated *in vitro* conditions were investigated and compared with conventional monophasic CPC. The results showed that different heat treatments of commercially available α -TCP allowed the formation of biphasic TCP cement precursor powder with a variety of α/β -TCP ratios. In a previous study, Zou *et al.*²⁴ and Li *et al.*⁹ showed that biphasic α/β -TCP particles can be prepared also by calcining an amorphous calcium phosphate precursor at a temperature ranging from 800 to 900 °C. Similar to Zou *et al.*²⁴, the current study also employed SAED to confirm that both α - and β -TCP polymorphs were present in single powder particles after heat treatment. It was, however, not possible to determine the spatial distribution of the α - and β -TCP polymorphs since the individual particles which were characterized by SAED agglomerated upon heat treatment. As

a consequence, injectable and self-setting BCPCs of variable α/β -TCP ratio were developed that were still self-setting based on the hydrolysis of the α -TCP phase. The resulting cements revealed significantly different mechanical properties and degradation characteristics which are discussed below in direct comparison to standard, β -TCP-free CPC.

The handling properties of the biphasic cement pastes of different α/β -TCP ratio differed significantly from the conventional CPC. Injectability, initial and final setting times increased considerably with increasing β -TCP content, which can be explained by the fact that β -TCP is not a setting reactant as it does not hydrolyze into HA. Nevertheless, all tested cements were injectable through 0.2 ml syringes without filter pressing (as caused by the homogeneous size of the reactant powders)²⁵, while cements hardened within clinically acceptable values of less than 15 min²⁶. This indicates that enough reactants are available for the hydration with water and for the formation of HA clusters to allow cement setting.

This hardening process is proceeded by hydrolysis of α -TCP into poorly crystalline HA. This HA phase is formed upon dissolution/reprecipitation of the soluble precursor phases, creating the supersaturation necessary to precipitate CaP and form a network of entangled HA nanocrystals which is chemically similar to biological apatites²⁷. Since the solubility and hydrolysis rate of the α -TCP is higher than β -TCP, the crystallization process of HA was controlled by the hydrolysis reaction of α -TCP into HA, whilst β -TCP was not reacting and remained chemically unchanged²⁸. In addition to the hydrolysis reaction of α -TCP, calcite and monetite are also known to react towards apatite, thereby providing an additional source for precipitation of nanosized-apatite crystals, which are responsible for the setting of cement and concomitant embedding of β -TCP. IR spectra of CPC and BCPC showed distinct differences. IR analysis of set CPC revealed bands at 600, 1022 and 1090 cm^{-1} which are characteristic for crystalline HA²⁹. Two $\nu_4 \text{PO}_4^{3-}$ peaks characteristic for HA were observed at 600 and 570 cm^{-1} , which split into multiple absorption peaks at 600, 578 and 548 cm^{-1} with increasing β -TCP content for BCPC. In addition, weak shoulder absorptions at 944 and 972 cm^{-1} were observed for BCPC which

also corresponded to the phosphate vibration of β -TCP^{30, 31}. For biphasic BCPCs, additional IR spectra bands appeared at 944-972 cm^{-1} which increased in intensity with increasing β -TCP ratio, thus confirming the incorporation of β -TCP into BCPCs. Besides, the lack of absorption bands at 700-750 indicated the absence of crystalline calcium carbonate phases such as calcite, aragonite and vaterite³⁰. PO_4^{3-} ions were partially substituted by CO_3^{2-} ions, resulting into a poorly crystalline B-type carbonated apatite structure. It was shown that the incorporation of CO_3^{2-} ions into PO_4^{3-} sites in HA disturb the lattice structure, reduce the crystallinity and substantially enhance solubility³². The morphology of the precipitated crystals of the set cements depended strongly on the thermal treatment of the precursor powders, since crystal shapes changed from platelet-like to needle-like with increasing β -TCP content. As reported in previous studies, the number of crystallite nuclei increases with increasing supersaturation, thereby giving rise to formation of plate-like crystals^{33, 34}. Our results indeed confirmed that CaP platelets are formed from soluble α -TCP precursors, which yielded high supersaturation, whereas CaP needles were formed from dual α/β -TCP of lower solubility. Consequently, it can be concluded that crystal morphology of calcium phosphate cements can be controlled by tailoring the solubility and reactivity of the TCP-precursors through variation of the ratio between soluble and less soluble polymorphs. Whereas the compressive strength of cements was not affected by soaking in PBS, the mechanical strength of set cements decreased strongly with increasing β -TCP content. The decrease in strength can be attributed to the lower degree of entanglement of HA nanocrystals during setting of the cements containing non-setting β -TCP. Moreover, the mechanical weakness of β -TCP as observed previously^{35, 36} also contributed to the decrease in strength of the biphasic BCPCs.

Since *in vivo* resorption of CaP ceramics is mainly controlled by their solubility (which depends on crystallinity, crystal shape and morphology as well as porosity), the dissolution of BCPCs was measured as a function of time by quantifying mass loss and calcium release upon soaking in saline solution. The *in vitro* results clearly indicated that the degradation rates of

biphasic cements containing sufficient amounts of β -TCP (i.e. more β -TCP than α -TCP) were more than twice as high as that of β -TCP-free CPC. Nevertheless, the amount of calcium release and mass loss did not increase linearly with increasing β -TCP content, suggesting that TCP-precursor powders should be composed by more than half of the β -TCP polymorph in order to improve the degradation rate of CPCs. Nevertheless, it should be realized that the saline solutions as used in the current experimental set-up were set at an almost neutral pH of 6.4, thereby reducing the dissolution of CaP considerably as compared to more acid testing conditions such as reported in previous studies³². Recently, it was postulated that calcium and phosphate ions directly influence the migration, proliferation and differentiation of osteoblasts precursor cells^{37, 38}. In that respect, the control over release of calcium as described herein would be a valuable tool to modulate cellular behavior and improve the osteoconductivity as well as degradability of apatitic CPCs.

5. Conclusion

In the current study biphasic α/β -TCP powders were produced by heat treatment of α -TCP, which were subsequently used as precursor powder for self-setting biphasic calcium phosphate cements. Due to the biphasic chemical composition of the precursor powders and resulting cements, differences in handling behavior, physicochemical properties and degradation characteristics were observed. In general, BCPCs revealed longer setting and injectability times as compared to monophasic CPCs which depended on the ratio between α - and β -TCP in the precursor powder. During hardening of the cements, the amount of apatite formation was inversely proportional to the extent of β -TCP in biphasic BCPC, whereas the predominant morphology of the precipitated crystals changed from platelets to needles with increasing β -TCP content. The hardening process was controlled by the transformation reaction of α -TCP into a mixed matrix consisting of HA and β -TCP. *In vitro* degradation studies indicated that the degradation rates of biphasic cements containing

sufficient amounts of β -TCP (i.e. more β -TCP than α -TCP) were more than twice as high compared to β -TCP-free CPC.

References

1. Ginebra M.P., Traykova T., Planell J.A. Calcium phosphate cements as bone drug delivery systems: A review. *J Control Rel* 2006;113:102-110.
2. Ooms E.M., Wolke J.G.C., van der Waerden J.P.C.M., Jansen J.A. Trabecular bone response to injectable calcium phosphate cement. *J Biomed Mater Res A* 2002;61:9-18.
3. Magee W.P., Ajkay N., Freda N., Rosenblum R.S. Use of fast-setting hydroxyapatite cement for secondary craniofacial contouring. *Plast Reconstr Surg* 2004;114:289-297.
4. Habraken W.J., Liao H.B., Zhang Z., Wolke J.G., Grijpma D.W., Mikos A.G., Feijen J., Jansen J.A. In vivo degradation of calcium phosphate cement incorporated into biodegradable microspheres. *Acta Biomater* 2010;6:2200-2211.
5. Guha A.K., Singh S., Kumaresan R., Nayar S., Sinha A. Mesenchymal cell response to nanosized biphasic calcium phosphate composites. *Colloids Surf B Biointerfaces* 2009;73:146-151.
6. Lanao F.R.P., Leeuwenburgh S.C., Wolke J.G., Jansen J.A. Bone response to fast-degrading, injectable calcium phosphate cements containing PLGA microparticles. *Biomaterials* 2011;32:8839-8847.
7. LeGeros R.Z., Lin S., Rohanizadeh R., Mijares D., LeGeros J.P. Biphasic calcium phosphate bioceramics: preparation, properties and applications. *J Mater Sci Mater Med* 2003;14:201-209.
8. Kon M., Ishikawa K., Miyamoto Y., Asaoka K. Development of calcium phosphate based functional gradient bioceramics. *Biomaterials* 1995;16:709-714.
9. Li Y., Weng W., Tam K.C. Novel highly biodegradable biphasic tricalcium phosphates composed of α -tricalcium phosphate and β -tricalcium phosphate. *Acta Biomater* 2007;3:251-254.

10. Jansen J.A., Ruijter J.E., Schaeken H.G., van der Waerden J.P.C.M., Planell J.A., Driessens F.C.M. Evaluation of tricalciumphosphate/hydroxyapatite cement for tooth replacement: An experimental animal study. *J Mater Sci Mater Med* 1995;6:653-657.
11. van de Watering F.C., van den Beucken J.J., Walboomers X.F., Jansen J.A. Calcium phosphate/poly(D,L-lactic-co-glycolic acid) composite bone substitute materials: Evaluation of temporal degradation and bone ingrowth in a rat critical-sized cranial defect. *Clin Oral Implants Res* 2012;23:151-159.
12. Heredia L.M.A., Bongio M., Bohner M., Cuijpers V., Winnubst L.A., van Dijk N., Wolke J.G., van den Beucken J.J., Jansen J.A. Processing and in vivo evaluation of multiphasic calcium phosphate cements with dual tricalcium phosphate phases. *Acta Biomater* 2012;8:3500-3508.
13. Nilsson M., Fernandez E., Sarda S., Lidgren L., Planell J.A. Characterization of a novel calcium phosphate/sulphate bone cement. *J Biomed Mater Res* 2002;61:600-607.
14. Sariibrahimoglu K., Leeuwenburgh S.C., Wolke J.G., Yubao L., Jansen J.A. Effect of calcium carbonate on hardening, physicochemical properties, and in vitro degradation of injectable calcium phosphate cements. *J Biomed Mater Res A* 2012;100:712-719.
15. Khairoun I., Boltong M.G., Driessens F.C., Planell J.A. Some factors controlling the injectability of calcium phosphate bone cements. *J Mater Sci Mater Med* 1998;9:425-428.
16. Fernandez E., Gil F.J., Ginebra M.P., Driessens F.C., Planell J.A., Best S.M. Calcium phosphate bone cements for clinical applications. Part II: precipitate formation during setting reactions. *J Mater Sci Mater Med* 1999;10:177-183.
17. Mirtchi A.A., Lemaître J., Hunting E. Calcium phosphate cements: Action of setting regulators on the properties of the β -tricalcium phosphate-monocalcium phosphate cements. *Biomaterials* 1989;10:634-638.

18. Dagang G., Kewei X., Yaxiong L. Physicochemical properties and cytotoxicities of Sr-containing biphasic calcium phosphate bone scaffolds. *J Mater Sci Mater Med* 2010;21:1927-1936.
19. Tao J., Jiang W., Zhai H., Pan H., Xu X., Tang R. Structural Components and Anisotropic Dissolution Behaviors in One Hexagonal Single Crystal of β -Tricalcium Phosphate. *Cryst Growth Des* 2008;8:2227-2234.
20. Suvorova E.I., Arkharova N.A., Buffat P.A. Transmission electron microscopy of Ca oxide nano- and microcrystals in α -tricalcium phosphate prepared by sintering of β -tricalcium phosphate. *Micron* 2009;40:563-570.
21. Fowler B.O., Moreno E.C., Brown W.E. Infra-red spectra of hydroxyapatite, octacalcium phosphate and pyrolysed octacalcium phosphate. *Arch Oral Bio* 1966;11:477-492.
22. Habibovic P., Juhl M.V., Clyens S., Martinetti R., Dolcini L., Theilgaard N., van Blitterswijk C.A. Comparison of two apatite ceramics in vivo. *Acta Biomater* 2010;6:2219-2226.
23. LeGeros R.Z., Trautz O.R., Klein E., LeGeros J.P. Two types of carbonate substitution in the apatite structure. *Experientia* 1969;25:5-7.
24. Zou C., Cheng K., Weng W., Song C., Du P., Shen G., Han G. Characterization and dissolution–reprecipitation behavior of biphasic tricalcium phosphate powders. *J Alloys Comp* 2011;509:6852-6858.
25. Habib M., Baroud G., Gitzhofer F., Bohner M. Mechanisms underlying the limited injectability of hydraulic calcium phosphate paste. Part II: Particle separation study. *Acta Biomater* 2010;6:250-256.
26. Khairoun I., Boltong M.G., Driessens F.C., Planell J.A. Effect of calcium carbonate on the compliance of an apatitic calcium phosphate bone cement. *Biomaterials* 1997;18:1535-1539.
27. Zimmermann R., Gabl M., Lutz M., Angermann P., Gschwentner M., Pechlaner S. Injectable calcium phosphate bone cement Norian SRS for the treatment of intra-articular compression fractures of the

- distal radius in osteoporotic women. *Arch Orthop Trauma Surg* 2003;123:22-27.
28. Sariibrahimoglu K., Leeuwenburgh S.C., Wolke J.G., Yubao L., Jansen J.A. Calcium Phosphates. *Tissue Engineering: Principles and Practices*, ed. Fisher JP, Mikos AG, Bronzino JD, Peterson DR. US: CRC Press; pg. 31-38, 2012.
 29. Rey C., Shimizu M., Collins B., Glimcher M.J. Resolution-enhanced fourier transform infrared spectroscopy study of the environment of phosphate ion in the early deposits of a solid phase of calcium phosphate in bone and enamel and their evolution with age: 2. Investigations in the ν_3 PO_4 domain. *Calcif Tissue Int* 1991;49:383-388.
 30. Peña J., Vallet-Regi M. Hydroxyapatite, tricalcium phosphate and biphasic materials prepared by a liquid mix technique. *J Eur Ceram Soc* 2003;23:1687-1696.
 31. Cacciotti I., Bianco A. High thermally stable Mg-substituted tricalcium phosphate via precipitation. *Ceram Inter* 2011;37:127-137.
 32. LeGeros R.Z. Biodegradation and bioresorption of calcium phosphate ceramics. *Clin Mater* 1993;14:65-88.
 33. Ginebra M.P., Driessens F.C.M., Planell J.A. Effect of the particle size on the micro and nanostructural features of a calcium phosphate cement: A kinetic analysis. *Biomaterials* 2004;25:3453-3462.
 34. Ginebra M.P., Fernandez E., Driessens F.C.M., Planell J.A. Modeling of the Hydrolysis of α -Tricalcium Phosphate. *Journal of the Am Ceram Soc* 1999;82:2808-2812.
 35. Tamimi F., Torres J., Bassett D., Barralet J., Cabarcos E.L. Resorption of monetite granules in alveolar bone defects in human patients. *Biomaterials* 2010;31:2762-2769.
 36. Gbureck U., Grolms O., Barralet J.E., Grover L.M., Thull R. Mechanical activation and cement formation of β -tricalcium phosphate. *Biomaterials* 2003;24:4123-4131.

37. Chai Y.C., Carlier A., Bolander J., Roberts S.J., Geris L., Schrooten J., van Oosterwyck H., Luyten F.B. Current views on calcium phosphate osteogenicity and the translation into effective bone regeneration strategies. *Acta Biomater* 2012;8:3876-3887.
38. Barradas A.M.C., Yuan H., van der Stok J., Le Quang H., Fernandes H., Chaterjea A., Hogenes M.C., Shultz K., Donahue L.R., van Blitterswijk C., de Boer J. The influence of genetic factors on the osteoinductive potential of calcium phosphate ceramics in mice. *Biomaterials* 2012;33:5696-5705.



Chapter 5

INFLUENCE OF THE PORE GENERATOR ON THE EVOLUTION OF THE MECHANICAL PROPERTIES AND THE POROSITY AND INTERCONNECTIVITY OF CALCIUM PHOSPHATE CEMENT

M.A. Lopez-Heredia, K. Saribrahimoglu, W. Yang, M. Bohner, D.
Yamashita, A. Kunstar, A.A. van Apeldoorn, E.M. Bronkhorst, R.P. Félix
Lanao, S.C.G. Leeuwenburgh, K. Itatani, F. Yang, P.Salmon J.G.C. Wolke
and J.A. Jansen

1. Introduction

Injectable calcium phosphate cements (CPCs) are excellent materials for bone grafting procedures. CPCs adapt to the bone defect, are biocompatible, osteoconductive and have a composition similar to that of natural bone^{1, 2}. On the other hand, their degradation behavior is poor when delivered as a solid and is controlled via a layer-by-layer mechanism, which hampers the bone-remodeling process^{3, 4}. Increasing the porosity and interconnectivity of CPCs will allow transport of body fluids within the CPC scaffolds, enhances their degradation as well as the possibility of the colonization of proteins and cells into the CPCs⁵. Several methods to obtain porous CPCs have already been studied^{6, 7}. One of the more common methods to increase the porosity of CPCs is by including degradable pore-generating (porogens) microparticles^{8, 9}. Relevant material properties, such as porosity and interconnectivity, can be affected by the amount, size and type of polymer, as used to prepare the microparticles^{10, 11}. Poly (D,L-lactic-co-glycolic acid) (PLGA) is a biodegradable material that can be used for such a purpose¹². PLGA degrades by a nonenzymatical hydrolytic mechanism and is a porogen, which can be loaded with drugs or proteins^{13, 14}. PLGA microparticles can be produced by a water-in-oil-in-water (W/O/W) double emulsion technique¹⁵⁻¹⁷. Several parameters - *i.e.* amount of solvent, temperature, emulsification and agitation - affect the size and morphology of PLGA microparticles produced by this technique¹⁸⁻²². Increasing the porosity reduces the mechanical properties of the material, which can have an effect of final clinical application²³. This has been confirmed by finite element and mathematical models²⁴⁻²⁶. These approaches permit the calculation of the expected stress and Young's modulus. Porosity on calcium phosphate (CaP) materials are defined as follow²⁷: macroporosity (330 - 100 μm), mesoporosity (100 - 10 μm) and microporosity (10 μm - 30 \AA). The effect of macroporosity has been studied extensively²⁸. Levensgood *et al.*²⁹ performed studies on the effect of pores on the microporous region, *i.e.* pores between 0.5 - 10 μm . However, a good correlation of CPC properties with pores in the mesoporous region (10-100 μm) has not been

performed²⁷. A better understanding of the effect of the incorporation of PLGA microparticles on the properties of a CPC is important for the development of resorbable CPC^{18, 30}. The aim of the present work was to study the bulk properties of CPC-PLGA composite materials, in which PLGA microparticles created porosity -mainly in the mesoporous region- and to evaluate the interconnectivity and the development of the mechanical properties of these materials by considering the degradation of the mesoporous porogen.

2. Materials and methods

2.1. Material preparation

CPC powders were prepared consisting of 85 wt% alpha-tricalcium phosphate (α -TCP; CAM Bioceramics BV, The Netherlands), 10 wt% dicalcium phosphate anhydrous (DCPA; JT Baker Chemical Co, USA) and 5 wt% precipitated hydroxyapatite (pHA; Merck, Germany). CPC powders were ball milled in a sequential milling pathway as described before³¹. Two types of PLGA 50:50 (Purac, The Netherlands) were used: (1) a high molecular weight (HMW, 44 kD) end-capped PLGA, and (2) a low molecular weight (LMW, 17 kD) acid-terminated PLGA. Microparticles were obtained by a ([water-in-oil]-in-water) double emulsion technique. Briefly, the PLGA was first dissolved in dichloromethane (DCM, Merck, Germany) in a weight-to-volume ratio of 1:4 for the HMW PLGA and 2:4 for the LMW PLGA. Subsequently, 0.5 ml of deionized water was added and vigorously stirred for a given time with an emulsifier (T25 digital Ika, Germany). Then, 6 ml of 0.3% polyvinyl alcohol (PVA, Acros Organics, The Netherlands) solution was added and this second emulsion was stirred again for the same given time. This second emulsion was poured into a mixture of 394 ml of 0.3% PVA and 400ml of 2% Isopropanol (Labscan limited, The Netherlands). The suspension was stirred for 1 h and then PLGA microparticles were allowed to precipitate. Thereafter, the supernatant was decanted. The microparticles were collected via centrifugation, lyophilized and stored at -20 °C. The speed of the emulsification process was adjusted to 8000 rpm and 30 sec and 3200 rpm

and 90 sec to obtain small (S) and big (B) microparticles, respectively. Particle size of the prepared microparticles was measured with optical microscopy (DM RBE Leica, Germany) and image analysis software (Qwin Leica, Germany). CPC and CPC-PLGA samples were obtained by mixing the CPC or CPC-PLGA powders with a 2% Na₂HPO₄ (Merck, Germany) solution in a liquid-to-powder ratio (L/P) of 0.4. Briefly, 1 g of powder was placed in an exit-closed 2 ml syringe. Then, 0.4 ml of the 2% Na₂HPO₄ solution was added to the powder and the piston was placed back into the syringe. The syringe was placed in a mixing apparatus (Silamat[®] Vivadent, Liechtenstein) and mixed for 20 seconds. CPC alone samples were considered as the controls. For the CPC-PLGA samples, 1 g was kept as the final powder amount per syringe in order to use the L/P of 0.4. When PLGA was added, the corresponding amount of CPC was reduced. 10, 20 and 30 wt% of PLGA were incorporated into the CPC.

Table 1. Conditions used for the different CPC-PLGA combinations at the mechanical tests. Each combination had element 1 and 2 added in different percentages (10, 20 and 30 wt%) and at different ratios (0:1, 1:1, 1:0), within these percentages. Small \approx 20 μ m. Big \approx 40 μ m. LMW and HMW mean low and high molecular weight PLGA, respectively.

Combination	Added particle 1	Added particle 2
0	CPC alone (control)	
1	Small-LMW	Small-HMW
2	Small-HMW	Big-HMW
3	Small-HMW	Big-LMW
4	Small-LMW	Big-LMW
5	Small-LMW	Big-HMW
6	Big-HMW	Big-LMW

Table 1 gives more details about the different parameters as used for each CPC combination used for the mechanical properties. As can be noticed,

two types of polymer were always used for each combination. Within these percentages three different ratios, *i.e.* 1:0, 1:1 0:1, between element 1 and 2 were evaluated for each percentage of PLGA used. A ratio 1:0 means that only the first element was added within the given percentage; a ratio 1:1 means that the percentage included half and half of each element and a ratio 0:1 means that only element 2 was added. Per combination, for each time point, percentage and ratio, six (n=6) samples were prepared (54 in total). CPC controls (n=6) were only prepared for each time point since no percentage, combination or ratio is considered here. After mixing, a paste was obtained and injected into Teflon® molds of 4.5 mm in diameter by 9.2 mm in height in order to obtain cylindrical-shaped samples. Samples were dried at 37 °C overnight to facilitate the subsequent sample demolding. In some cases, when studying only structural parameters, basic samples were created. In this case, CPC-PLGA samples contained only the loading percentages (10, 20 and 30 wt%), the different sizes (S and B) and combination of sizes (S-B) without considering the type of polymer. Once again, six (n=6) samples were prepared per basic condition of loading percentage, size and ratio.

2.2. Material characterization

2.2.1. Morphological analysis

Scanning electron microscopy (SEM; JEOL 6310, JEOL, Japan) was used to examine the morphology of the PLGA particles, the CPC and the CPC-PLGA samples. CPC samples were used as controls. The specific surface area (SSA; Gemini 2360, Micromeritics, USA) of the CPC and basic CPC-PLGA samples, with polymer burned out, was characterized by nitrogen adsorption using the Brunauer, Emmett and Teller model³². Porosity of these samples was measured with the weight-lost method described by Habraken *et al.*¹³. Briefly, samples with a loaded amount of PLGA were weighted, then the PLGA was burned at 650 °C for 6 h and the samples were weighted again. SSA and porosity measurements were performed on four samples (n=4).

2.2.2. PLGA degradation and CPC transformation

Raman spectroscopy and X-ray diffraction (XRD) were used to analyze PLGA degradation and CPC transformation. To study the degradation of PLGA, 50 mg of microparticles were immersed in 10 ml of phosphate-buffered saline solution (Gibco, the Netherlands). CPC transformation was performed on CPC samples without PLGA. To study the CPC transformation three cylindrical samples, with the aforementioned dimensions, were immersed in a flask with 20 ml of Ringer's solution. Apatite is soluble in Ringer's solution but not in serum. This allows simulating also the dissolution of the cement *in vitro*, which is closer to an *in vivo* situation. Immersion time periods for all assays were 0 (no immersion), 3, 7, 21 and 56 days. When applicable, degradation and transformation solutions were renewed every week. At the end of the respective immersion periods, the samples were retrieved and freeze dried to perform subsequently the analysis. CPC samples were gently crushed with an agate (SiO₂) pestle and mortar.

Raman measurements were performed using a home-built confocal Raman spectrometer^{33, 34}. A Krypton ion laser (Coherent, Innova 90K, Santa Clara, CA) with an emission wavelength of 647.1 nm was used as the excitation source. Raman PLGA analysis was performed with an immersion objective (63x Neofluar; Carl Zeiss, Germany). This objective was used to illuminate the sample as well as to collect the Raman-scattered photons in the epi-detection mode. CPC Raman analysis was performed with an atmospheric objective (40x, Carl Zeiss, Germany). Raman spectra were acquired in the spectral image mode. In this measurement mode, a single full spectrum was obtained by single point measurement with the laser beam with a laser power of 35mW over each sample in 10s. XRD (PW3710 Philips, The Netherlands) was performed with a Cu K α radiation source with a wavelength of 1.5405 Å at a voltage of 40 kV and a current of 30 mA. Spectra were collected for 2 θ values of 3° to 70° in a continuous mode.

2.2.3. Pore interconnectivity

To determine pore interconnectivity, images of cylindrical CPC and basic CPC-PLGA samples were acquired with a high resolution micro-Computer Tomography scanner (μ -CT; Skyscan 1172, Skyscan, Belgium). A resolution of 3 μm , with acquisition conditions of 49 KV, 179 μA , rotation step of 0.25° , Al filter of 0.5 mm and exposure time of 2000 ms were used. NRecon[®] (Skyscan, Belgium) software, with an Instarecon[®] (InstaRecon Inc., USA) engine, was used to reconstruct the acquired image slices. Around 1500 slices per sample were generated. Reconstructed images were processed with CTAn software (SkyScan, Belgium). A custom processing was applied to selected regions of interest (ROIs) of the samples fitting it exactly (shrink-wrapped boundary). Adaptive thresholding was applied based on localized analysis of density, to minimize partial volume effect and thickness biasing. 3D parameters were based on analysis of a Marching Cubes type model with a rendered surface³⁵. Calculation of 2D areas and perimeters was based on the Pratt algorithm³⁶. Morphometric parameters measured by CT-analyzer have been validated on both virtual objects and aluminum foil and wire phantoms^{37, 38}. Model construction was done by the “Double time cubes” method³⁹. Interconnectivity was evaluated by making the ROI’s boundary (Shrink-wrap procedure) to follow a volume of a given specific size (voxel) of 0, 12, 24, 48 or 96 μm and measuring how much volume was occupied by these objects in comparison to the total porosity available. Analysis of the total porosity (Standard 3D analysis) included the close and open porosity, while a process performed with a volume of 0 μm gave only the open porosity.

2.2.4. Mechanical characterization

The compressive strength (σ_c) and modulus of Elasticity (E) of the samples were measured with a mechanical testing bench (858 MiniBionixII[®], MTS, USA) at a cross-head speed of $0.5 \text{ mm}\cdot\text{min}^{-1}$. Samples were tested after 0, 3, 7, 21 and 56 days of immersion in Ringer’s solution at 37 °C. Three CPC, or CPC-PLGA, cylindrical samples - for each possible condition presented at section 2.1. - were immersed in a flask with 20 ml of

Ringer's solution. Six samples per condition (n=6, two flasks) were tested. When applicable, solution was renewed every week.

2.3. Statistical analysis

Statistical analysis was performed by applying linear regression to the experimental data obtained from the mechanical tests. An analysis of the relation between the independent variables, *i.e.* time, percentage, type of polymer and particle size, was performed. The reference for the independent variables was 0 day, 10%, LMW and S particle size, respectively. These analyses were done separately for σ_c and E as independent variables. The regression analysis gave the coefficients of the relation between the independent variables and their significance. For testing a threshold of 0.05 for significance and 95% confidence intervals were used. Statistics were performed by using SPSS software (version 16; SPSS Inc, USA).

3. Results

3.1. Morphological analysis

Figure 1a depicts a representative image of the spherical PLGA microparticles obtained via the double emulsion process. The specific manufacturing parameters described earlier allowed producing small (S) and big (B) PLGA microparticles. B- and S-PLGA LMW microparticles were found to measure 42.47 ± 1.14 and 19.10 ± 0.07 μm in diameter, respectively. B- and S-PLGA HMW microparticles measured 34.14 ± 3.39 and 18.22 ± 0.45 μm , respectively.

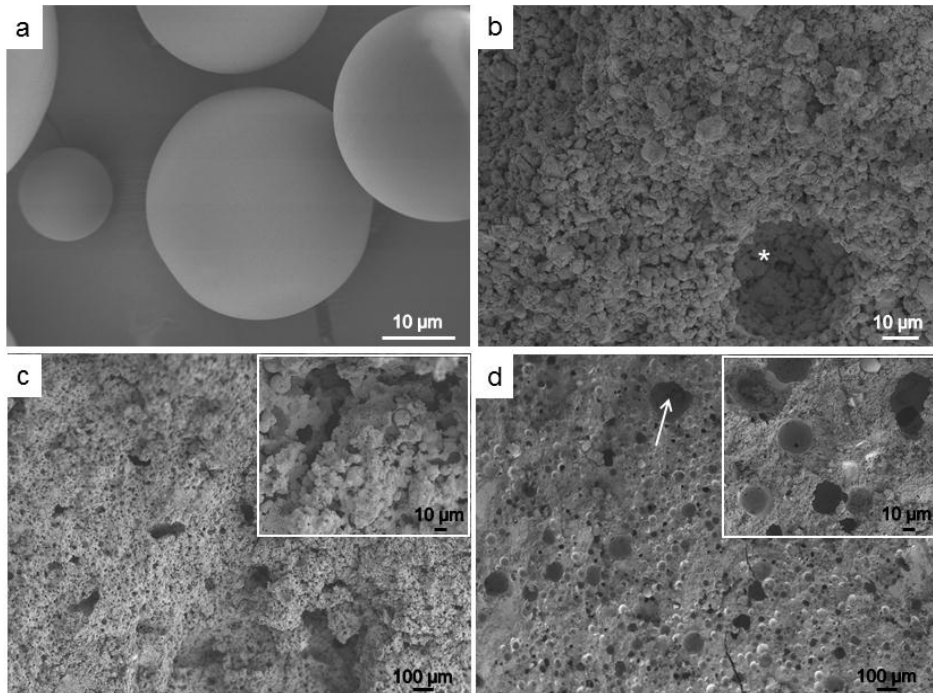


Figure 1. SEM images of (a) PLGA particles obtained by the double-emulsion process; (b) CPC alone showing a mesopore (*) created by air entrapment; (c) CPC loaded with 30 wt.% of small ($\sim 20 \mu\text{m}$) LMW PLGA particles; and (d) CPC loaded with 10 wt.% of big ($\sim 40 \mu\text{m}$) HMW PLGA particles. Frames inside (c) and (d) are close-ups of these samples. The arrow on (d) shows a pore of a size of $\sim 100 \mu\text{m}$.

SEM revealed that CPC (Figure 1b) showed a microstructure with only microporosity due to the dissolution-precipitation hardening mechanism, as is the consequence of the mixing of CPC powder with the liquid phase. The incorporation of PLGA microparticles appeared to increase the mesoporosity of the CPC (Figure 1c, d). Figure 1d shows a pore of around $100 \mu\text{m}$ in diameter. The increment of porosity by adding PLGA was confirmed by the porosity measurements (Figure 2a). The relationship between the micro- and mesoporosity was found to be linear (Figure 2b).

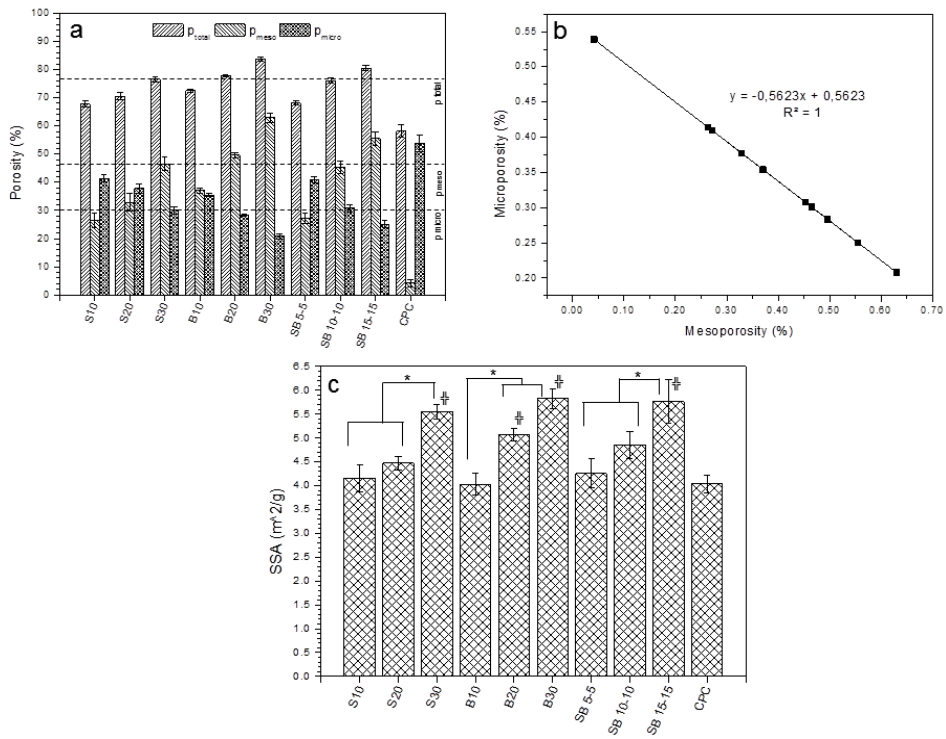


Figure 2. (a) Porosity, (b) relationship between micro- and mesoporosity and (c) SSA for the different basic CPC-PLGA samples. Lines in (a) indicate the minimal porosities values that were found for samples to be significant in (c). S: Small particles ($\approx 20 \mu\text{m}$). B: Big particles ($\approx 40 \mu\text{m}$) and SB: Mixture of small and big particles. Numbers next to prefixes are the weight percentages of PLGA loaded into the CPC. ‡: Significant different ($p < 0.05$) versus CPC samples. *: Significant different ($p < 0.05$).

SSA (Figure 2c) was shown to be influenced by the amount and size of the incorporated porogen. For S microparticles, the incorporation of 30 wt% resulted in a significantly increased SSA compared with the incorporation of lower percentages. In contrast, for B microparticles, 20 wt% had already a significant effect on SSA. Incorporation of both microparticle sizes in a 1:1 ratio had only a significant effect when 30 wt% was included. Comparison with the control CPC revealed the same significant behavior for these samples CPC-PLGA that were significant among their groups. For the significant compositions ($p < 0.05$), the minimal total and mesoporosity

was at least 77% and 47%, respectively, while the microporosity had a maximal value of 30% (Figure 2a).

3.2. PLGA degradation and CPC transformation

Raman spectrometry (Figure 3) provided information about the degradation rate of PLGA microparticles and transformation of the CPC material. A clear degradation of the PLGA polymers after immersion was shown by Raman spectroscopy (Figure 3a, b). Depending on the type of polymer, the decrease on the ester bonds ($\approx 1767 \text{ cm}^{-1}$) occurred at different rates. For LMW, it changed at a rate of 1.47% per day and for the HMW at 1.35% per day. As a result, the 50% degradation state was reached at 34 days and 36.5 days for LMW and HMW PLGA, respectively. Raman of CPC revealed the characteristic PO_4 bands in the spectrograms (Fig. 3c)⁴⁰. However, no clear transformation was observed during immersion time.

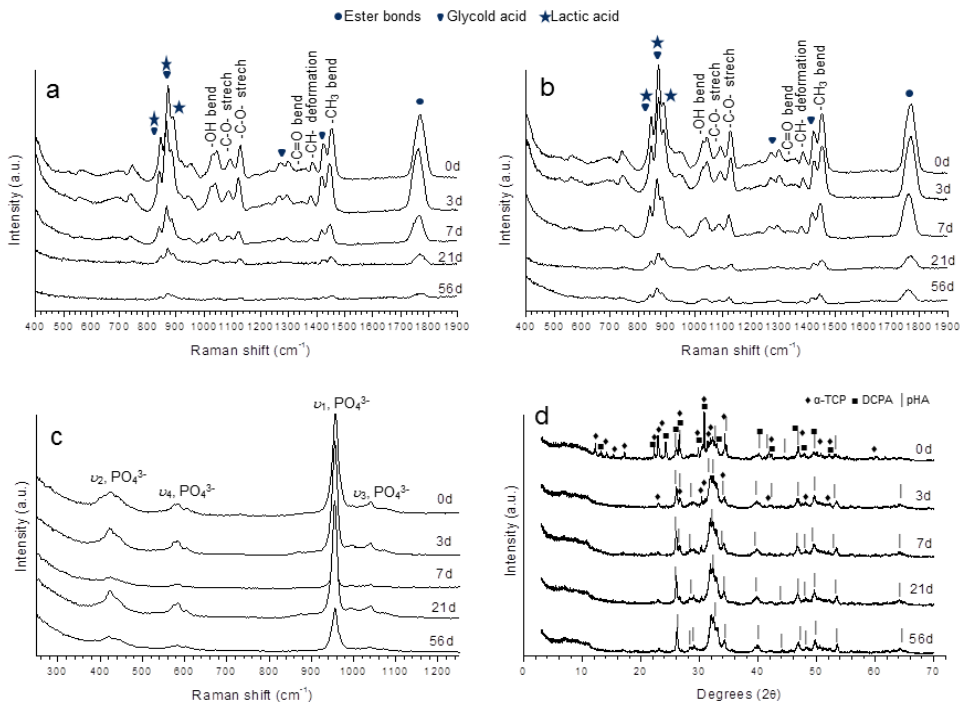


Figure 3. Raman spectra of (a) LMW PLGA, (b) HMW PLGA and (c) CPC and (d) XRD spectra of CPC after the different immersion times used in this study.

In contrast, XRD analysis (Fig. 3d) of CPC gave better information about the transformation process. After 3 days of immersion, some α -TCP was still detected, but after 7 days the CPC was completely hydrolyzed into an apatite CaP type.

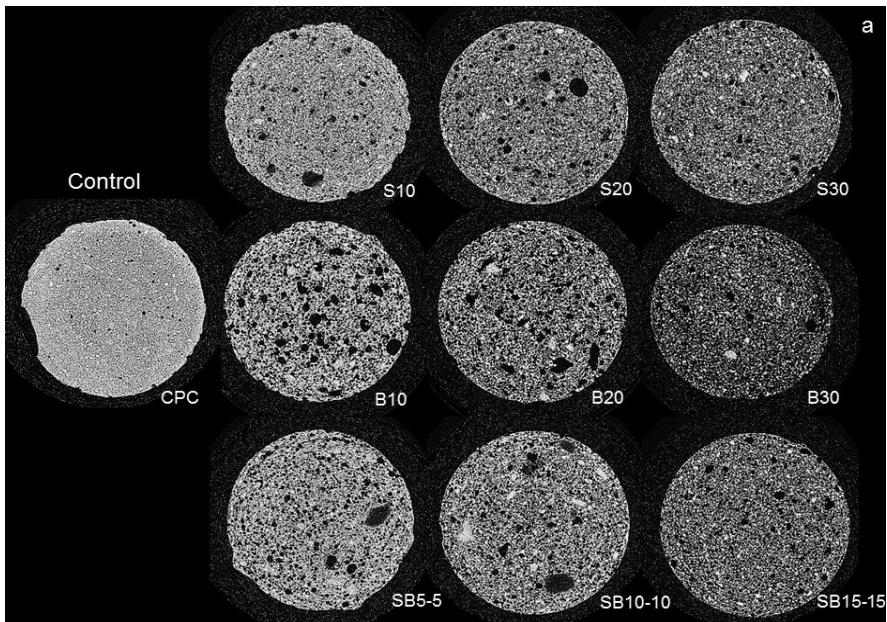


Figure 4. Representative μ -CT cross-sections, 4.5 mm in diameter, of the different basic CPC-PLGA samples. S: Small particles ($\approx 20 \mu\text{m}$). B: Big particles ($\approx 40 \mu\text{m}$) and SB: Mixture of small and big particles. Numbers next to prefixes are the weight percentages of PLGA loaded into the CPC.

3.3. Pore interconnectivity

μ -CT of CPC and CPC-PLGA samples (Figure 4) allowed the observation of differences in the mesoporous morphology. μ -CT showed that the pores, as made by the porogens, were round and smooth. PLGA loaded samples were more porous than the CPC control, as evidenced by a less whiter image, indicating less presence of CPC or a less dense material. This change in morphology was found to be dependent upon the amount, size and ratio of the incorporated microparticles. These observations corroborate the porosity and SSA measurements. μ -CT interconnectivity analysis

showed clearly that the loading amount and size of porogen had an effect on this property (Figure 5).

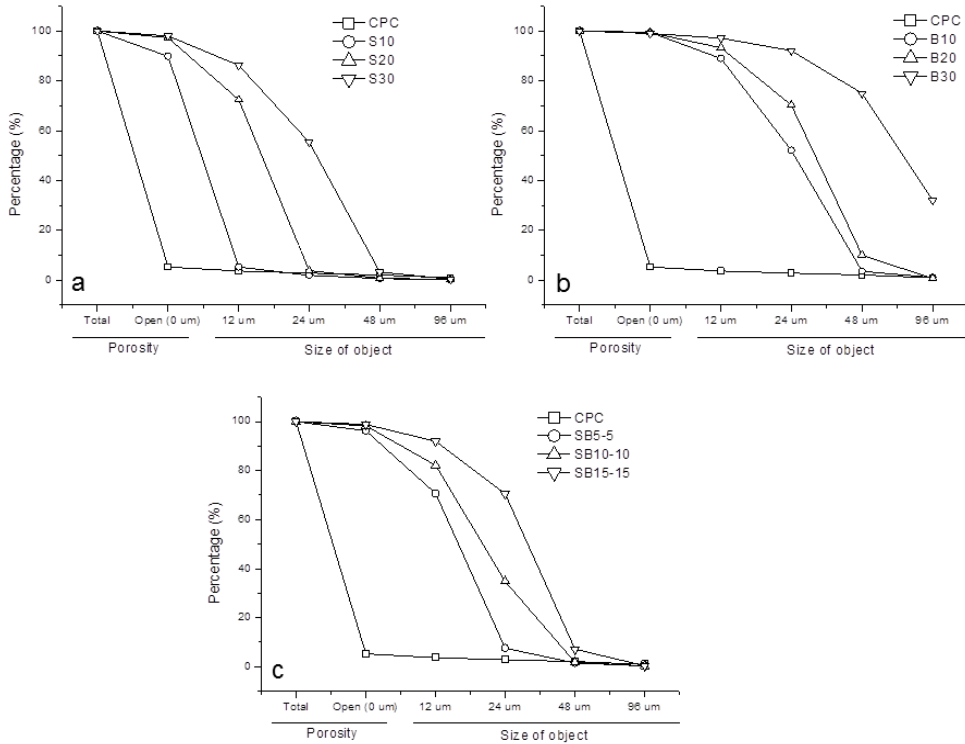


Figure 5. Percentage of porosity available that is interconnected to allow the penetration of an object of a given size in the CPC with (b) Small ($\approx 20 \mu\text{m}$) PLGA particles, (c) Big ($\approx 40 \mu\text{m}$) PLGA particles and (d) Mixture of small and big (S-B, ratio 1:1) PLGA particles versus the CPC alone. S: Small particles ($\approx 20 \mu\text{m}$). B: Big particles ($\approx 40 \mu\text{m}$) and SB: Mixture of small and big particles. Numbers next to prefixes are the weight percentages of PLGA loaded into the CPC.

The ability of volume objects of 0 (open porosity), 12, 24, 48 and $96 \mu\text{m}$ to occupy a given percentage of the available porosity was influenced by the amount and size of the microparticles. CPC has mainly a closed microporosity and almost no objects can penetrate into it. The addition of PLGA increases the percentage of total open porosity and porosity available to objects of sizes ranging from 12 to $96 \mu\text{m}$. Depending on the

particle size -or ratio- and the percentage loaded, the percentage of available open porosity changes. The addition of 20 or 30 wt% of S-PLGA to CPC, or a ratio 1:1, had an evident effect on the total open porosity. Loading B-PLGA, even at the lower amount of 10 wt%, increased the total open porosity to almost 100%. In the same manner, the percentage of porosity accessible to larger objects increases as a function of the particle size -or ratio- and the percentage loaded. For a CPC with 30 wt% of S-PLGA, the maximal object size able to enter the composite is 48 μm but in a percentage slightly higher than zero. Using a ratio of 1:1 maintains this limitation, but increased the percentage to almost 10%. On the other hand, 30 wt% of B-PLGA allows a maximal object size of 96 μm to invade around 30% of the total porosity. The rest of the samples are in between the aforementioned behaviors. Samples with a lower weight percentage and smaller particle size were closer to a non-interconnected sample. An increase in the size and amount of microparticles makes the CPC-PLGA samples to move away from a closed porosity situation, i.e. 0 μm , towards a larger interconnected porosity accessible for larger objects, i.e. 96 μm . Figure 6 show that the mean size of the open pores for the CPC control was the lowest with a value around 42 μm . For samples with small microparticles and 1:1 ratios, as the loaded amount increases the mean particle size decreases. For CPC with S-PLGA it went from 58 to 50 μm for loads of 10 and 30 wt%.

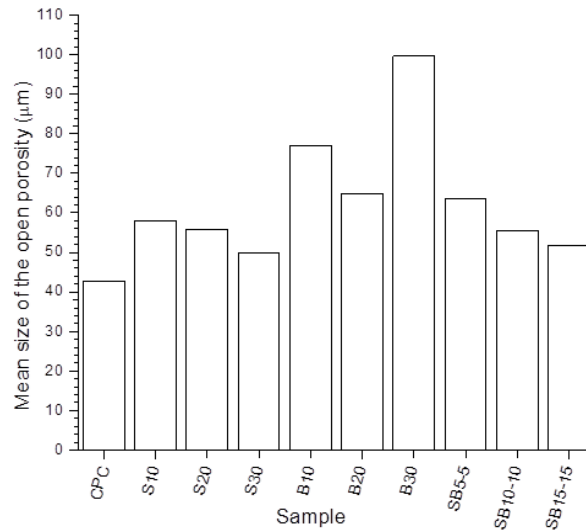


Figure 6. Mean size of the open porosity for the different CPC-PLGA basic samples. S: Small particles ($\approx 20 \mu\text{m}$). B: Big particles ($\approx 40 \mu\text{m}$) and SB: Mixture of small and big particles. Numbers next to prefixes are the weight percentages of PLGA loaded into the CPC.

For CPC samples with 1:1 ratios it changed from 64 to 52 μm for the same percentages mentioned before. However adding only B-PLGA microparticles produced the biggest mean size as it was around 78 μm for a 10 wt% and 100 μm for a 30 wt%. These behaviors may be related to the pore size distributions (Fig. 7). Figure 7 shows that a CPC sample with 30 wt% B-PLGA has the broader pore size distribution compared to the rest of the samples.

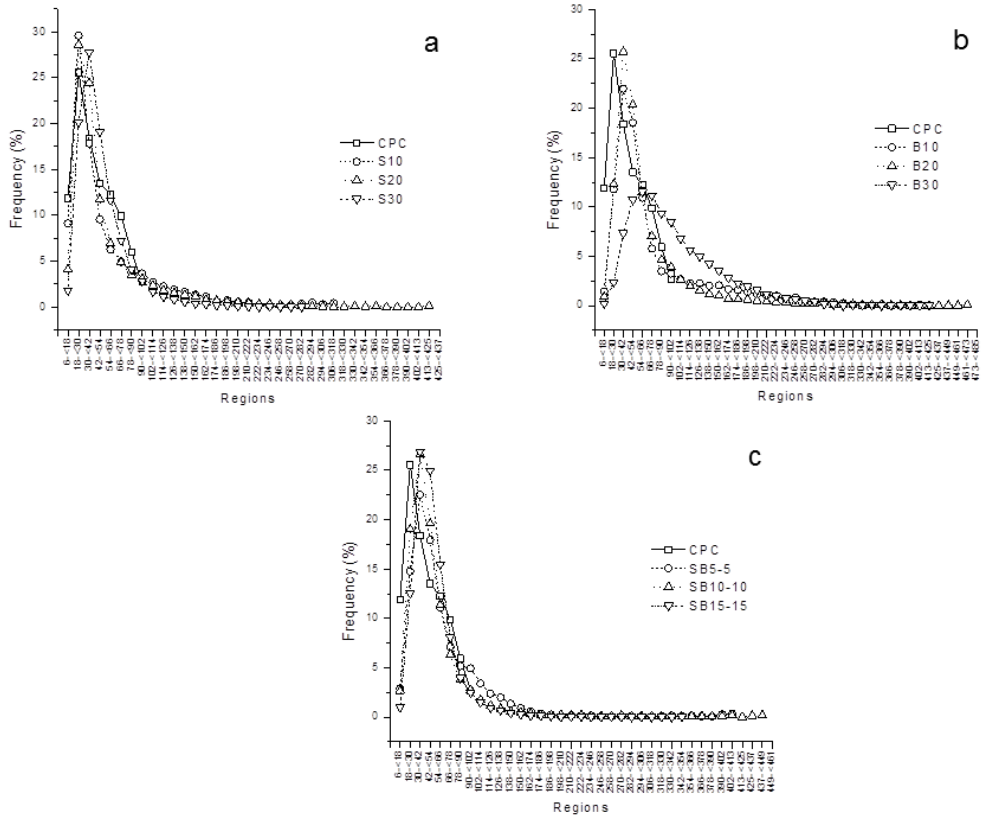


Figure 7. Percentage distribution (or frequency) of the porosity size regions available on their open porosity in the CPC with (a) Small ($\approx 20 \mu\text{m}$) PLGA particles, (b) Big ($\approx 40 \mu\text{m}$) PLGA particles and (c) Mixture of small and big (S-B, ratio 1:1) PLGA particles versus the CPC alone. S: Small particles ($\approx 20 \mu\text{m}$). B: Big particles ($\approx 40 \mu\text{m}$) and SB: Mixture of small and big particles. Numbers next to prefixes are the weight percentages of PLGA loaded into the CPC.

3.4. Mechanical characterization and statistical analysis

Figure 8 shows the general results of the mechanical tests as well as the fitted curves for these results. The amount of loaded PLGA, independent of the size and PLGA type, had the most noticeable effect on the σ_c values. Compared to CPC, before immersion (0 day), the σ_c of CPC-PLGA samples loaded with 10 wt% PLGA was reduced by 35% of that of the CPC control. This reduction went down to 55% of the CPC control for CPC-PLGA samples loaded with 30 wt% PLGA. After the different immersion times

these values continued to decrease while maintaining the differences between the percentages of PLGA loaded. The different compositions showed a similar effect during the immersion times without obvious differences between the sizes, PLGA type or their ratios. Comparison of the development of the mechanical properties for the different combinations (Figure 8b) versus the percentages of PLGA loaded (Figure 8a) indicates that the range of σ_c values for the combinations, *i.e.* when considering polymer type and particle size, is narrower than those for the percentages, *i.e.* when considering only the amount loaded. The fitted curves clearly show that the σ_c and E values of CPC increases towards an immersion period of 7 days and then decrease again. Nevertheless, this effect was not significant.

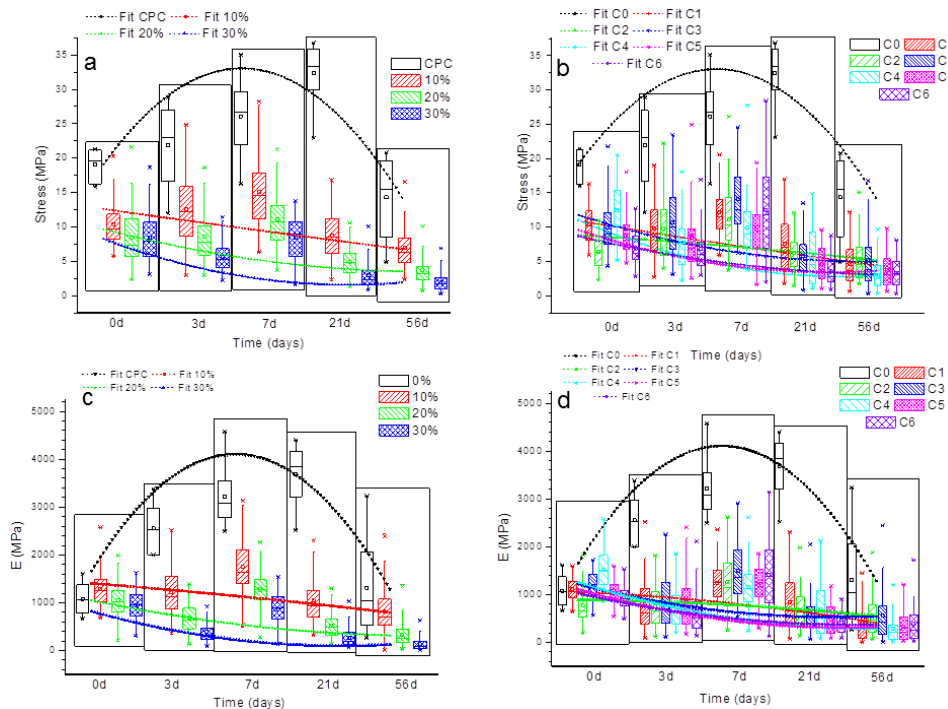


Figure 8. Grouped results of the mechanical properties, with their fitting curves, for the CPC-PLGA samples according to the percentage of PLGA loaded into the CPC (a. c) and according to the different combinations of particle size and polymer type presented in Table 1 (b. d).

Statistical analysis (Table 2 and Table 3) confirmed that the major influencing parameters for the mechanical properties were the percentage of porogen loaded and immersion time. 30 wt% of PLGA and 56 days of immersion produced the more negative coefficients, in a significant way ($p < 0.001$), for σ_c and E . Coefficients indicate the effect that the given parameters will have compared with a CPC sample with 10 wt% S-PLGA without immersion (0 day). Since CPC serves as the control and its properties at all immersion times are better than for all CPC-PLGA samples, control CPC groups were not considered in the statistical analysis. The results for the coefficients and significances, as listed in Tables 2 and 3, show that: (1) the use of LMW and HMW PLGA was not a significant parameter for the obtained σ_c , (2) the use of LMW and HMW PLGA, or HMW PLGA alone, was not a significant parameter for the obtained E and (3) an immersion period of 3 days did not affect the σ_c measurements. The combination of LMW and HMW PLGA microparticles, HMW PLGA microparticles alone or 7 days of immersion time produced a positive coefficient on the statistical analysis of the mechanical properties, i.e. these parameters help to the strength of the material.

Table 2. Statistical analysis of the parameters for the independent variables for the stress (adjusted $R^2 = 0.599$) compared against a CPC sample with 10 wt% S-PLGA LMW at 0 days considered as the constant. LMW and HMW mean low and high molecular weight PLGA, respectively. Small $\approx 20 \mu\text{m}$. Big $\approx 40 \mu\text{m}$. The confidence interval indicates the reliability of the estimate.

Parameter	Coefficient	Significance	95% Confidence Interval	
			Lower bound	Upper bound
Constant ^b	13.10	$p < 0.001$	12.64	13.56
20 wt%	-3.41	$p < 0.001$	-3.77	-3.06
30 wt%	-5.27	$p < 0.001$	-5.63	-4.91
Mix: LMW – HMW	0.26	0.219	-0.15	0.67
HMW	0.66	$p < 0.001$	0.33	0.99
Mix: Small - Big	-1.31	$p < 0.001$	-1.72	-0.90
Big	-2.87	$p < 0.001$	-3.21	-2.54
3 days	-0.21	0.381	-0.67	0.26
7 days	2.42	$p < 0.001$	1.95	2.88
21 days	-3.58	$p < 0.001$	-4.04	-3.12
56 days	-4.95	$p < 0.001$	-5.41	-4.49

Table 3. Statistical analysis of the parameters for the independent variables for the modulus of elasticity (adjusted $R^2 = 0.620$) compared against a CPC sample with 10 wt% S-PLGA LMW at 0 days considered as the constant. LMW and HMW mean low and high molecular weight PLGA, respectively. Small $\approx 20 \mu\text{m}$. Big $\approx 40 \mu\text{m}$. The confidence interval indicates the reliability of the estimate.

Parameter	Coefficient	Significance	95% Confidence Interval	
			Lower bound	Upper bound
Constant ^b	1558.39	$p < 0.001$	1505.32	1611.46
20 wt%	-447.75	$p < 0.001$	-488.87	-406.63
30 wt%	-701.47	$p < 0.001$	-742.59	-660.35
Mix: LMW – HMW	33.00	0.171	-14.23	80.24
HMW	35.88	0.065	-2.19	73.95
Mix: Small - Big	-87.91	$p < 0.001$	-135.14	-40.67
Big	-203.87	$p < 0.001$	-241.95	-165.80
3 days	-331.64	$p < 0.001$	-384.73	-278.55
7 days	199.07	$p < 0.001$	145.99	252.16
21 days	-486.39	$p < 0.001$	-539.48	-433.30
56 days	-678.21	$p < 0.001$	-731.30	-625.12

4. Discussion

The present work aimed to characterize the effect of incorporating PLGA, with mesoporous sizes, on the properties of CPC. Different loading percentages of PLGA were used (10, 20 and 30 wt%). Within these percentages, two different particle sizes (S and B) using two types of polymers (HMW and LMW), were prepared by a double emulsification process. In addition, the ratio between the type and size (Table 1) was changed within the percentages to better understand the effect of incorporating mesoporous and biodegradable PLGA on the properties of the final CPC.

Several studies have already been performed using porogens and CPC¹¹⁻¹³. Nevertheless, a clear reason -in terms of porosity and interconnectivity- for choosing certain sizes and percentages as included into the CPC has not been provided. In this study, the double emulsion process was a limiting factor. Both polymers have different molecular weights, which affects the stability of the PLGA-DCM solutions during the manufacturing of the microparticles. In the same PLGA-DCM proportions a LMW-PLGA is less stable than a HMW-PLGA. This stability increases when more LMW-PLGA is added into the DCM. The finally obtained particle size is also affected by the teeth relationship of the rotor-stator and the distance between these. Nevertheless, by increasing the amount of LMW PLGA in DCM, similar particles sizes compared with the HMW PLGA microparticles and without having to change the aforementioned parameters were obtained.

The current formulation of CPC was chosen on basis of the characteristics as required for clinical application and other properties as related to the materials^{31, 41}. A maximum of 30 wt% of microparticle loading was selected since this has been reported to be the percentage that generates a good biological response, while maintaining the scaffold stability¹¹. In any case, a certain degree of sample stability is needed, during demolding and handling steps involved in the study. If scaffolds are not solid enough they will collapse during this procedure. However, *in vivo* these requirements may be different. Compared to our previous study³¹, the measured SSA of

the presently prepared CPC was low ($21.5 \text{ m}^2 \cdot \text{g}^{-1}$ vs $4 \text{ m}^2 \cdot \text{g}^{-1}$). Evidently, there is an effect of the thermal treatment, as used to burn the PLGA, on the SSA. Previous studies on the effect of thermal treatments on α -TCP or HA corroborate with this observation^{42, 43}. Still, the significant differences, as observed for the various samples, can be considered valid since all samples received this treatment. As SSA increases, the biological response to a given CPC should be better and its resorption should be faster. In our case, a higher SSA could mean either less agglomerated or smaller CaP crystals. CPC transformation could better be detected by XRD than by Raman. Raman did not allow the observation of clear differences in the CPC transformation. This limited detection of the CPC transformation by Raman can be due to the technique, which analyses small regions (spatial resolution $\sim 700 \text{ nm}$) of the sample as compared to XRD. As a consequence, Raman microspectroscopy could have measured regions where the crystallinity was different from the rest of the sample due to the lack of open porosity. This has been signaled before⁴⁴. Hence, the intensity of the peaks at a given immersion time is affected and does not allow the observation of a clear tendency. One possibility to compensate for this could be to perform a high number of randomized measurements on a sample.

Several studies have been performed on the effect of macroporosity on CPC properties^{45, 46}. Levengood *et al.*²⁹ studied the role of microporosity, i.e. $0.5 - 10 \text{ }\mu\text{m}$ on ceramic materials. However, mesoporosity has also been found to be able to support bone ingrowth^{47, 48}. Lu *et al.*⁴⁹ studied the role of pore interconnectivity for porous CaP. They found that $50 \text{ }\mu\text{m}$ is the minimum interconnection size to assure bone formation. Malafaya *et al.*⁵⁰ proposed a $53 \text{ }\mu\text{m}$ as minimum, since *in vivo* lower values than this will not be relevant for bone ingrowth. Loading 30 wt% of B-PLGA into the CPC may be creating enough clusters of PLGA microparticles to allow interconnected spaces for objects of $96 \text{ }\mu\text{m}$ by creating a broader pore distribution. The effect of particles clusters on interconnectivity has been studied deeply by Descamps *et al.*^{43, 49, 51} If the particle size is increased, the loading amount may be reduced while keeping the same interconnectivity. However, using

smaller particles would increase the general porosity of the cement, producing a faster resorption. In addition, it should be also easier to inject smaller particles, *e.g.* 30 μm vs. 200 μm .

Interconnectivity and pore-size distribution results must be considered together in order to understand the materials properties better. Air-entrapment may create mesopores in the structure of a CPC without porogens. The resulting mesopores are of similar size as the mesoporosity introduced by the porogens. Hence, such “air-entrapped” mesopores indeed affect to some extent the mechanical properties of a CPC without porogen and contribute to the total porosity. However, since their number is low and the distance from each other is far, CPC samples present an interconnectivity analysis with an almost inexistent open porosity. Having a broad pore size distribution but lacking the right interconnectivity will not allow an optimal bone formation. Nevertheless, the development of the mechanical properties and the CPC bulk properties will also be expected to change. The differences and reduction in mechanical properties are related to the discontinuity as induced by these PLGA microparticles on the CPC continuous matrix as well as their degradation, which creates an empty void over a period of time⁵². In our case, this degradation happens at the same time that hydrolysis of the α -TCP and crystal growth of the apatite CaP type occurs in the CPC. The combined phenomenon of crystal growth and PLGA degradation explains the “improvement” in mechanical properties at 7 days of immersion in Ringer’s solution with any of the polymers. At 7 days, CPC has reached a full transformation from α -TCP to calcium deficient apatite and only around 10% of the PLGAs are hydrolyzed. This behavior will differ if the porogen degrades, or the CPC transforms, differently than the currently used materials⁵³.

The effect of the loading of mesoporous PLGA microparticles on the mechanical and bulk properties, such as porosity, SSA and interconnectivity, can be used to tune a desired *in vivo* response by playing with the CaP phases, as present in the CPC, while still maintaining specific material properties. In addition, due to PLGA degradation by hydrolysis, the surrounding pH of the space, as occupied by the porogen, can be

modified. This can influence the characteristics of the CPC and the cellular response, like the presence of macrophages and/or inflammatory reaction, which can support then the degradation of the CPC^{54,55}.

These characteristics, plus the degradation behavior of the porogen, can be used as an indicator of how bone ingrowth should be stimulated/generated in order to maintain or increase the mechanical properties and match those of the ingrowing bone. We know that, for the materials used here, 10% of the PLGA will be degraded within 7 days, and that 50% of the porosity has to be filled with immature bone at 35 days.

5. Conclusion

The design of this study focused on the little-known effect of the mesoporous region in CPC. The influence of the mesoporosity, as created by a PLGA porogen loaded into a CPC, on the bulk properties was demonstrated. A clear and tangible effect of the loading amount, particle size and mixing ratios on the interconnectivity and mechanical properties was found. Maximal mesoporosity and minimal microporosity values were found to create a significant surface area, while allowing specific interconnectivity percentages of objects of specific sizes and mechanical stability. On basis of the obtained data from the results of this study, we recommend the use of porogens with a minimum size of 40 μm , and incorporated at an amount of 30 wt% in CPC, as appropriate. Future efforts should be directed to the degradation and resorption of the CPC material tuned with PLGA microparticle degradation.

References

1. Jansen J.A., Ooms E., Verdonschot N., Wolke J.G.C. Injectable calcium phosphate cement for bone repair and implant fixation. *Orthop Clin North Am* 2005;36:89-95.
2. LeGeros R.Z. Properties of osteoconductive biomaterials: Calcium phosphates. *Clin Orthop Relat Res* 2002;395:81-98.

3. Bohner M. Physical and chemical aspects of calcium phosphates used in spinal surgery. *Eur Spine J* 2001;2:S114-121.
4. Ooms E.M., Wolke J.G., van der Waerden J.P., Jansen J.A. Trabecular bone response to injectable calcium phosphate (Ca-P) cement. *J Biomed Mater Res A* 2002;1:9-18.
5. del Real R.P., Ooms E., Wolke J.G., Vallet-Regi M., Jansen J.A. In vivo bone response to porous calcium phosphate cement. *J Biomed Mater Res A* 2003;1:30-36.
6. Almirall A., Larrecq G., Delgado J.A., Martinez S., Planell J.A., Ginebra M.P. Fabrication of low temperature macroporous hydroxyapatite scaffolds by foaming and hydrolysis of an alpha-TCP paste. *Biomaterials* 2004;17:3671-3680.
7. Barralet J.E., Grover L., Gaunt T., Wright A.J., Gibson I.R. Preparation of macroporous calcium phosphate cement tissue engineering scaffold. *Biomaterials* 2002;23:3063-3072.
8. Dorozhkin S.V. Bioceramics of calcium orthophosphates. *Biomaterials* 2010;31:1465-1485.
9. Habraken W.J.E.M., Zhang Z., Wolke J.G.C., Grijpma D.W., Mikos A.G., Feijen J., Jansen J.A. Introduction of enzymatically degradable poly(trimethylene carbonate) microspheres into an injectable calcium phosphate cement. *Biomaterials* 2008;29:2464-2476.
10. Link D.P., van den Dolder J., Jurgens W.J.F.M., Wolke J.G.C., Jansen J.A. Mechanical evaluation of implanted calcium phosphate cement incorporated with PLGA microparticles. *Biomaterials* 2006;27:4941-5017.
11. Ruhe P.Q., Hedberg E.L., Padron N.T., Spauwen P.H.M., Jansen J.A., Mikos A.G. Biocompatibility and degradation of poly(DL-lactic-co-glycolic acid)/calcium phosphate cement composites. *J Biomed Mater Res Part A*. 2005;74A:533-544.

12. Bodde E.W., Habraken W.J., Mikos A.G., Spauwen P.H., Jansen J.A. Effect of polymer molecular weight on the bone biological activity of biodegradable polymer/calcium phosphate cement composites. *Tissue Eng* 2009;15:3183-191.
13. Habraken W.J., Wolke J.G., Mikos A.G., Jansen J.A. Injectable PLGA microsphere/calcium phosphate cements: physical properties and degradation characteristics. *J Biomater Sci* 2006;17:1057-1074.
14. Shive M.S., Anderson J.M. Biodegradation and biocompatibility of PLA and PLGA microspheres. *Adv Drug Deliv Rev* 1997;28:5-24.
15. Fujiwara M., Shiokawa K., Tanaka Y., Nakahara Y. Preparation and formation mechanism of silica microcapsules (hollow sphere) by water/oil/water interfacial reaction. *Chem Mater* 2004;16:5420-5426.
16. Ha C.S., Gardella J.A. Surface chemistry of biodegradable polymers for drug delivery systems. *Chem Rev* 2005;105:4205-4232.
17. Sahoo S.K., Panda A.K., Labhasetwar V. Characterization of porous PLGA/PLA microparticles as a scaffold for three dimensional growth of breast cancer cells. *Biomacromolecules* 2005;6:1132-1139.
18. Cui C.J., Schwendeman S.P. Surface entrapment of polylysine in biodegradable poly(DL-lactide-co-glycolide) microparticles. *Macromolecules* 2001;34:8426-8433.
19. Hai M., Bernath K., Tawfik D., Magdassi S. Flow cytometry: A new method to investigate the properties of water-in-oil-in-water emulsions. *Langmuir* 2004;20:2081-2085.
20. Shum H.C., Lee D., Yoon I., Kodger T., Weitz D.A. Double emulsion templated monodisperse phospholipid vesicles. *Langmuir* 2008;24:7651-7643.
21. Yang S., Liu H.R., Zhang Z.C. Fabrication of novel multihollow superparamagnetic magnetite/polystyrene nanocomposite

- microspheres via water-in-oil-in-water double emulsions. *Langmuir* 2008;24:1395-1401.
22. Yang Y.Y., Chia H.H., Chung T.S. Effect of preparation temperature on the characteristics and release profiles of PLGA microspheres containing protein fabricated by double-emulsion solvent extraction/evaporation method. *J Control Rel* 2000;69:81-96.
 23. Karageorgiou V., Kaplan D. Porosity of 3D biomaterial scaffolds and osteogenesis. *Biomaterials* 2005;26:5474-5491.
 24. Lacroix D., Chateau A., Ginebra M.P., Planell J.A. Micro-finite element models of bone tissue-engineering scaffolds. *Biomaterials* 2006;27:5326-5334.
 25. Pecqueux F., Tancret F., Payraudeau N., Bouler J.M. Influence of microporosity and macroporosity on the mechanical properties of biphasic calcium phosphate bioceramics: Modelling and experiment. *J Eur Ceram Soci* 2010;30:819-829.
 26. Zhang J.T., Tancret F., Bouler J.M. Fabrication and mechanical properties of calcium phosphate cements (CPC) for bone substitution. *Mater Sci Eng C* 2011;31:740-747.
 27. Le Ray A.M., Gautier H., Bouler J.M., Weiss P., Merle C. A new technological procedure using sucrose as porogen compound to manufacture porous biphasic calcium phosphate ceramics of appropriate micro- and macrostructure. *Ceram Int* 2010;36:93-101.
 28. Ginebra M.P., Delgado J.A., Harr I., Almirall A., Del Valle S., Planell J.A. Factors affecting the structure and properties of an injectable self-setting calcium phosphate foam. *J Biomed Mater Res A* 2007;80:351-361.
 29. Lan Levengood S.K., Polak S.J., Wheeler M.B., Maki A.J., Clark S.G., Jamison R.D., Wagoner J.J.A.J. Multiscale osteointegration as a new paradigm for the design of calcium phosphate scaffolds for bone regeneration. *Biomaterials* 2010;31:3552-3563.

30. Hindmarsh J.P., Su J.H., Flanagan J., Singh H. PFG-NMR analysis of intercompartment exchange and inner droplet size distribution of W/O/W emulsions. *Langmuir* 2005;21:9076-9084.
31. Heredia M.A.L., Bohner M., Zhou W., Winnubst A.J., Wolke J.G., Jansen J.A. The effect of ball milling grinding pathways on the bulk and reactivity properties of calcium phosphate cements. *J Biomed Mater Res B Appl Biomater* 2011;98:68-79.
32. Brunauer S., Emmett P.H., Teller E. Adsorption of Gases in Multimolecular Layers. *J Am Chem Soci* 1938;60:309-319.
33. Van Apeldoorn A.A., Van Manen H.J., Bezemer J.M., De Bruijn J.D., Van Blitterswijk C.A., Otto C. Raman imaging of PLGA microsphere degradation inside macrophages. *J Am Chem Soci* 2004;126:1326-1337.
34. van Manen H.J., Lenferink A., Otto C. Noninvasive Imaging of Protein Metabolic Labeling in Single Human Cells Using Stable Isotopes and Raman Microscopy. *Anal Chem* 2008;80:9576-9582.
35. Lorensen W.E., Cline H.E. Marching cubes: a high resolution 3D surface construction algorithm: *Computer graphics* 1987;21:163-169.
36. Pratt W.K. *Digital image processing*. New York: Wiley; 1991.
37. Salmon P. Loss of chaotic trabecular structure in OPG-deficient juvenile Paget's disease patients indicates a chaogenic role for OPG in nonlinear pattern formation of trabecular bone. *J Bone Miner Res* 2004;19:695-702.
38. Salmon P.L., Liu X., Sasov A. A post-scan method for correcting artefacts of slow geometry changes during micro-tomographic scans. *J Xray Sci Technol* 2009;17:161-174.
39. Bouvier D.J. Double-Time Cubes: A Fast 3D Surface Construction Algorithm for Volume Visualization. *Proc Int Conf Imaging Science Systems and Technology*; Las Vegas, 1997.

40. Silva C.C., Sombra A.S.B. Raman spectroscopy measurements of hydroxyapatite obtained by mechanical alloying. *J Phy and Chem Solids* 2004;65:1031-1033.
41. Liao H., Walboomers X.F., Habraken W.J.E.M., Zhang Z., Li Y., Grijpma D.W. Injectable calcium phosphate cement with PLGA, gelatin and PTMC microspheres in a rabbit femoral defect. *Acta Biomater* 2011;7:1752-1759.
42. Bohner M., Brunner T.J., Doebelin N., Tang R., Stark W.J. Effect of thermal treatments on the reactivity of nanosized tricalcium phosphate powders. *J Mater Chem* 2008;18:4460-4467.
43. Descamps M., Hornez J.C., Leriche A. Effects of powder stoichiometry on the sintering of [beta]-tricalcium phosphate. *J Ceramic Soci* 2007;27:2401-2406.
44. Combes C., Miao B., Bareille R., Rey C. Preparation, physical-chemical characterisation and cytocompatibility of calcium carbonate cements. *Biomaterials* 2006;27:1945-1954.
45. Ginebra M.P., Espanol M., Montufar E.B., Perez R.A., Mestres G. New processing approaches in calcium phosphate cements and their applications in regenerative medicine. *Acta Biomater* 2010;6:2863-2873.
46. Miño-Fariña N., Muñoz-Guzón F., López-Peña M., Ginebra M.P., del Valle-Fresno S., Ayala D., Gonzalez C.A. Quantitative analysis of the resorption and osteoconduction of a macroporous calcium phosphate bone cement for the repair of a critical size defect in the femoral condyle. *The Veter J* 2009;179:264-272.
47. Boby J.D., Pilliar R.M., Cameron H.U., Weatherly G.C. The optimum pore size for the fixation of porous-surfaced metal implants by the ingrowth of bone. *Clin Orthop Relat Res* 1980;150:263-270.
48. Itala A.I., Ylanen H.O., Ekholm C., Karlsson K.H., Aro H.T. Pore diameter of more than 100 microm is not requisite for bone ingrowth in rabbits. *J Biomed Mater Res* 2001;58:679-683.

49. Lu J.X., Flautre B., Anselme K., Hardouin P., Gallur A., Descamps M., Thierry B. Role of interconnections in porous bioceramics on bone recolonization in vitro and in vivo. *J Mater Sci Mater Med* 1999;10:111-1120.
50. Malafaya P.B., Santos T.C., van Griensven M., Reis R.L. Morphology, mechanical characterization and in vivo neo-vascularization of chitosan particle aggregated scaffolds architectures. *Biomaterials* 2008;29:3914-3926.
51. Descamps M., Duhoo T., Monchau .F, Lu J., Hardouin P., Hornez J.C., Leriche A. Manufacture of macroporous [beta]-tricalcium phosphate bioceramics. *J Ceramic Soci* 2008;28:149-157.
52. Tancret F., Bouler J.M., Chamousset J., Minois L.M. Modelling the mechanical properties of microporous and macroporous biphasic calcium phosphate bioceramics. *J Ceramic Soci* 2006;26:3647-3656.
53. Fernández E., Vlad M.D., Gel M.M., López J., Torres R., Cauch J.V., Bohner M. Modulation of porosity in apatitic cements by the use of alpha-tricalcium phosphate-calcium sulphate dihydrate mixtures. *Biomaterials* 2005;26:3395-3404.
54. Fellah B.H., Delorme B., Sohier J., Magne D., Hardouin P., Layrolle P. Macrophage and osteoblast responses to biphasic calcium phosphate microparticles. *J Biomed Mater Res A* 2010;93:1588-1595.
55. Fellah B.H., Josselin N., Chappard D., Weiss P., Layrolle P. Inflammatory reaction in rats muscle after implantation of biphasic calcium phosphate micro particles. *J Mater Sci Mater Med* 2007;18:287-294.



Chapter 6

TUNING THE DEGRADATION RATE OF CALCIUM PHOSPHATE CEMENTS BY INCORPORATING MIXTURES OF POLY(LACTIC-CO-GLYCOLIC ACID) MICROSPHERES AND GLUCONO-DELTA-LACTONE MICROPARTICLES

Kemal Sariibrahimoğlu, Jie An, Bart van Oirschot, Arnold W.G. Nijhuis, Rhandy Eman, Jacqueline Alblas, Joop G.C. Wolke, Jeroen J.J.P. van den Beucken, Sander C.G. Leeuwenburgh, John A. Jansen

1. Introduction

Bone tissue has the ability to repair itself, but when bone defects exceed a critical size (which depends on a wide variety of factors including species and anatomical site), this self-healing capacity of bone is not sufficient and additional bone grafts are required to facilitate complete healing of autografts. Autografts are considered the gold standard for bone grafting purposes, although its clinical use is associated with disadvantages including limited supply donor site morbidity and the need for additional surgery. Calcium phosphate ceramics (CaP) based materials represent a promising alternative to auto- or allograft due to the off-the-shelf availability, biocompatibility and osteoconductive properties. Pure CaPs are available in different forms such as pre-made granules and blocks, which are difficult to handle from a clinical point of view. The injectable and self-setting form of the CaP ceramics is calcium phosphate cement (CPC) which was developed to overcome these handling difficulties and achieve optimal defect filling¹⁻³.

Numerous *in vivo* studies have confirmed the beneficial biological and clinical handling behavior of cements that harden owing to hydrolysis of alpha-tricalcium phosphate (α -TCP) precursor powders to nanocrystalline hydroxyapatite (HA) as end products of the setting reaction^{4, 5}. After setting, this nanostructured HA matrix is highly osteocompatible, but its low solubility at physiological pH of 7.4^{6, 7} inhibits degradation and hence complete regeneration of bone defects in time^{2, 4, 8}. To increase the degradation rate, macro- and microporosity can be introduced in CPCs. To this end, several methods have been described such as introduction of water-soluble mannitol crystals, or the creation of porosity using *in situ* formation of carbon dioxide bubbles^{9, 10}. A more recent strategy involves the creation of macroporosity into CPCs by incorporation of biodegradable acid-producing polymeric porogens.

Acid-producing porogens composed of poly(D,L-lactic-co-glycolic) acid (PLGA) were shown to exhibit suitable properties in terms of tissue response and degradation profile¹¹. PLGA degrades by hydrolysis of ester groups in the polymer backbone¹². Degradation of PLGA leads to the

formation of porosity within the ceramic matrix and the release of innocuous acidic monomers (lactic and glycolic acid) which decrease the pH locally, thereby inducing accelerated dissolution of the CPC, since most of the calcium phosphate ceramics dissolve faster under acidic conditions^{5, 13}. The rate of PLGA degradation/erosion strongly depends on its chemical structure such as molecular weight (MW) and co-polymer composition. Nevertheless, degradation of PLGA proceeds in terms of months rather than weeks^{14, 15}. Therefore, the use of alternative acid-producing porogen was explored to dissolve CPCs at a faster rate yet in a controlled manner.

Glucono-delta-lactone (GDL) is a natural food-additive that is cheap, easily available and used as controllable acidifier of milk products. GDL received its GRAS (Generally Recognized As Safe) status in 1986 by the Food and Drug Administration (FDA) for use as curing, pickling and pH controlling agent¹⁶. Commercially available GDL microparticles can be mixed directly as porogens with the powder phase of CPCs. In aqueous systems, GDL rapidly hydrolyzes into gluconic acid within hours to days, thereby leading to a local acidification, which is an appealing material to be used as porogen for CPC and may facilitate the dissolution of the surrounding CPC matrix.

Lanao *et al.*¹⁷ recently showed that the use of a CPC containing either PLGA or GDL increased the amount of new bone formed in a rabbit femoral condyle implantation model with a faster bone ingrowth observed for cements containing 10 wt% of GDL vs. cements containing higher amounts of PLGA (43 wt%). This effect was attributed to a faster acidification of CPC containing GDL compared to PLGA-containing CPC, whereas it was observed that CPC containing high amounts of GDL (30 wt%) did not degrade due to the compact structure resulted from high acidification.

Based on these promising results, it was hypothesized that mixtures of both fast-degrading GDL and slow-degrading PLGA porogens would allow for more precise tuning of the degradation rate compared to the single use of either PLGA or GDL, but no studies had been performed yet to confirm this hypothesis.

Therefore, the effect of incorporating PLGA, GDL or mixtures thereof on the degradation of CPCs was systematically analyzed *in vitro* by analyzing the pH, release of acidic by-products, morphology, crystallinity, mechanical strength and mass loss of the CPCs as a function of soaking time in phosphate buffered saline (PBS). CPCs were implanted for 12 weeks at ectopic sites (intramuscular) to evaluate the soft tissue response and at orthotopic sites (transverse processes of the goat spine)¹⁸⁻²¹ to evaluate bone ingrowth.

2. Materials and methods

2.1. Materials

CPC powder consisted of a mixture of 95% alpha-tricalcium phosphate (α -TCP; CAM Bioceramics, Leiden, the Netherlands) and 5% precipitated hydroxyapatite (pHA; Merck, Darmstadt, Germany). Na_2HPO_4 was purchased from Merck (Darmstadt, Germany).

Poly(lactic-co-glycolic acid) (PLGA) Purasorb[®] was obtained from Purac Biomaterials (Gorinchem, the Netherlands). Purasorb[®] PDLG 5002A ($M_w = 17$ kDa, acid terminated, lactide/glycolide (L/G) ratio of 50/50) L:G = 50:50) was used to prepare microspheres. Polyvinyl alcohol (PVA; 88% hydrolyzed, $M_w = 22$ kDa) was obtained from Acros (Geel, Belgium) and isopropanol (IPN; analytical grade), dichloromethane (DCM; analytical grade) and D-(+)-Glucono-delta-lactone were obtained from Merck (Darmstadt, Germany). Gluconic acid solution was supplied by Sigma-Aldrich (Zwijndrecht, the Netherlands).

2.2. Preparation and characterization of PLGA

Dense PLGA microspheres were prepared by a single emulsion technique^{11, 20}. Briefly, 0.2 g of PLGA was dissolved in 2 mL of DCM in a 20 mL glass tube. This solution was transferred into a stirred beaker containing 100 mL of 0.3% PVA solution. Subsequently, 50 mL of 2% IPN solution was added. The solution was stirred for one hour. The microspheres were allowed to settle for 1h and the clear solution was decanted. The remaining suspension was centrifuged and the clear solution on top was aspirated.

Finally, the microspheres were frozen, freeze-dried for 24 h and stored at -20°C.

The average size of the PLGA and GDL porogens was determined by an optical microscope equipped with a digital camera (Leica/Leitz DM RBE Microscope system, Leica Microsystems AG, Wetzlar, Germany) using a sample size of at least 300 porogens. In addition, the morphology of the microspheres was observed by means of Scanning Electron Microscopy (SEM, JEOL 6310) at an accelerating voltage of 10 kV.

2.3. Preparation of cements

The cement precursors (α -TCP and pHA) were grinded in a laboratory ball mill for 5.5 h at 500 rpm in order to obtain a homogeneous particle-size distribution⁷. The particle size distribution of the precursors (α -TCP: 8.7 ± 3.0 μm and pHA: 4.5 ± 1.9 μm) was determined by using laser diffraction (Mastersizer-2000, Malvern Inst. Ltd., U.K).

Table 1 provides an overview of the composition, abbreviations and total porosity of all tested groups which contained either no porogen, 43 wt% PLGA, 10 or 20 wt% GDL, or mixtures of PLGA (30 wt%) and GDL (5 or 10 wt%). These compositions were selected based on previous studies performed at our laboratory¹¹. The total amount of powder was kept constant at 1.2 g for each formulation.

Subsequently, the amount of liquid phase was optimized to obtain cement formulations that exhibited comparable initial setting times (3-4 min). It was observed that considerably lower amounts of liquid phase (3 w/v% aqueous solution of Na_2HPO_4) were needed for GDL-containing formulations to obtain handling properties similar to pure CPC or composites containing PLGA. Therefore, 420 μL , 420 μL , 380 μL and 380 μL of aqueous Na_2HPO_4 solution were added to pure CPC, CPC65-PLGA30-GDL5, CPC67-PLGA43 and CPC90-GDL10, respectively, whereas 240 μL of aqueous Na_2HPO_4 solution were added to the powder precursor phase for CPC80-GDL20 and CPC60-PLGA30-GDL10.

After combining all liquid and powder precursor compounds as well as organic additives (PLGA and/or GDL), the reactants were mixed

vigorously for 30 seconds in 2 mL syringes (Silamat[®] mixing apparatus, Vivadent, Schaan, Liechtenstein) and the cement was injected into Teflon molds (6 mm height x 8 mm diameter) to obtain cylindrical substrates. Initial and final setting times of the different CPC pastes were assessed using Gillmore needles (ASTM C266). Briefly, a bronze block was used as mold containing holes of 6 mm diameter and 12 mm height. The mould was placed in a water bath at 37°C. Samples of each formulation were mixed and injected into the mould and initial and final setting time was determined.

Total porosity was determined by measuring the weight of pre-set CPC discs (Table 1). The composites were placed in a furnace at 650°C for 2 h to burn out PLGA and GDL. Subsequently, porosity was calculated using equations as described previously⁴.

$$\text{Total porosity} = (1 - (M_{\text{burnt}}/V * \rho_{\text{HA}})) * 100\% \quad (1)$$

where M_{burnt} is the average sample mass after burning out the polymer (g), V is the sample volume (cm^3), and ρ_{HA} is the density of hydroxyapatite (g/cm^3).

2.4. *In vitro* degradation studies

Variations in pH of the soaking buffer were measured up to soaking time of 6 weeks. Therefore, 1.2 g of pre-set CPC was placed in 1.5 mL of Phosphate Buffered Saline (PBS) and incubated at 37 °C on a shaker table (60 rpm) for 6 weeks²⁰.

To investigate the physicochemical, mechanical and degradation properties *in vitro*, pre-set cements were incubated in 20 mL of PBS at 37 °C for up to 12 weeks (n=3). The solution was renewed every week and the initial solution pH was 7.4. After each time point, we monitored the release rates of glycolic or gluconic acid, compressive strengths, morphology and total mass loss.

The release rate of acidic by-products glycolic acid and gluconic acid in PBS was analyzed as a measure for the degradation of PLGA and GDL,

respectively, by Reverse Phase High Performance Liquid Chromatography (RP-HPLC) (n=3). Standard curves (concentrations: from 0 to 10 g/L) were prepared by using standard solutions of lactic acid and gluconic acid. The system consisted of a Hitachi L2130 HPLC pump, a Hitachi L-2400UV detector, a Hitachi L-2200 auto sampler and an Atlantis dC18 column (Waters, 250 mm x 4.6 mm, 5 μ m). Two mobile phases were used; 1% acetonitrile in 20 mM NaH₂PO₄ at pH= 2.2 (mobile phase A) and 100% acetonitrile (mobile phase B) as solvents to vary the eluting strength of the mobile phase in a systematic manner. The gradient elution was carried out by linear replacement of initial mobile phase component A by mobile phase component B within 30 minutes. The flow rate was 0.5 mL per minute, the injection volume 40 μ L and the UV detection wavelength 210 nm.

The compressive strength of the samples (6 mm height x 8 mm diameter) as a function of soaking time was measured with a mechanical testing bench (858 MiniBionixII®, MTS, USA) at a cross-head speed of 0.5 mm min⁻¹. Cylindrical samples were tested after 0, 1, 2, 6 and 12 weeks of immersion in 20 mL of PBS at 37°C (n=3).

The crystal structure of the CPCs was evaluated as a function of soaking time after crushing pre-set samples before and after soaking for 2 and 12 weeks in 20 mL of PBS at 37°C using X-Ray diffraction (XRD; Philips PW3710, The Netherlands). XRD was performed with a CuK α radiation source having a wavelength of 1.54 Å at a voltage of 40 kV and a current of 30 mA. Patterns were collected from 10° to 40° 2 θ at a step size of 0.05° and a counting time of 20 seconds at each step. The morphology of the set cements was evaluated by scanning electron microscopy (SEM, JEOL 6301) after soaking in PBS for 2 weeks and 12 weeks. Prior to SEM examination, all samples were mounted on aluminium stubs using carbon tape and sputter coated with gold-palladium.

Degradation rates of the various CPCs upon soaking in PBS were evaluated by monitoring the total mass loss as compared to the initial weight of samples which was determined by removing injected samples from the mold followed by air-drying and weighing. Soaked samples were weighed after each time point after drying at 37°C for one week (n= 4). In addition,

the total mass loss caused by degradation of organic additives was determined by calculating the cumulative release of lactic and glycolic acid in the supernatant solutions as described above.

Table 1. Composition, porosity values and setting times of the various CPC materials.

Abbreviations	Powder phase			Liquid phase	Setting times (min)		Total Porosity (vol%)
	CaP (wt%)	PLGA (wt%)	GDL (wt%)	Liquid (μ L)	Initial	Final	
CPC	100	-	-	420	3.3 \pm 0.5	5 \pm 1	40 \pm 4
CPC67-PLGA43	67	43	-	380	3.3 \pm 0.5	18 \pm 2	75 \pm 5
CPC90-GDL10	90	-	10	380	3.3 \pm 0.3	17 \pm 6	54 \pm 5
CPC80-GDL20	80	-	20	240	9 \pm 4	206 \pm 12	60 \pm 4
CPC65-PLGA30-GDL5	65	30	5	420	3.0 \pm 0.5	12 \pm 3	70 \pm 5
CPC60-PLGA30-GDL10	60	30	10	240	3.8 \pm 0.5	160 \pm 10	76 \pm 5

2.5. *In vivo* implantation study

Ten adult Dutch milk goats with a weight between 45 and 50 kg were used as experimental animals. The protocol was approved by the Animal Ethical Committee of the Radboud University Nijmegen Medical Centre (Approval no: RU-DEC 2011-228) and the national guidelines for the care and use of laboratory animals were applied.

Postoperatively, Finadyne[®] (Interver BV, Boxmeer, the Netherlands) was administered for two days to reduce post-operative pain. Subsequently, the goats were intubated and connected to an inhalation ventilator with a constant volume of a mixture of nitrous oxide, isoflurane, and oxygen. Before the insertion of the implants, each animal was immobilized on its back and the hind limbs were shaved, washed, and disinfected with povidoneiodine. Twenty polyacetal cassettes (23 mm height x 13 mm

length x 12 mm wide), designed for fixation to the transverse process of the goat lumbar spine, were used. Two spinal cassettes per goat consisting of two sidewalls each holding three empty gaps (12 mm height x 7 mm length x 4 mm wide) separated by polyacetal sheets, were implanted bilaterally on the transverse process of the L1-L4 vertebrae of the 10 goats^{18, 19, 21}. Prior to the implantation, all components were sterilized using gamma radiation (25-50 kGy; Isotron BV, Ede, the Netherlands). After shaving and disinfection of the dorsal thoracolumbar area, a middle skin incision was made to expose the paraspinal muscle to enable implantation of the cages. Cassettes were mounted after thoroughly decorticating and flattening of the underlying bone (until bleeding surface was obtained) to ensure direct contact. After implantation of the cassettes, each empty space was filled with injectable cements according to the above-mentioned procedure with the same materials tested *in vitro* (section 2.3 and Table 1: pure CPC was excluded) according a randomized scheme (Table 2)^{19, 21}. Based on the results of the above-mentioned *in vitro* degradation studies, pure CPC scaffolds were excluded from the evaluation of the *in vivo* orthotopic and intramuscular implantation.

For intramuscular implantation, pre-set cement discs were prepared by injection of the cements (section 2.3 and Table 1) into Teflon® molds of 6 mm in height by 8 mm in diameter to obtain cylindrical samples. The samples in the mold were left to set at 37 °C. Cylinders of cement were removed from the mold and sterilized using gamma radiation (25-50 kGy; Isotron BV, Ede, the Netherlands). Subsequently, these discs were implanted into pockets of about 3 cm which were created in the paravertebral muscle by blunt dissection. After implantation of the cements into these pockets, the muscle fascia was closed with non-resorbable sutures and the skin closed with two 3-0 Vicryl® (Johnson and Johnson, St. Stevens-Woluwe, Belgium) resorbable sutures. In this way, each goat received in total 5 intramuscular implants (Table 1: pure CPC was excluded). Surgeries were performed under general inhalation anesthesia with a combination of isoflurane, nitrous oxide, and oxygen. Postoperative pain relief (Buprenorphin, Shering-Plough, The Netherlands) was given to

each animal. Animals were sacrificed at 12 weeks after implantation by an overdose of pentobarbital (Organon, Oss, The Netherlands) and the implants were retrieved by removing the transverse processes.

Table 2 Randomized scheme of the orthotopic implantations of CPC samples on top of goat transverse processes (A: Empty, B: CPC67-PLGA43, C: CPC90-GDL10, D: CPC80-GDL20, E: CPC65-PLGA30-GDL5, F: CPC60-PLGA30-GDL10).

	Left	Right
Goat 1	ABC	FED
Goat 2	AFE	BCD
Goat 3	EDC	FAB
Goat 4	FED	ABC
Goat 5	EFA	DCB
Goat 6	BAF	CDE
Goat 7	CBA	DEF
Goat 8	AEF	DCB
Goat 9	CDE	BAF
Goat 10	DEF	CBA

2.6. Histological processing

The explanted samples from bone (orthotopic site) were fixed in 4% formaldehyde for 48 hours, dehydrated in a graded series of ethanol (70-100%) and embedded in methylmethacrylate (MMA). After polymerization, at least three 20 µm sagittal cross sections were prepared using a sawing microtome technique (Leica, Nussloch, Germany). Sections were stained with methylene blue/basic fuchsin and examined with a light microscope equipped with a digital camera (Axio Imager Microscope Z1, Carl Zeiss Micro imaging GmbH, Göttingen, Germany).

The retrieved intramuscular specimens were fixed in 4% formaldehyde for 48 hours and decalcified in an ethylenediamine tetraacetic acid (EDTA) solution (10%) and dehydrated in a graded series of ethanol (70-100%). Finally, the specimens were embedded in paraffin and sectioned (5 µm) using a standard microtome (RM 2165, Leica). Sections were stained with hematoxylin and eosin (HE). Tissue response was examined by measuring

the thickness of the capsule area surrounding the pre-set intramuscular implants using light microscopy (Leica Microsystems AG, Wetzlar, Germany) and quantitative microscopy software (Q-win, Leica Microsystems AG, Wetzlar, Germany). Moreover, a histological grading scale (Table 3) was used to evaluate material degradation as well as the response of the soft tissues surrounding the implant in terms of tissue infiltration.

Table 3 Histological grading scale of the tissue reaction.

Evaluation	Response	Score
Tissue infiltration in surface pores/polymeric microspheres	Tissue in pores contains fibrous tissue	3
	Tissue in pores is mostly fibrous tissue with inflammatory cells	2
	Tissue in pores is mainly inflammatory cells	1
	No porosity open for tissue in-growth	0
Degradation of the CPC	CPC complete disintegrated	3
	CPC lost integrity, and is severely fragmented	2
	Surface erosion of the CPC, minimal degradation of polymer microsphere	1
	No obvious degradation of the CPC, polymer microspheres remained	0
Capsule quantitatively	Histological slides were analyzed by measuring the capsule thickness	

2.7. Histomorphometry

Bone formation was quantified using computer-based image analysis techniques (Leica Qwin Pro-image analysis system, Wetzlar, Germany) of at least three histological sections per specimen. The region of interest (ROI) was defined as the area inside the polyacetal cassette between the original parietal bone surface and a perpendicular height of 4 mm¹⁰. To

determine the amount of bone ingrowth, newly formed bone was determined by color recognition (pixel value detection) and expressed as a percentage of the ROI. The maximum height of bone ingrowth was determined as the longest perpendicular distance between the original bone surface and newly formed bone within the ROI.

2.8. Statistical analysis

Data is represented in this article as a function of mean values. Significant differences between the groups were determined using analysis of variance (ANOVA) with Tukey-Kramer Multiple Comparison Tests. For all statistics, GraphPad InStat (GraphPad Software, San Diego CA, US) was used. Results were considered significant at p -values lower than 0.05 ($p < 0.05$).

3. Results

3.1. Characteristics of porogens and cement formulations

The prepared acid-producing PLGA porogens displayed a spherical morphology after freeze-drying as shown in Figure 1A, while GDL porogens are irregular in shape (Figure 1B). The average size of the spheres was $95 \pm 15 \mu\text{m}$ and the average particle size of GDL porogens was equal to $380 \pm 80 \mu\text{m}$ (Figure 1B).

All experimental groups were shown in Table 1. The porogens incorporated into CPC were burned-out to measure the porosity of the CPC. Porogen-free CPC had an intrinsic total porosity of $40 \pm 4\%$. Volumetric percentages of the porosity in the CPCs increased from $54 \pm 5\%$ to $60 \pm 4\%$ with increasing GDL content from 10% to 20%, respectively. Highest total porosity values of $75 \pm 5\%$, $70 \pm 5\%$ and $76 \pm 5\%$ were measured for CPC67-PLGA43, CPC65-PLGA30-GDL5 and CPC60-PLGA30-GDL10 compositions, respectively.

Setting times (Table 1) measurements confirmed that initial setting times (3-3.5 min.) were equal for all cement formulations except for the cement containing the highest amount of GDL (CPC80-20GDL), which revealed longer initial setting times of about 9 min whereas final setting times (Table

1) varied from 5 min for pure CPC to 206 min for CPC80-GDL20 (which contained the highest amount of GDL).

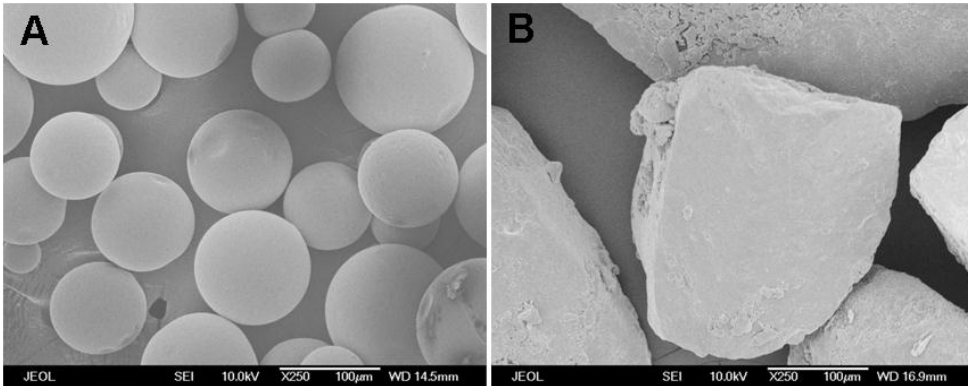


Figure 1. SEM micrographs of [A] PLGA microspheres and [B] GDL microparticles.

3.2. *In vitro* degradation studies

Variations in pH of the buffer medium upon soaking of pre-set CPCs are shown in Figure 2A. A gradual pH decrease from the initial pH of 7.4 to 5.8 ± 0.1 after 6 weeks was recorded for pure CPC. A drastic drop to lower pH values of about 3.3 ± 0.1 was observed after 6 weeks for PLGA-containing samples. A rapid initial pH decrease from 7.4 to 6.4 ± 0.1 within 3 h followed by almost constant pH values was detected for CPCs containing GDL irrespective of the amount of GDL (10 or 20 wt%).

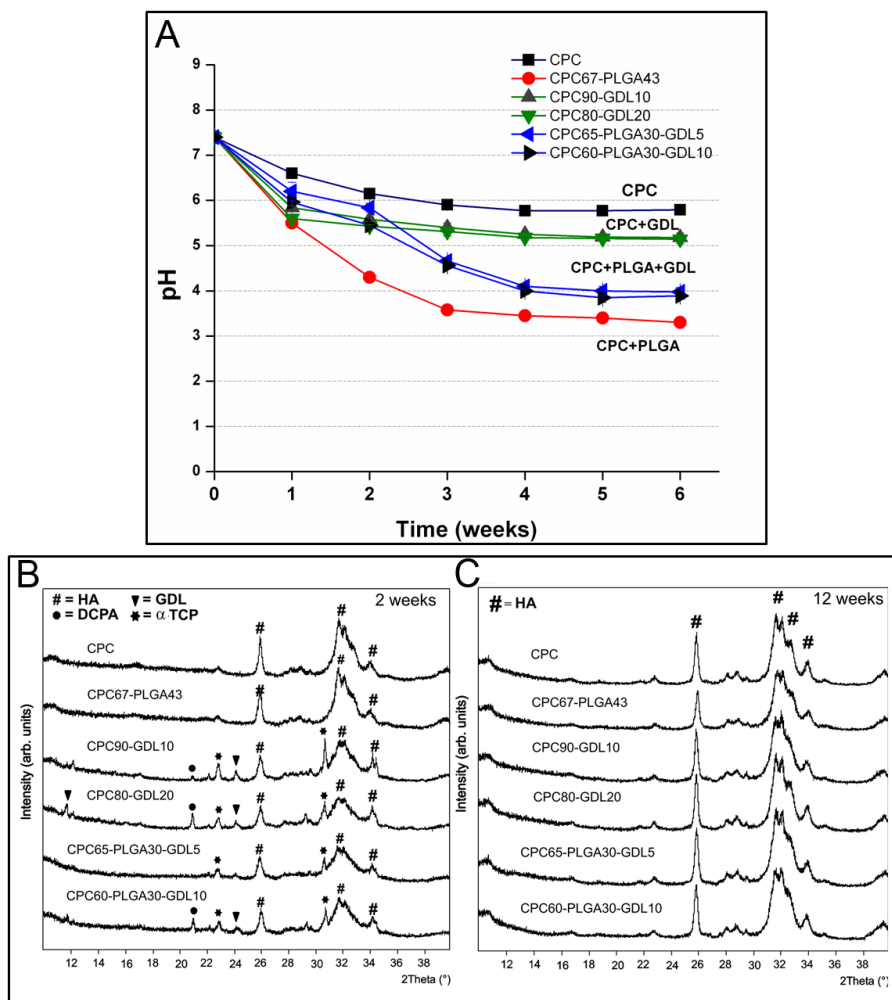


Figure 2. [A] Variations in pH of the soaking medium as a function of time. After 6 weeks, the pH of all experimental groups remained constant until 12 weeks (average for n=3, error bars represent standard deviation), [B] X-Ray diffraction patterns of the CPC cements after immersion in PBS solution for 2 weeks and, [C] X-Ray diffraction patterns of the CPC cements after immersion in PBS for 12 weeks.

Regarding the crystallographic properties of the various CPCs, the typical reflection peaks characteristic for HA at $2\theta = 31.7^\circ$ (112) and 25.9° (002) appeared after 2 weeks of incubation in medium for all CPCs (Figure 2B). Brushite (DCPD) peaks ($2\theta = 11.8^\circ$ and 21.9°) and α -TCP peak ($2\theta =$

30.9°) were identified in GDL-containing CPCs. After 12 weeks of incubation in PBS, DCPA and α -TCP peaks were absent and only peaks characteristic for HA were observed, indicating that all CPCs fully transformed towards HA (Figure 2C).

In order to monitor the morphological appearance before and after soaking in PBS for 2 and 12 weeks, SEM images were taken from CPC67-PLGA43, CPC80-GDL20 and CPC60-PLGA30-GDL10 as representative examples for CPCs containing either PLGA, GDL or a mixture thereof (Figure 3).

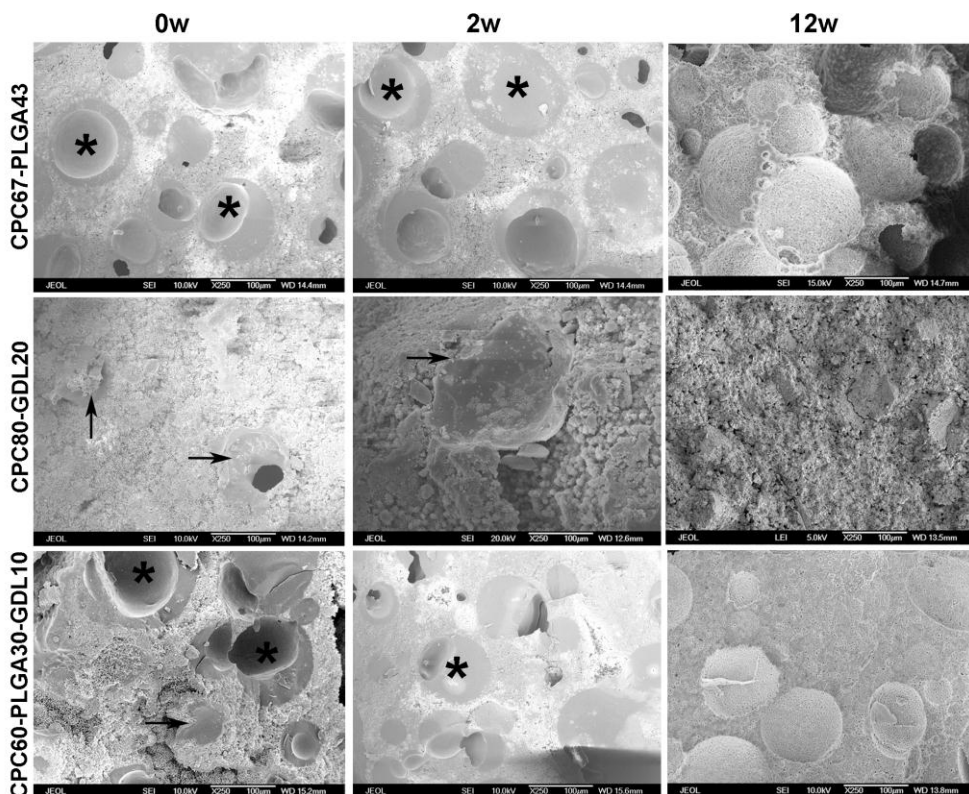


Figure 3. SEM pictures of CPC67-PLGA43, CPC80-GDL20 and CPC60-PLGA30-GDL10 samples after injection (0 weeks), 2 weeks and 12 weeks of incubation (PLGA:* and GDL: →).

Before and after 2 weeks of soaking in PBS, PLGA porogens embedded in CPC were clearly visible, whereas the majority of GDL porogens disappeared already after 2 weeks of soaking in PBS leaving behind a dense

ceramic matrix. PLGA porogens were not detected anymore after 12 weeks of incubation and spherical macroporous structures were present inside the ceramic matrix. From week 2 to week 12, no visible changes in the overall morphology were observed for CPC80-GDL20 and CPC90-GDL10 substrates. Composites containing mixtures of PLGA porogens and GDL porogens, on the other hand, showed macroporous morphology similar to CPCs containing PLGA porogens.

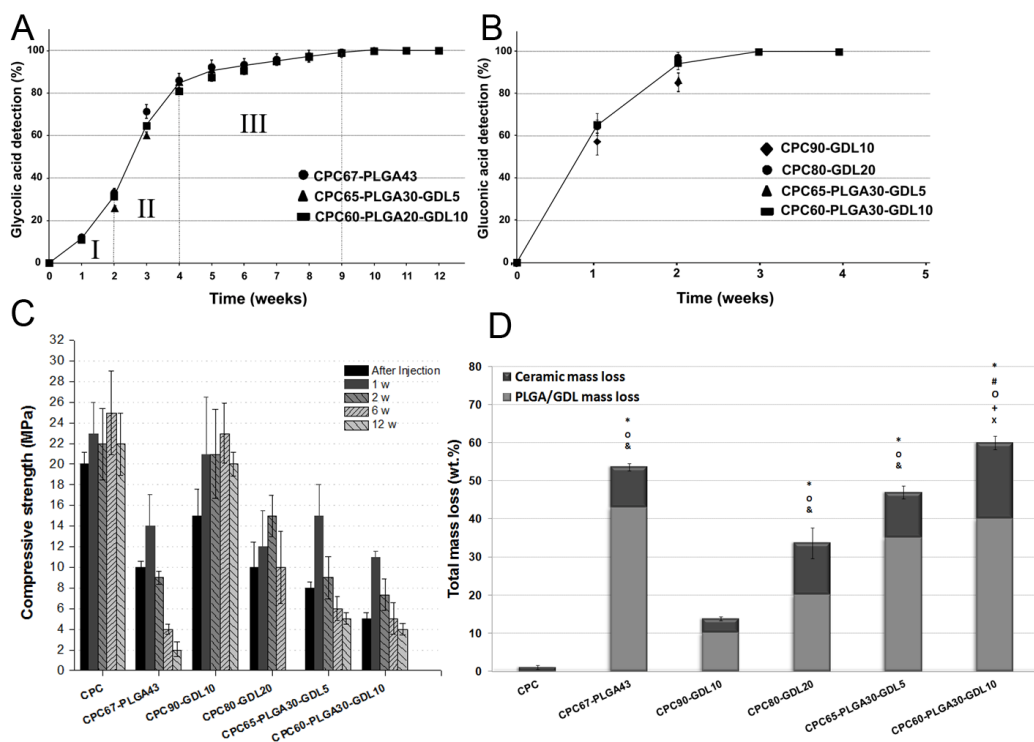


Figure 4. [A] Glycolic acid (PLGA), and [B] gluconic acid (GDL) release detected by RP-HPLC (average for $n=3$, error bars represent standard deviation), [C] compressive strength of the CPCs as a function of soaking time in PBS for up to 12 weeks (average for $n=3$, error bars represent standard deviation of independent experiments), [D] degradation of CPCs after 12 weeks of soaking in PBS (average for $n=3$, error bars represent standard deviation). Statistically significant differences with CPC, CPC67-PLGA43, CPC90-GDL10, CPC80-GDL20, CPC65-PLGA30-GDL5 and CPC60-PLGA30-GDL10 are indicated by: *, #, O, x, + and &, respectively.

The release kinetics of glycolic (Figure 4A) and gluconic acid (Figure 4B) were monitored using RP-HPLC. According to the release of glycolic acid, the degradation profile of PLGA from all PLGA-containing samples was similar and consisted of three stages. The initial release for 2 weeks was slow (stage I) followed by an accelerated release that lasted until the end of week 4 (stage II), whereafter release slowed down again from week 4 to week 12 (stage III). Release of GDL from GDL-containing samples, on the other hand, occurred much faster characterized by almost complete degradation of GDL within the first 2 weeks for all GDL-containing samples (*i.e.* 90-95% of gluconic acid release).

Pure CPC revealed compressive strengths of 20-25 MPa, which remained constant for the entire duration of the soaking experiment ($P > 0.05$) (Figure 4D). Compressive strengths of composites containing PLGA microspheres and/or GDL microparticles increased from initial setting to one week of soaking in PBS. Subsequently, compressive strengths of composites containing PLGA decreased to 2 ± 1 MPa after 12 weeks whereas composites containing 10% of GDL revealed a constant compressive strength of about 20 MPa comparable to pure CPC. Compressive strengths of composites containing CPC80-GDL20, on the other hand, were considerably lower (~ 10 -14 MPa) and disintegrated after 6 weeks of incubation in PBS.

Total mass loss of the composites as a function of soaking time is given in Figure 4D for both ceramic and organic components. Pure ceramic (CPC) barely degraded and the majority of the ceramic was still present after 12 weeks. CPCs containing organic additives revealed considerable mass loss values ranging from 10-60 wt%. After 12 weeks, the organic additives were completely dissolved and measured PLGA-GDL mass losses corresponded perfectly with the initial amount of PLGA and/or GDL. The amount of degradation of the ceramic matrix was lowest for samples containing 10 wt% GDL (3.7 ± 1.4 wt%) and highest for cements containing the maximum amount of organic additives (CPC60-PLGA30-GDL10) which revealed ceramic mass loss values of 20 ± 2 wt%.

3.3. Histology of pre-set intramuscularly implanted cements

All 10 goats exhibited good health and did not show any wound complications. Light microscopical analysis revealed that the shape of the intramuscular implants was partly remained after 12 weeks of implantation except for the cement containing the highest amount of GDL (CPC80-20GDL). A thick capsule was observed surrounding the implants (Figure 5A). The microsphere cavities of all PLGA-containing CPCs were filled with fibrous tissue and occasionally inflammatory cells were present (Figures 5A). Quantification of the histological results of the intramuscular implantation (Figure 5B) revealed that the highest fibrous capsule thickness was measured for CPC80-GDL20. Similar degradation patterns were observed for all experimental groups containing PLGA microspheres (Figure 5C). Limited degradation of CPC90-GDL10 (Figure 5A and 5C) was observed while CPC80-GDL20 almost completed degraded and the pores were mainly filled with inflammatory cells and fibroblasts (Figure 5A and Figure 5B).

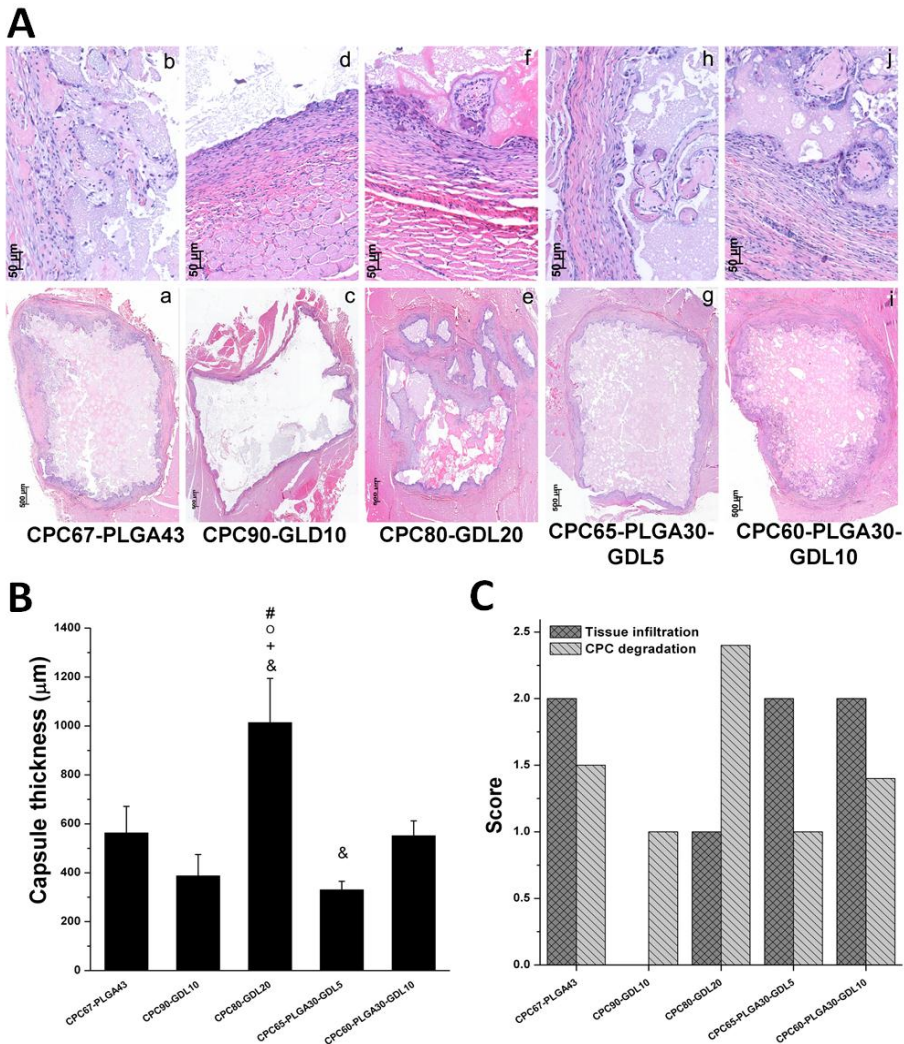


Figure 5. [A] Histological evaluation of the scaffolds implanted in paravertebral muscle of goats after 12 weeks at low and high magnifications; [a, b] CPC67-PLGA43, [c, d] CPC90-GDL10, [e, f] CPC80-GDL20, [g, h] CPC65-PLGA30-GDL5 and [i, j] CPC60-PLGA30-GDL10. Black arrows indicate the presence of tissue infiltration in pores. [B] Capsule thickness (μm) evaluation of the samples after 12 weeks of implantation (average for $n=6$, error bars represent standard deviation, statistically significant differences with CPC67-PLGA43, CPC90-GDL10, CPC80-GDL20, CPC65-PLGA30-GDL5 and CPC60-PLGA30-GDL10 are indicated by: #, O, x, + and &, respectively. [C] Scoring of the tissue infiltration and CPC degradation in ectopic site.

3.4. Histology of cements injected on transverse processes

An overview of representative histological sections of all experimental groups after 12 weeks of implantation is depicted in Figure 6A. Examination of the sections after 12 weeks of implantation revealed variable amounts of cement degradation in the ROI. The bone contact surface of the CPC67-PLGA43 implants showed a rough appearance with spherical cavities caused by degradation of acid-producing PLGA porogen within CPC. However, non-degraded GDL and PLGA porogens were also visible using light microscopy (Figure 6A). The degradation in the periphery of the PLGA-containing CPC implants allowed vertical bone growth in the contact region (Figure 6A). The newly formed bone followed the contour of the pores which were created by the degradation of the porogens. Viable cells are visible. CPC90-10GDL cements presented a compact, dense structure confirming that these CPC-based formulations did neither degrade nor were substituted by new bone tissue (Figure 6A). CPC80-GDL20 samples revealed minor degradation of the implant at the peripheral area and limited new vertical bone growth occurred throughout these degraded implant margins (Figure 6A).

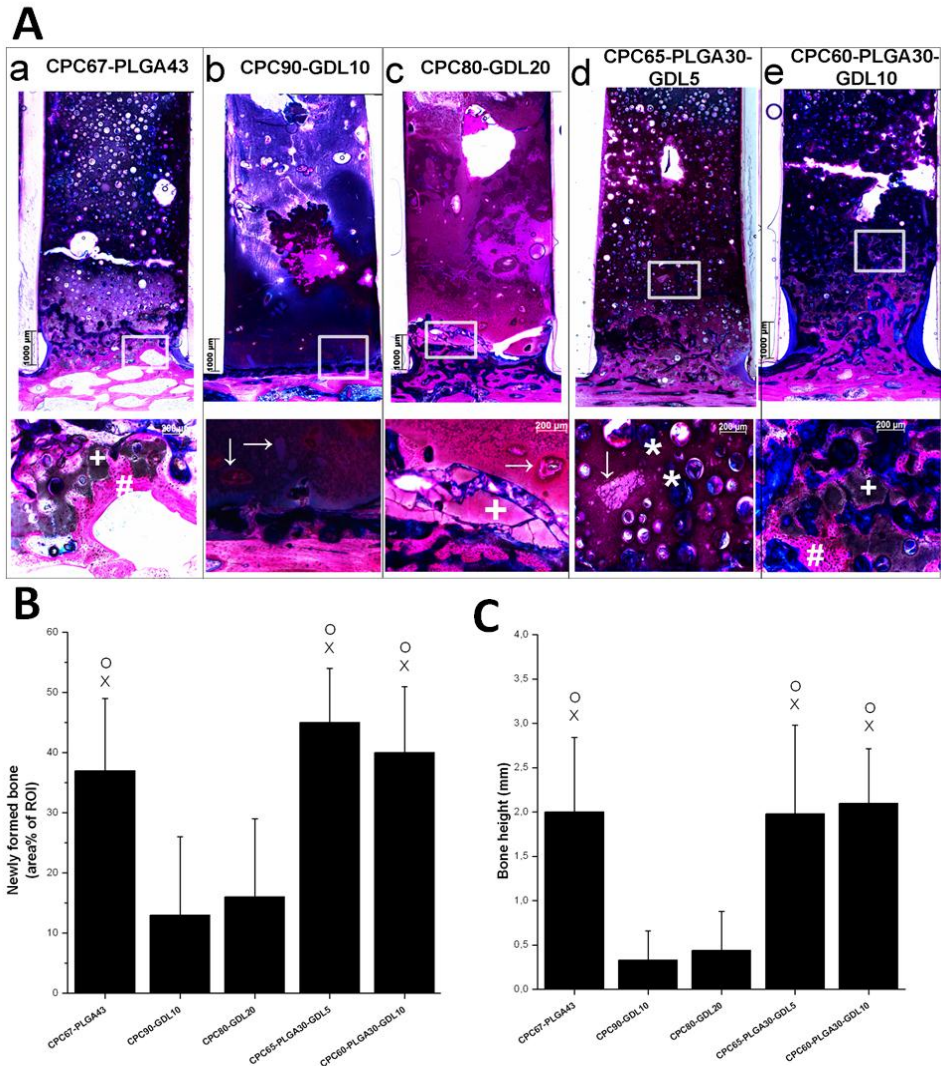


Figure 6. [A] Representative histological sections of implanted cassettes; [a] CPC67-PLGA43, [b] CPC90-GDL10, [c] CPC80-GDL20, [d] CPC65-PLGA30-GDL5 and [e] CPC60-PLGA30-GDL10 (Bone: #, CPC:+, GDL: → and PLGA: *). [B] Newly formed bone (%) within the region of interest (ROI), and [C] bone height (mm) after 12 weeks of orthotopic implantation on goat transverse processes. Statistically significant differences with CPC67-PLGA43, CPC90-GDL10, CPC80-GDL20, CPC65-PLGA30-GDL5 and CPC60-PLGA30-GDL10 are indicated by: #, O, x, + and &, respectively (average for n=10, error bars represent standard deviation).

Quantitative evaluation of new bone formation within the ROI revealed that the amount and height of newly formed bone varied considerably among the experimental groups (Figure 6B and Figure 6C). The amount of newly formed bone was 37-45% at ROI in the CPC67-PLGA43, CPC65-PLGA30-GDL5 and CPC60-PLGA30-GDL10 PLGA groups. For the same experimental groups, the maximum vertical bone height reached to 1.98-2.1 mm. Significantly less new bone formation on CPC90-GDL10 and CPC80-GDL20 (13-16%) within the ROI compared to implants containing PLGA (with or without GDL). No significant differences were observed between CPC90-GDL10 and CPC80-GDL20 samples for either bone area or oppositional bone height (0.3-0.45 mm).

4. Discussion

The goal of the current study was to control the degradation rate of calcium phosphate cements by incorporating mixtures of fast-degrading acid-producing GDL porogens and/or slow-degrading PLGA porogens. To this end, the physicochemical, mechanical and degradation properties were studied *in vitro*. To test our hypothesis also *in vivo*, the selection of the animal model is essential. The goat transverse process model which represents the initial bone formation in posterolateral spinal fusion was selected since this model was shown to be highly efficient for the screening of multiple experimental materials using a limited amount of animals^{18, 19}. Thus, CPCs were implanted at ectopic (intramuscular) and orthotopic implantation sites (transverse processes of the spine) in goats.

4.1. *In vitro* degradation studies

After ball-milling, the particle size distribution of the precursor powder was homogeneous which was beneficial in view of the potential risk for filter pressing²². Hence, cement pastes could be injected easily through 2 ml syringes with orifice diameters of 1.7 mm.

The initial setting times could be optimized to values between 3-4 min for all formulations by varying the amount of liquid phase, except for CPC80-

GDL20 which revealed considerably longer initial setting times of about 9 min. Final setting times increased moderately vs. strongly with increasing amount of PLGA vs. GDL, respectively, and exceeded clinically accepted values of less than 20 min^{23, 24} for composites containing 20 wt% of GDL or a combination of 30 wt% PLGA and 10 wt% GDL. This data indicates that large volumes of GDL interfered with the entanglement of nanoscale hydroxyapatite crystals and prevented proper setting of these cement compositions. In fact, the transformation reaction from α -TCP precursor powders to precipitated HA crystals was suppressed by the presence of GDL due to the high acidification during hardening which instead promoted the (partial) formation of the acid CaP phase brushite (DCPD)^{25, 26}.

By monitoring pH and release of acidic by-products in solution as well as the morphology, crystallinity, and total mass loss of the cements as a function of soaking time in PBS, we observed that PLGA incorporated in CPC matrices degraded by a slow hydrolysis process that lasted for up to 10 weeks. PLGA porogens dissolved faster than the surrounding ceramic matrix. Moreover, the pH reduction associated with the production of acidic by-products lactic and glycolic acid reduced the pH values as low as 3-3.5, which induced severe dissolution of the ceramic matrix and corresponding loss of mechanical strength similar to previously reported studies²⁷⁻³². The initial mechanical strength of cements after setting decreased strongly with increasing PLGA content. This decrease in strength can be attributed to the lower degree of entanglement of HA nanocrystals during setting of the cements containing low amounts of HA-forming precursors, thereby reducing the amount of load-bearing matrix phase. CPCs containing acid-producing GDL porogens, on the other hand, revealed a completely different pattern of *in vitro* degradation. Upon contact with aqueous PBS, GDL dissolved at a much faster rate than PLGA as reflected by an almost complete release of its hydrolysis reaction product gluconic acid (90-95%) within two weeks. This phenomenon can be understood from the fact that hydrolysis of polymers such as PLGA generally proceeds at a faster rate than hydrolysis of a small molecule such as GDL. SEM analysis revealed

that GDL did act as microporogen, since morphologies of cements were dense without the presence of macropores for the entire duration of the study. In contrast to cements containing PLGA (whose strength decreased considerably with increasing time), the introduction of GDL did not reduce the compression strength of CPC after prolonged soaking, emphasizing again that GDL microparticles did not act as porogen.

XRD analysis confirmed the residual presence of GDL in the cements after 2 weeks of soaking, but RP-HPLC analysis revealed that almost all GDL (90-95%) was dissolved after 2 weeks. This discrepancy could be explained by the fact that complete hydrolysis of GDL particles embedded in CPC was inhibited by dense ceramic structure. The amounts of mass loss related to PLGA and/or GDL degradation after 12 weeks, however, matched precisely with the initial amounts of porogen. The amount of degradation of the ceramic matrix after 12 weeks could be controlled from 4 wt% to 16 wt% by increasing the initial amount of acid-producing GDL porogens from 10 wt% to 20 wt%. Since dissolution of GDL was shown to occur during the first two weeks of soaking, we speculate that this degradation of the ceramic matrix was also obtained within the first two weeks of soaking. This speculation was confirmed by the fact that the mechanical strength of GDL-containing cements did not decrease - as observed for cements containing PLGA - after 2 weeks of soaking.

Cements containing mixtures of PLGA (30 wt%) and GDL (5-10%) exhibited initial setting time of 3-3.8 min, while the addition of 10 vs. 5 wt% resulted into a dramatic increase of the final setting time from 12 to 160 min, confirming that the addition of 20 wt% GDL was detrimental to the setting of the cement by phase transformation of α -TCP to HA. Incorporation of 30 wt% PLGA and 5% GDL into CPC was associated with a ceramic matrix degradation of about 12 ± 1 wt%, whereas extensive ceramic degradation of 20 ± 2 wt% was observed for cements containing 30 wt% of PLGA and 10% of GDL. These values exceeded the ceramic mass loss of 10 ± 1 wt% observed for cements containing a higher initial amount of organic additive (*i.e.* 43 wt% of PLGA). Despite the as yet unresolved problems related to delaying effect of GDL on final setting, these results

suggest that the combination of GDL microparticles (up to a maximum of 10 wt%) with PLGA microspheres offers the possibility to increase the amount and rate of ceramic matrix degradation while maintaining comparable or even higher compressive strength values after 12 weeks of soaking due to the dense morphology characteristic for GDL-containing cements.

4.2. *In vivo* degradation studies

Upon intramuscular implantation, all samples containing PLGA and/or GDL microspheres/particles revealed ingrowth of connective tissue. Such tissue was characterized by the presence of fibroblasts as well as several types of inflammatory cells (eg. granulocytes, multinucleated giant cells). The most pronounced reaction was observed around CPCs containing 20 wt% of GDL where inflammatory cells were abundantly present between the implant surface and the surrounding fibrous capsule. It can be attributed to rapid degradation, fragmentation into small particles which may cause friction at the soft interface and/or excessive release of inorganic or organic degradation by-products resulting into inflammatory responses. The fibrous tissue capsule was also significantly thicker around CPCs containing 20% of GDL (~1000 μm) vs. a capsule thickness between 300-600 μm for the other experimental groups. Scoring of cement degradation after 12 weeks of intramuscular implantation was also significantly higher for cements containing 20 wt% of GDL. Moreover, quantification of bone ingrowth (expressed as newly formed bone and maximum bone height) from the transverse processes into cements containing 10 wt% or 20 wt% of GDL revealed that bone ingrowth was impeded by the dense morphology that resulted from incorporation of GDL porogens. Therefore, we concluded that the addition of 20 wt% of GDL was excessive since the addition of 20 wt% of GDL resulted into i) clinically unacceptable setting times, ii) formation of fibrous capsules, and iii) reduced bone ingrowth. The incorporation of 10 wt% of GDL resulted into a lower capsule thickness after intramuscular implantation, but the extent of bone ingrowth upon orthotopic implantation was as low as observed for cements containing 20

wt% of GDL. Cements containing mixtures of GDL and PLGA revealed values for bone ingrowth and bone height similar to cements containing PLGA microspheres only.

Obviously, these results are in contrast to the obtained *in vitro* results, where the amount of cement degradation could be controlled by the amount of organic additive. We speculate that these differences are caused by a lack of perfusion of body fluids into the cements upon implantation onto transverse processes of goats. As a result, the access of these fluids into the interior of these cements was limited which reduced the rate of hydrolysis of the organic additives into acid monomers, thus reducing the release rate of acidic degradation by-products which are responsible for the *in situ* formation of porosity. These results are in contrast to results obtained by Lanao *et al.*¹⁷ who observed that the addition of 10 wt% of GDL resulted into accelerated cement degradation after 2 weeks and almost full degradation after 12 weeks of implantation into femoral condyles of rabbits. In this respect, it should be emphasized that condylar defects are more perfused than augmentation models^{10, 17, 33, 34} such as implantation onto the transverse process.

The amounts of CPC degradation and concomitant bone ingrowth were lower than previous studies^{35, 36}, which is most likely related to slow hydrolysis rates of the PLGA microspheres due to poor perfusion of body fluids into the CPC. As a consequence, it can be concluded that under the current experimental conditions the slow formation of pores upon PLGA degradation or the formation of dense ceramic matrices upon dissolution of GDL microparticles rendered calcium phosphate cements containing PLGA and/or GDL unsuitable for bone augmentation. In addition, it was concluded that the selected animal model was not suitable to quantify the degradation of the CPC at orthotopic sites. It should be emphasized that the selected bone augmentation model strongly differs from orthotopic implantation sites such as femoral condyle or cranial bone defects, which was another limitation of the selected animal model. Generally, inter-animal variations are an intrinsic part of animal testing. The variations in bone formation, material degradation and inflammation were slightly

higher, however, than previous orthotopic studies^{35, 36, 37}, which might be related to the fact that orthotopic implantation sites such as femoral condyles facilitate a more precisely defined region of interest than the augmentation model as selected for the current study. Therefore, future strategies focusing on acceleration of the degradation of CPCs will focus on the use of orthotopic animal models (e.g. femoral condyle model) that allow for i) penetration of body fluids throughout the cement, and ii) precise definition of the region of interest for histomorphometrical analysis.

5. Conclusion

In the current goat study, the combination of acid-producing GDL and PLGA porogens did not facilitate improved bone ingrowth into apatitic calcium phosphate cements in a bone augmentation model on the transverse processes of goats despite a proven accelerating effect on the *in vitro* degradation.

References

1. Magee W.P., Nicolás A., Nicola F., Richard R. Use of fast-setting hydroxyapatite cement for secondary craniofacial contouring. *Plast Reconstr Surg* 2004;114:289-297.
2. Ooms E.M., Wolke J.G.C., van de Heuvel M.T., Jeschke B., Jansen J.A. Histological evaluation of the bone response to calcium phosphate cement implanted in cortical bone. *Biomaterials* 2003;24:989-1000.
3. Brown W.E., Chow L.C. A New Calcium Phosphate, Water-setting Cement. *Cements Research Progress*, P.W. Brown, Ed., Westerville, OH: Am Ceram Soc 1986;352-379.
4. Van de Watering F.C.J., van den Beuken J.J., Walboomers X.F., Jansen J.A. Calcium phosphate/poly(D,L-lactic-co-glycolic acid) composite bone substitute materials: evaluation of temporal degradation and bone ingrowth in a rat critical-sized cranial defect. *Clin Oral Implan Res* 2012;23:151-159.

5. Ooms E.M., Wolke J.G.C., van der Waerden J.P.C.M., Jansen J.A. Trabecular bone response to injectable calcium phosphate (Ca-P) cement. *J Biomed Mater Res* 2002;61:9-18.
6. Bose S., Tarafder S. Calcium phosphate ceramic systems in growth factor and drug delivery for bone tissue engineering: a review. *Acta Biomater* 2012;8:1401-1421
7. Sariibrahimoglu K., Leeuwenburgh S.C.G., Wolke J.G.C., Yubao L., Jansen J.A. Effect of calcium carbonate on hardening, physicochemical properties, and *in vitro* degradation of injectable calcium phosphate cements. *J Biomed Mater Res Part A* 2012;100:712–719.
8. Rey C., Drouet C., Somrani S. Bioceramics and their applications: tricalcium phosphate-based ceramics. In: Kokubo T, editor. *Japan Medical Materials*. Cambridge: Woodhead: CRC Press; vol. 326-340, 2008.
9. Xu H.H.K., Weir D.M., Burguera E.F., Fraser A.M. Injectable and macroporous calcium phosphate cement scaffold. *Biomaterials* 2006;27:4279-4287.
10. Klijn R.J., van den Beucken J.J.J.P., Lanao R.P.F., Veldhuis G., Leeuwenburgh S.C., Wolke J.G.C., Meijer G.J., Jansen J.A. Three different strategies to obtain porous calcium phosphate cements: comparison of performance in a rat skull bone augmentation model. *Tissue Eng Part A*, 2012;18:1171-1182.
11. Lanao R.P.F., Leeuwenburgh S.C.G., Wolke J.G.C., Jansen J.A. Bone response to fast-degrading, injectable calcium phosphate cements containing PLGA microparticles. *Biomaterials* 2011;32:8839-8847.
12. Grizzi I., Garreau H., Li S., Vert M. Hydrolytic degradation of devices based on poly(DL-lactic acid) size-dependence. *Biomaterials* 1995;16:305-311.
13. LeGeros R.Z. Biodegradation and bioresorption of calcium phosphate ceramics: review paper. *Clinic Mater* 1993;14:65-88.
14. Lanao R.P.F., Jonker A.M., Wolke J.G.C., Jansen J.A, van Hest J.C.M., Leeuwenburgh S.C.G. Physicochemical properties and

- applications of poly(lactic-co-glycolic acid) for use in bone regeneration. *Tissue Eng B* 2013;19:1-11.
15. Bodde E.W.H., Habraken W.J.E.M., Mikos A.G., Spauwen P.H.M., Jansen J.A. Effect of polymer molecular weight on the bone biological activity of biodegradable polymer/calcium phosphate cement composites. *Tissue Eng A* 2009;15:3183-3191.
 16. Parke S.A., Birch G.G., MacDougall D.B., Stevens D.A. Tastes, structure and solution properties of D-Glucono-1,5-lactone. *Chem Senses* 1997;22:53-65.
 17. Lanao F.R.P., Sariibrahimoglu K., Wang H., Wolke J.G.C., Jansen J.A, Leeuwenburgh S.C.G. Accelerated calcium phosphate cement degradation due to incorporation of glucono delta-lactone microparticles. Accepted for publication in *Tissue Engineering Part A*, doi:10.1089/ten.TEA.2012.0427.
 18. Kruyt M.C., Wilson C.E., de Bruijn J.D., van Blitterswijk C.A., Oner C.F., Verbout A.J., Dhert W.J.A. The effect of cell-based bone tissue engineering in a goat transverse process model. *Biomaterials* 2006;27:5099-5106.
 19. Habibovic P., Kruyt M.C., Juhl M.V., Clyens S., Martinetti R., Dolcini L., Theilgaard N., van Blitterswijk C.A. Comparative *in vivo* study of six hydroxyapatite-based bone graft substitutes. *J Orthopaed Res* 2008;26:1363-1370.
 20. Habraken J.E.M.W., Wolke J.G.C, Mikos A.G., Jansen J.A. PLGA microspheres/calcium phosphate cement composites for tissue engineering: *in vitro* release and degradation characteristics. *J Biomater Sci-Polym E* 2008;19:1171-1188.
 21. Kruyt M.C., Delawi D., Habibovic P., Oner C.F., van Blitterswijk C.A., Dhert W.J.A. Relevance of bone graft viability in a goat transverse process model. *J Orthopaed Res* 2009;27:1055-1059.
 22. Böhner M., Baroud G. Injectability of calcium phosphate pastes. *Biomaterials* 2005;26:1553-1563.
 23. Khairoun I., Boltong M.G., Driessens F.C.M., Planell J.A. Some factors controlling the injectability of calcium phosphate bone cements. *J Mater Sci: Mater Med* 1998;9:425-428.

24. Takagi S., Chow L.C., Ishikawa K. Formation of hydroxyapatite in new calcium phosphate cements. *Biomaterials* 1998;19:1593-1599.
25. LeGeros R.Z., Lin S., Rohanizadeh R., Mijares D., LeGeros J.P. Biphasic calcium phosphate bioceramics: preparation, properties and applications. *J Mater Sci Mater Med* 2003;14:201-209.
26. Fernandez E., Gil F.J., Ginebra M.P., Driessens F.C.M., Planell J.A., Best S.M. Calcium phosphate bone cements for clinical applications. Part I: solution chemistry. *J Mater Sci - Mater Med* 1999;10:169-176.
27. He F., Ye J. In vitro degradation, biocompatibility, and in vivo osteogenesis of poly(lactic-co-glycolic acid)/calcium phosphate cement scaffold with unidirectional lamellar pore structure. *J Biomed Mater Res A* 2012;100A:3239-3250.
28. Anderson J.M., Shive M.S. Biodegradation and biocompatibility of PLA and PLGA microspheres. *Adv Drug Deliver Rev* 1997;28:5-24.
29. Meyer F., Wardale J., Best S., Cameron R., Rushton N., Brooks R. Effects of lactic and glycolic acid on human osteoblasts: a way to understand PLGA involvement in PLGA/calcium phosphate composite failure. *J Orthopaed Res* 2012;30:864-871.
30. Leroux L., Hatim Z., Frèche M., Lacout J.L. Effects of various adjuvants (Lactic acid, glycerol, and chitosan) on the injectability of a calcium phosphate cement. *Bone* 1999;25:31S-34S
31. Habraken W.J.E.M., Liao H.B., Zhang Z., Wolke J.G.C., Grijpma D.W., Mikos A.G., Feijen J., Jansen J.A. *In vivo* degradation of calcium phosphate cement incorporated into biodegradable microspheres. *Acta Biomater* 2010;6:2200-2211.
32. Heredia L.M.A., Sariibrahimoglu K., Yang W., Bohner M., Yamashita D., Kunstar A., van Apeldoorn A.A., Bronkhorst E.M., Lanao R.P., Jansen J.A. Influence of the pore generator on the evolution of the mechanical properties and the porosity and interconnectivity of a calcium phosphate cement. *Acta Biomater* 2012;8:404-414.

33. Delawi D., Kruyt M.C., Huipin Y., Vincken K.L., de Bruijn J.D., Oner F.C., Wouter J.A.D. Comparing autograft, allograft and tricalcium phosphate ceramic in a goat instrumented posterolateral fusion model. *Tissue Eng C* 2013;19:1-8.
34. Sengupta D.K., Truumees E., Patel C.K., Kazmierczak C., Hughes B., Elders G., Herkowitz H.N. Outcome of local bone versus autogenous iliac crest bone graft in the instrumented posterolateral fusion of the lumbar spine. *Spine* 2006;31:985
35. Lanao R.P.F., Leeuwenburgh S.C.G., Wolke J.G.C., Jansen, J.A. Bone response to fast-degrading, injectable calcium phosphate cements containing PLGA microparticles. *Biomaterials* 2011;32:8839-8847.
36. Lanao R.P.F., Hoekstra J.W.M., Wolke J.G.C., Leeuwenburgh S.C.G., Plachokova A.S., Boerman O.C., van den Beucken J.J.J.P., Jansen, J.A. Porous calcium phosphate cement for alveolar bone regeneration. *J Tissue Eng Regen Med*. doi: 10.1002/term. 1546.
37. Hoekstra J.W., Klijn R.J., Meijer G.J., van den Beucken J.J.J.P., Jansen J.A. Maxillary sinus floor augmentation with injectable calcium phosphate cements: a pre-clinical study in sheep. *Clin Oral Implants Res* 2013;24:210-216.



Chapter 7

CONTROLLED RELEASE OF PLATINUM-BISPHOSHONATE COMPLEXES FROM INJECTABLE CALCIUM PHOSPHATE CEMENTS FOR TREATMENT OF BONE TUMORS

Kemal Saribrahimoglu, Michele Iafisco, Nicola Margiotta,
Joop G.C. Wolke, John A. Jansen, Sander C.G. Leeuwenburgh

1. Introduction

Bone tissue exhibits a remarkable regenerative capacity owing to the concerted action of bone-forming osteoblasts and bone-resorbing osteoclasts. Nevertheless, large critical size bone defects require a bone substitute that fills the defect and facilitates tissue regeneration. Treatment of such large bone defects is even more challenging for patients that exhibit a compromised health. A particularly challenging health condition for bone healing involves surgical treatment of bone tumors. Bone tissue is both the most common organ affected by metastatic cancer and the site that produces the greatest morbidity for patients¹⁻³. Treatment of bone tumors is highly dependent on the type of bone tumor and may include (a combination of) surgery, medication, chemotherapy and/or radiotherapy⁴⁻⁸. Local surgical therapy is generally favored if a margin of tumor-free tissue can be preserved around the tumor⁹, since intralesional surgery will lead to a very high risk of local recurrence irrespective of preoperative chemo- or radiotherapy. After tumor resection by curettage or aspiration, a large contained defect is left that needs to be reconstructed using autografts allografts or alloplasts. Autologous bone harvested from the iliac crest or fibula is currently the gold standard of care. Nevertheless, surgical treatments such as tumor resection and/or autologous bone graft harvesting are often intolerable for patients with co-morbid conditions and limited life expectancy. In addition to the devastating effect of cancer on bone tissue, treatments such as radio- and chemotherapy reduce bone health as well. Local, targeted delivery of chemotherapeutics would allow efficient delivery of anti-cancer drugs to the tumor while minimizing the toxic side effects of these drugs. To this end, novel biomaterials are currently developed that are able to reconstruct bone defects created by tumor resection and release chemotherapeutic drugs in a controlled and sustained manner.

Injectable, self-setting calcium phosphate cements (CPCs) have been developed as synthetic bone substitutes in view of their similarity to the mineral component of bone tissue¹⁰. In addition, CPCs are injectable and can be molded to fill irregular defect shapes. CPCs that maintain a high

local concentration of the drug would represent an ideal therapeutic strategy after tumor resection. Previously, Lopez-Heredia et al.⁶ loaded pre-set CPC disks with the chemotherapeutic drug paclitaxel by simple adsorption. This method did not allow loading chemotherapeutic drugs into injectable CPCs, while the total amount of paclitaxel release was very limited. During the past decade, nanotechnology has emerged as an additional tool to improve the efficacy of drug delivery for cancer therapies. Iafisco et al.¹¹ recently developed hydroxyapatite (HA) nanoparticles for the local delivery of two chemotherapeutic platinum-bisphosphonate (Pt-BP) complexes, i.e., complex A (bis-{ethylenediamineplatinum(II)}-2-amino-1-hydroxyethane-1,1-diyl-bisphosphonate (EDPAB)) and complex B (bis-{ethylenediamineplatinum(II)}-medronate (EDPM)). Both Pt-BP complexes were developed to target traditional cisplatin-based drugs to bone tissue. Moreover, the presence of bisphosphonate ligands allowed for efficient loading of these complexes onto synthetic HA nanoparticles. The results indeed revealed a high loading capacity of the HA nanoparticles for the Pt-BP complexes, while the release of chemotherapeutically active Pt was shown to proceed in a sustained manner. Nevertheless, drug-loaded nanoparticles cannot be injected directly into bone defects due to the risk of excessive leakage of nanoparticles into the surrounding tissues.

Herein, we present a novel method to confine drug-loaded HA nanoparticles inside apatitic CPCs in an attempt to develop CPCs with a sustained chemotherapeutic efficacy. To this end, HA nanoparticles loaded with Pt-BP complexes were added to the cement powder phase at different amounts ranging from 5 to 20 wt%. Poly(D,L-lactic-co-glycolic) acid (PLGA) porogens were used to render apatitic CPCs degradable. The morphology and crystal phases of the drug-loaded cements were studied after setting using Scanning Electron Microscopy (SEM) and X-Ray Diffraction (XRD), respectively, while the cement setting times were studied using Gillmore needles. The release profiles of the Pt-BP complexes were investigated in vitro by soaking drug-loaded cements into Phosphate Buffered Saline (PBS) followed by quantification of both Ca and

Pt release for up to 4 weeks using Inductively Coupled Plasma Optical Emission Spectroscopy (ICP-OES).

2. Materials and Methods

2.1. Materials

The powder phase of the CPC powder consisted of a mixture of α -tricalcium phosphate (α -TCP; CAM Bioceramics, Leiden, the Netherlands) and precipitated hydroxyapatite as prepared in our laboratory (see section 2.2 for further details). Na_2HPO_4 was purchased from Merck (Darmstadt, Germany). Poly(lactic-co-glycolic acid) (PLG, Purasorb[®] PDLG 5002A, $M_w = 17$ kDa, acid terminated, L:G = 50:50) from Purac Biomaterials (Gorinchem, the Netherlands). Polyvinyl alcohol (PVA; 88% hydrolyzed, $M_w = 22$ kDa) was obtained from Acros (Geel, Belgium) while isopropanol (IPN; analytical grade) and dichloromethane (DCM; analytical grade) were obtained from Merck (Darmstadt, Germany). Pt-BP complexes bis-{ethylenediamineplatinum(II)}-2-amino-1-hydroxyethane-1,1-diyl-bisphosphonate (EDPABm $M_w = 898$) and bis-{ethylenediamineplatinum(II)}-medronate (EDPM, $M_w = 682$) were prepared as described previously¹².

2.2. Synthesis of hydroxyapatite nanoparticles

Apatitic particles were synthesized according to a method reported by Liou et al.¹³ and Iafisco et al.¹¹. Briefly, apatite nanocrystals were precipitated by slow addition (1 drop s^{-1}) of an aqueous solution of H_3PO_4 (50 mM) to a suspension of $\text{Ca}(\text{CH}_3\text{COO})_2$ (83 mM) at a stoichiometric Ca/P ratio (1.67) while keeping the pH at a constant value of 10 by the addition of a $(\text{NH}_4)\text{OH}$ solution at 25°C . The reaction mixture was stirred at room temperature for 24 hours, after which stirring was suspended and the mixture was left standing for 2 hours to sediment the nanoparticles. Subsequently, the suspension was centrifuged (6000 rpm, 10 min) in Falcon 50 mL conical centrifuge tubes, washed with water three times, and freeze-

dried for 24 hours. Dry HA powder was grinded in a laboratory ball mill for 1 h at 500 rpm in order to obtain a homogeneous particle size distribution.

2.3. Synthesis of drug-loaded hydroxyapatite nanoparticles

Pt-BP complexes were loaded onto HA nanoparticles according to the method described by Iafisco et al.¹¹. Briefly, an aliquot (1.5 mL) of Pt-BP complex solution (0.5 mg/mL) was added to 10 mg of HA nanoparticles in a 20 mL glass tube. After vortexing for 15 s, this suspension was maintained in a bascule bath at 37°C shaking at 60 rpm for one week. Thereafter, the suspension was centrifuged 3 min at 1000 rpm in Falcon 15 mL conical centrifuge tubes, followed by removal of the supernatant and washing (2x using water) of the drug-loaded nanoparticles. The drug remained after washing was considered to be effectively bound to the apatite nanocrystals.

The total adsorption of Pt-BP complexes onto HA nanoparticles was quantified after dissolving 1 g of drug-loaded HA nanoparticles in 1 wt% nitric acid. After complete dissolution of these drug-loaded nanoparticles the concentration of calcium and platinum ions were determined by Inductively Coupled Plasma-Optical Emission Spectrometry (ICP-OES, Liberty 200, Varian, Clayton South, Australia).

2.4. Preparation of PLGA microspheres

Dense PLGA microspheres were prepared by a single emulsion technique¹⁴. 0.2 g of PLGA was dissolved in 2 mL of DCM in a 20 mL glass tube. This solution was transferred into a stirred beaker containing 100 mL of 0.3% PVA solution. Subsequently, 50 mL of 2% IPN solution was added. The solution was stirred for one hour. The microspheres were allowed to settle for one hour and the clear solution was decanted. The remaining suspension was centrifuged and the clear solution on top was aspirated. Finally, the microspheres were frozen, freeze-dried for 24 hours and stored at -20°C. The average size of the PLGA microspheres was determined as 95±15 µm by an optical microscope equipped with a digital camera (Leica/Leitz DM

RBE Microscope system, Leica Microsystems AG, Wetzlar, Germany) using a sample size of at least 300 microspheres.

2.5. Preparation of CPCs containing drug-free and drug-loaded hydroxyapatite nanoparticles

The cement precursor powder (α -TCP) were grinded in a laboratory ball mill for 5.5 h at 500 rpm yielding a particle size of 8.7 ± 3.0 μm as determined by laser diffraction (Mastersizer-2000, Malvern Inst. Ltd., U.K). Drug-loaded, freeze-dried HA nanoparticles were added to this cement powder phase at various weight ratios ranging between 5 to 20 wt% (see Table 1 for an overview of the abbreviations and composition of all experimental groups). The PLGA content was fixed at 40 wt% while PLGA-free CPCs were included as controls.

Cement pastes were obtained by homogeneous mixing of precursor powders with a 3% Na_2HPO_4 (Merck, Germany) solution at a liquid-to-powder ratio (L/P) of 0.40 mL/g. Briefly, 1 g of precursor powder was placed in an exit-closed 2 ml syringe (orifice diameter 1.7 mm). Subsequently, the solution was added to the powder. The syringe was placed in a mixing apparatus (Silamat® Vivadent, Liechtenstein) and mixed for 30 seconds. After mixing, a paste was obtained and injected into Teflon® molds of 5 mm in diameter by 3.85 mm in height to obtain cylindrical cement samples ($W_{\text{av.}} = 90$ g). The samples in the mold were setting at 37°C.

2.6. Physicochemical characterization of CPCs

The initial and final setting times of the various cement pastes were assessed using Gillmore needles according to ASTM C266. A bronze block containing 6 holes (6 mm in diameter, 12 mm in height) was used as a mold. The mold was placed in a water bath at body temperature (37 °C). Samples of each formulation were mixed and injected into the mold. The Gillmore needles were carefully lowered onto the surface of the freshly shaped cement paste and kept there for 3 seconds. The setting time was recorded when penetration was not observed anymore (n = 3).

The crystal structure of the CPCs was evaluated as a function of soaking time after crushing pre-set samples before and after soaking for 28 days in 10 mL of HEPES buffer at 37°C. X-Ray diffraction (XRD; Philips PW3710, The Netherlands) was used to analyze the effect of microparticles on set CPC compositions. XRD was performed with a CuK α radiation source having a wavelength of 1.54 Å at a voltage of 40 kV and a current of 30 mA. Patterns were collected from 10° to 40° 2 θ , a step size of 0.05° and a counting time of 20 seconds/step. The morphology of the set cements was evaluated by scanning electron microscopy (SEM, JEOL 6301). Prior to SEM examination, all samples were mounted on aluminum stubs using carbon tape and sputter coated with gold-palladium.

2.7. In vitro quantification of Pt and Ca release from CPCs

Hardened, drug-loaded CPCs were soaked in 10 mL of HEPES buffer saline solution (10 mM) containing sodium chloride ions (NaCl, 0.20 M). After 1, 3, 5, 9, 18 and 28 days of soaking, buffers were removed to determine Pt and Ca concentrations and replaced with fresh buffer. The Pt and Ca concentrations in the buffers were quantified using ICP-OES (Liberty 200, Varian, Clayton south, Australia). For the Pt assay the selected analytical wavelength was 265 nm. Cumulative Pt and Ca release amounts were calculated relative to total amount of Pt adsorbed onto HA nanoparticles prior to incorporation in CPC (see section 2.3).

2.8. Statistical analysis

Data is represented in this article as a function of mean values. Statistical analyses were performed using GraphPad InStat (GraphPad Software, San Diego CA, US). Significant differences between the groups were determined using analysis of variance (ANOVA) with Tukey-Kramer Multiple Comparison Tests.

3. Results and discussion

ICP analysis revealed that 1 mg of drug-loaded HA contained 0.0145 ± 0.0004 mg (1.45 wt%) and 0.0138 ± 0.0001 mg (1.38 wt%) Pt for EDPAB and EDPM-loaded HA, respectively. The initial amount of Pt-BP complexes in the loading solutions was equal to 0.075 mg/mL which corresponded to 0.033 mg/mL and 0.042 mg/mL Pt for EDPAB and EDPM loaded HA, respectively (by compensating for the differences in molecular weight of both complexes). Consequently, the loading efficiencies in HA particles were $43 \pm 2\%$ and $34 \pm 3\%$ for aminated EDPAB vs. amino-free EDPM complexes, respectively. These values are lower than previous findings by Iafisco et al.¹¹ who observed that 100% of EDPAB and 60% of EDPM were loaded onto HA nanoparticles within 6 days. We did not sieve the HA nanoparticles after prior to drug loading whereas Iafisco et al.¹¹ used HA granular fractions having dimensions ranging from 100 to 150 μm which might have caused differences in specific surface area and corresponding drug adsorption.

Table 1. Abbreviations, compositions and setting times of the various CPC materials.

Abb.	α -TCP (wt%)	PLGA (wt%)	Drug-free HA (wt%)	Drug-loaded HA ¹ (wt%)	Setting times (min) ²	
					Initial	Final
CPC1	55	40	5		4.5 ± 0.5	18 ± 1
CPC2	55	40	-	5	4.5 ± 0.5	21 ± 2
CPC3	50	40	-	10	8.5 ± 0.3	45 ± 6
CPC4	40	40	-	20	8 ± 0.4	55 ± 12
CPC5	40	40	20	-	3.5 ± 0.5	14 ± 3
CPC6	95	-	-	5	3.5 ± 0.5	5.5 ± 1
CPC7	80	-	-	20	4.2 ± 0.5	28 ± 2
CPC8	95	-	5	-	3.3 ± 0.5	5 ± 1

¹HA nanoparticles were loaded with either complex A (aminated EDPAB) or complex B (amino-free EDPM).

²Initial and final setting times did not depend on the type of drug loading (complex A or B) so values are only given for CPCs loaded with complex A (aminated EDPAB)

All CPC formulations used in this study were injectable through syringes. The shortest setting times (i.e. 4-5 min for initial and 18-21 min for final setting) were observed for drug-free CPCs and CPCs containing 5 wt% of drug-loaded HA nanoparticles (Table 1). Setting times of the cement pastes increased with increasing amount of drug-loaded HA up to initial and final setting times of 8 and 55 min, respectively. Generally, the type of Pt-BP complex (EDPAB or EDPM) did not affect the setting time of the CPC paste.

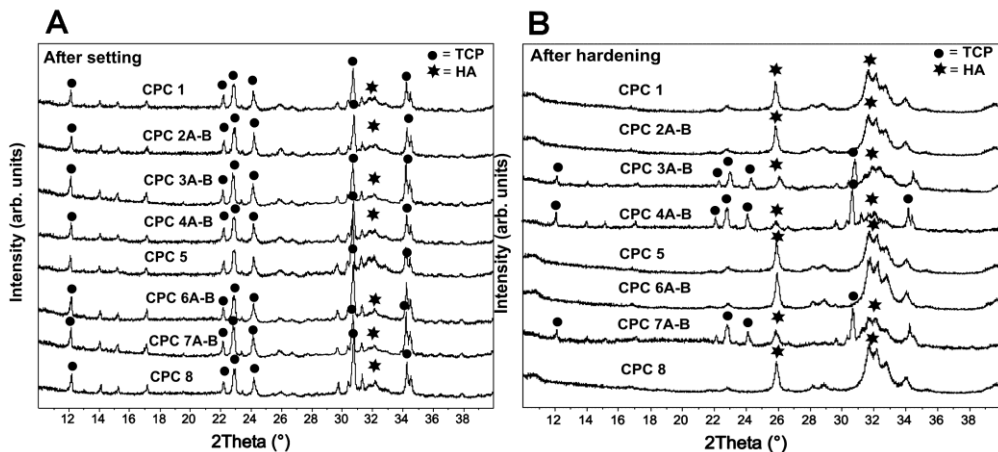


Figure 1. X-ray diffraction patterns of the CPCs [A] after setting and [B] after hardening in HEPES buffer for 28 days. No obvious differences were observed between Complex A- and Complex B-containing cement groups.

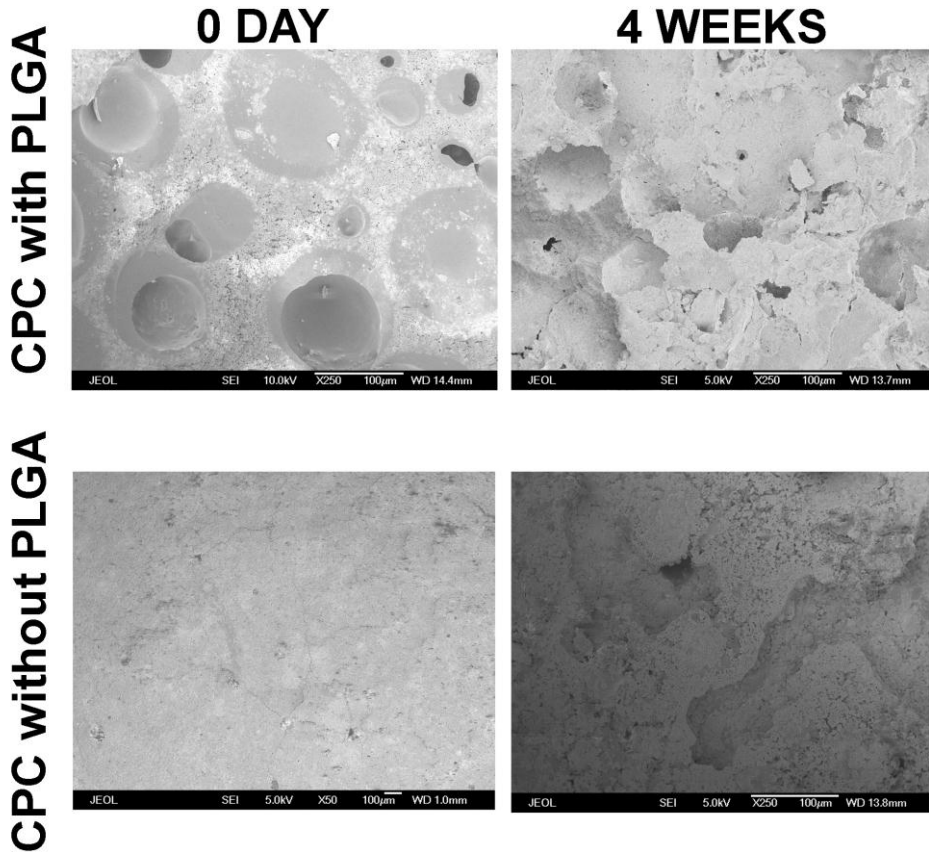


Figure 2. Scanning electron micrographs of CPC4 (CPC with 40 wt% PLGA and 20 wt% of drug-loaded HA) and CPC8 (CPC without PLGA) samples after injection (0 days) and 28 days of incubation in HEPES buffer (pH=7.0, 37 °C)

Figure 1 shows the XRD patterns of the cements before (Figure 1A) and after (Figure 1B) hardening for 28 days in HEPES buffer (pH=7.0) at 37 °C. The typical reflection peaks characteristic for HA at $2\theta = 31.7^\circ$ (112) and 25.9° (002) appeared after 28 days of incubation for all experimental groups (Figure 1B) confirming that the hardening reaction proceeded by hydrolysis of α -TCP into poorly crystalline HA. The presence of drug-loaded HA nanoparticles delayed this transformation from α -TCP towards poorly crystalline HA at high contents of Pt-BP complexes (10 and 20 wt% of drug-loaded HA) as evidenced by the presence of intense reflection peaks characteristic of α -TCP. This phenomenon can be attributed to the

lower amount of transformable α -TCP precursor powder as well as the inhibiting effect of bisphosphonates on cement setting as described previously by Panzovola et al.¹⁵ for setting of cement containing amino-bisphosphonates alendronate and pamidronate.

SEM images were taken from CPCs with (CPC4, 40 wt% PLGA, 20 wt% drug-loaded HA) or without PLGA microspheres (CPC8, 5 wt% drug-free HA) before and after soaking for 4 weeks in HEPES buffer (Figure 2). After setting, PLGA microspheres embedded in CPC were clearly visible, but these microspheres were not observed anymore after 28 days of incubation resulting into the formation of a macroporous morphology. CPCs without PLGA exhibited a dense morphology both before and after soaking in HEPES.

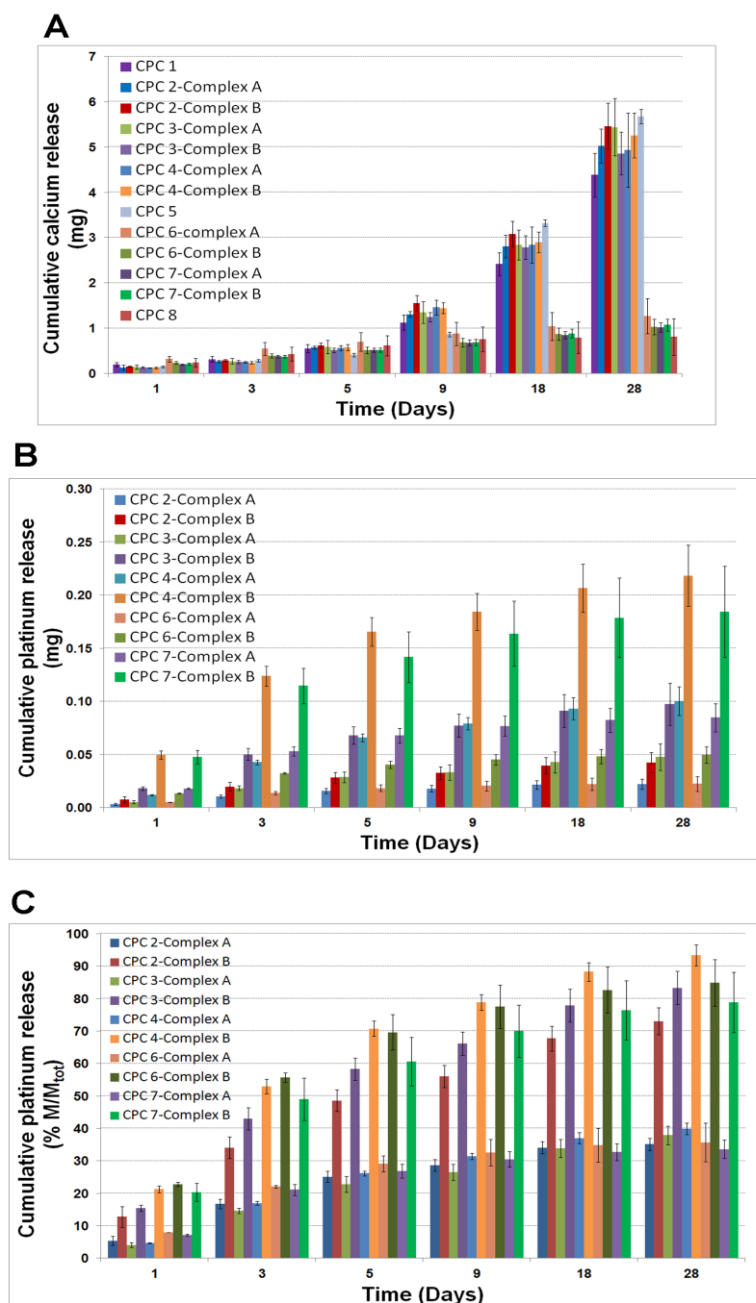


Figure 3. Cumulative release amounts of [A] calcium (mg), [B] platinum (mg) and [C] released mass percentages of Pt ions as a function of soaking time in HEPES buffer.

The release experiments showed that the release of calcium ions from all cements increased with increasing incubation time (Figure 3A). Considerably higher amounts of calcium release were observed upon incorporation of PLGA microspheres CPC which confirmed that the cements degraded gradually within 4 weeks of soaking in HEPES as observed in several publications from our laboratory^{14, 16, 17}. The amounts of Pt release increased with increasing amount of drug-loaded HA particles in CPC, but the biggest effect on the Pt release kinetics was caused by the type of Pt-BP complex (Figures 3B and 3C). After 28 days of incubation in HEPES buffer, 93 ± 3 wt% of the originally loaded Pt was released from CPC4 containing 20 wt% of complex B (amino-free EDPM) whereas only 40 ± 2 wt% of Pt was released from CPC4 containing 20 wt% of complex A (aminated EDPAB) (Figure 3C). These results correspond to Iafisco et al.¹¹ who observed that the affinity of complex A (aminated EDPAB) for HA was greater than complex B (amino-free EDPM) owing to the positively charged NH_3^+ moiety of complex A.

The incorporation of PLGA microspheres into CPCs did not affect the release rate of Pt. These results indicate that Pt release from the cements was faster than the degradation of PLGA microspheres. Therefore, it can be concluded that release was not controlled by degradation of the cement matrix but by the diffusion of the complexes through nanopores. Figure 3B indicated that amount of cumulative Pt release increased from 0.043 mg via 0.097 mg to 0.220 mg by increasing the amount of drug-loaded HA from 5 via 10 to 20 wt.% HA) in CPC, respectively, confirming that the release of Pt-BP complexes proceeded in a dose-dependent manner.

4. Conclusion

The current study demonstrated that Pt-BP complexes can be released in a sustained manner at rates which can be controlled by varying the HA-binding affinity of the Pt-BP complexes as well as the amount of drug-loaded HA nanoparticles.

References

1. Lee R.J., Saylor P.J., Smith M.R. Treatment and prevention of bone complications from prostate cancer. *Bone* 2011;48:88-95.
2. Boanini E., Torricelli P., Gazzano M., Giardino R., Bigi A. Alendronate–hydroxyapatite nanocomposites and their interaction with osteoclasts and osteoblast-like cells. *Biomaterials* 2008;29:790-796.
3. Smith M.R., McGovern F.J., Zietman A.L., Fallon M.A., Hayden D.L., Schoenfeld D.A., Kantoff P.W., Finkelstein J.S. Pamidronate to prevent bone loss during androgen-deprivation therapy for prostate cancer. *The new england journal of medicine* 2001;345:948-955.
4. Barroug A., Kuhn L.T., Gerstenfeld L.C., Glimcher M.J. Interactions of cisplatin with calcium phosphate nanoparticles: in vitro controlled adsorption and release. *Journal of Orthopaedic Research* 2004;22:703-708.
5. Diel I.J., Solomayer E.F., Costa S.D., Gollan R., Wallwiener D., Kaufmann M., Bastert G. Reduction in New Metastases in Breast Cancer with Adjuvant Clodronate Treatment. *New England Journal of Medicine* 1998;339:357-363.
6. Heredia L.M.A., Kamphuis G.J., Thune P.C., Oner F.C., Jansen J.A., Walboomers X.F. An injectable calcium phosphate cement for the local delivery of paclitaxel to bone. *Biomaterials* 2011;32:5411-5416.
7. Draenert F.G., Draenert K. Methotrexate-Loaded Polymethylmethacrylate bone cement for local bone metastasis therapy: pilot animal study in the rabbit patellar groove. *Chemotherapy* 2008;54:412-416.
8. Tahara Y., Ishii Y. Apatite cement containing cis-diamminedichloroplatinum implanted in rabbit femur for sustained release of the anticancer drug and bone formation. *J Orthop Sci* 2001;6:556-565.
9. Bölling T., Harges J., Dirksen U. Management of bone tumors in paediatric oncology. *Clin Oncol (R Coll Radiol)* 2013;25:19-26.

10. Ginebra M.P., Canal C., Espanol M., Pastorino D., Montufar E.B. Calcium phosphate cements as drug delivery materials. *Adv Drug Deliv Rev* 2012;64:1090-1110.
11. Iafisco M., Palazzo B., Martha G., Margiotta N., Piccinonna S., Natilde G., Gandin V., Marzano C., Roveri N. Nanocrystalline carbonate-apatites: role of Ca/P ratio on the upload and release of anticancer platinum bisphosphonates. *Nanoscale* 2012;4:206-217.
12. Margiotta N., Ostuni R., Gandin V., Marzano C., Piccinonna S., Natilde G. Synthesis, characterization, and cytotoxicity of dinuclear platinum-bisphosphonate complexes to be used a prodrugs in the local treatment of bone tumors. *Dalton Trans* 2009;28:10904-10913.
13. Liou S.C., Chen S.Y., Lee H.Y., Bow J.S. Structural characterization of nano-sized calcium deficient apatite powders. *Biomaterials* 2004;25:189-196.
14. Lanao F.R.P., Leeuwenburgh S.C., Wolke J.G., Jansen J.A. In vitro degradation rate of apatitic calcium phosphate cement with incorporated PLGA microspheres. *Acta Biomater* 2011;7:3459-3468.
15. Panzavolta S., Torricelli P., Bracci B., Bigi A. Alendronate and Pamidronate calcium phosphate bone cements: Setting properties and in vitro response of osteoblast and osteoclast cells. *J Inorg Biochem* 2009;103:101-106.
16. Habraken W.J., Wolke J., Mikos A.G., Jansen J.A. Injectable PLGA microsphere/calcium phosphate cements: Physical properties and degradation characteristics. *J Biomed Sci Poly Ed* 2006;17:1057-1074.
17. Sariibrahimoglu K., Leeuwenburgh C.G.S., Wolke J.G.C., Li Y., Jansen J.A. Effect of calcium carbonate on hardening, physicochemical properties and in vitro degradation of injectable calcium phosphate cements. *J Biomed Mater Res A* 2012;100A:712-719.



Chapter 8

**SUMMARY, CLOSING REMARKS AND
FUTURE PERSPECTIVES**

**SAMENVATTING, SLOTOPMERKINGEN EN
TOEKOMSTPERSPECTIEF**

1. Summary

Calcium phosphate-based apatitic cements (CPCs) are promising materials for bone repair in the field of dentistry, orthopedics and reconstructive surgery. CPCs can be shaped to fit complex shapes using minimally invasive surgery which would benefit both patients and surgeons. CPCs are biocompatible and osteoconductive, but their slow degradation often results in an incomplete tissue regeneration. Therefore, degradable implants are often preferred to achieve complete bone regeneration. The main goal of the research described in the current thesis was to develop CPCs that can degrade in a controlled manner without compromising clinical handling and mechanical properties. To this end, two chemical strategies to modify the ceramic phase of injectable CPCs were explored aiming at increasing the solubility of the ceramic matrix. In addition, the influence of two types of organic additives, i.e. polymeric poly(lactic-co-glycolic acid) (PLGA) microspheres and glucono-delta-lactone (GDL) microparticles, on the degradation of CPCs was investigated as well. Finally, the suitability of injectable scaffolds composed of a porous polyurethane matrix and strontium-substituted hydroxyapatite nanoparticles for bone regeneration was explored as a potential alternative to injectable CPCs.

Chapter 2 provides an overview of the literature on calcium phosphate based bone substitute materials currently used for hard tissue regeneration by focusing on the relationship between the physiochemical properties of calcium phosphate ceramics and their capacity to facilitate the process of bone regeneration.

One of the main disadvantages of apatitic calcium phosphate cements (CPCs) is their slow degradation rate, which limits complete bone regeneration. Carbonate (CO_3^{2-}) is the common constituent of bone and it can be used to improve the degradability of the apatitic calcium phosphate ceramics. In **chapter 3** we aimed to examine the effect of calcite (CaCO_3) incorporation on the degradation rate of apatitic CPC. To this end, the CaCO_3 amount (0–4–8–12 wt.%) and its particle size (12.0 μm -coarse or 2.5 μm -fine) were systematically investigated. In comparison to calcite-free CPC, the setting time of CPCs was delayed with increasing CaCO_3

incorporation. Reduction of the CaCO_3 particle size in the initial powder increased the injectability time of the paste. During hardening of the cements, the increase in calcium release was inversely proportional to the extent of CO_3^{2-} incorporation into the apatite lattice. The morphology of the carbonate-free product consisted of large needle-like crystals, whereas small plate-like crystals were observed for carbonated apatites. Compressive strength decreased with increasing CaCO_3 content. In vitro accelerated degradation tests demonstrated that calcium release and dissolution rate from the set cements increased with increasing the incorporation of CO_3^{2-} , whereas differences in CaCO_3 particle size did not affect the in vitro degradation rate under accelerated conditions.

In **chapter 4** we pursued another ceramic-based strategy to overcome the lack of degradability of apatitic CPC by developing biphasic CPCs (BCPCs) through incorporation of tricalcium phosphate (TCP) in both α - and β -polymorphs. The aim of this study was to prepare and analyze the physicochemical properties of BCPCs based on dual-phase α/β -TCP as obtained by heat treatment of pure α -TCP. The handling and mechanical characteristics of the samples as well as the in vitro degradation behavior were investigated and compared with a standard CPC made of monophasic α -TCP. The results showed that different heat treatments of commercially available α -TCP allowed the formation of biphasic calcium phosphate powder with a variety of α/β -TCP ratios. The use of biphasic powder particles as a reactant for CPCs resulted into increased setting and injectability times of the final biphasic BCPCs. During hardening of the cements, the amount of apatite formation decreased with increasing β -TCP content in the biphasic precursor powders. The morphology of the monophasic CPC consisted of plate-like crystals, whereas needle-like crystals were observed for biphasic BCPCs. In vitro degradation tests demonstrated that dissolution rate and corresponding calcium release from the set cements increased considerably with increasing β -TCP content, suggesting that apatitic CPCs can be rendered degradable by using biphasic α/β -TCP as powder precursor phase.

Porosity and interconnectivity are important properties of calcium phosphate cements (CPCs) and bone-replacement materials. Porosity of CPCs can be obtained by adding organic degradable pore-generating particles (porogens), which can add porosity to the CPC. Porosity affects the mechanical properties of CPCs, which is relevant for the final clinical application. In **chapter 5** we focused on the effect of combinations of these polymeric porogens on the properties of CPC, such as specific surface area, porosity and interconnectivity and compressive strength. CPC powder was mixed with different amounts of PLGA porogens with different molecular weight and porogen size. The major factors affecting the properties of the CPC were related to the amount of porogen loaded and the porogen size; the molecular weight did not show a significant effect. A minimal porogen size of 40 μm at a polymer content of 30 wt% seems to provide the CPC mechanical properties, porosity and interconnectivity applicable for clinical applications. Properties studied here, and induced by the porogen and CPC can be used as a guide to evoke a specific host-response to keep the CPC integrity and to generate an explicit bone ingrowth.

In **chapter 6** we investigated if degradation of apatite-forming cements can be tuned by incorporating acid-producing, slow-resorbing poly(D,L-lactico-glycolic) acid (PLGA) microspheres and fast-resorbing glucono-delta-lactone (GDL) microparticles, or mixtures thereof. The physicochemical, mechanical and degradation characteristics of these CPC formulations were systematically analysed upon soaking in phosphate buffer saline. In parallel, various CPC formulations were implanted intramuscularly and orthotopically on top of the transverse process of goats followed by analysis of soft tissue response and bone ingrowth after 12 weeks. *In vitro* degradation of GDL was almost completed after two weeks, as evidenced by characterization of release of gluconic acid while PLGA-containing CPCs released glycolic acid throughout the entire study period of 12 weeks, resulting in decreased compressive strengths. Extensive *in vitro* degradation of the CPC matrix was observed upon simultaneous incorporation of 30% PLGA and 10% GDL. Histomorphometrical evaluation of intramuscularly implanted samples revealed that all CPCs exhibited degradation which was

accompanied by an increase in capsule thickness. In *in vivo* goat transverse process model, incorporation of 43% PLGA, 30% PLGA-5% GDL and 30% PLGA-10% GDL in CPC significantly increased bone formation and resulted in a higher amounts of newly formed bone and bone height as compared to both 10% GDL and 20% GDL-containing CPC samples. In summary, the combination of GDL microparticles and PLGA microspheres did not facilitate improved bone ingrowth into apatitic calcium phosphate cements in a bone augmentation model on the transverse processes of goats despite a proven accelerating effect on the *in vitro* degradation.

Since CPCs were rendered degradable by incorporation of PLGA microspheres in previous studies, the goal of **chapter 7** was to load α -tricalcium phosphate-(α -TCP) based calcium phosphate cements (CPCs) with novel hydroxyapatite-binding, cytostatic platinum-bisphosphonate (Pt-BP) complexes to investigate their potential as vehicle for local delivery of chemotherapeutic drugs. Platelet-shaped hydroxyapatite (HA) nanoparticles were synthesized at room temperature using a wet-chemical reaction between calcium acetate and phosphoric acid. These HA particles were subsequently loaded with two types of Pt-BP complexes of different binding affinity to hydroxyapatite, i.e., bis-{ethylenediamineplatinum(II)}-2-amino-1-hydroxyethane-1,1-diyl-bisphosphonate (EDPAB) and bis-{ethylenediamineplatinum(II)}-medronate (EDPM). HA nanoparticles loaded with Pt-BP complexes were added to the cement powder phase at different amounts ranging from 5 to 20 wt%. Poly(D,L-lactic-co-glycolic) acid (PLGA) porogens were used to render apatitic CPCs degradable. The morphology and crystal phases of the drug-loaded cements were studied after setting using Scanning Electron Microscopy (SEM) and X-Ray Diffraction (XRD), respectively, while the cement setting times were studied using Gillmore needles. The release profiles of the Pt-BP complexes were investigated *in vitro* by soaking drug-loaded cements into Phosphate Buffered Saline (PBS) followed by quantification of both Ca and Pt release for up to 28 days using Inductively Coupled Plasma-Optical Emission Spectroscopy (ICP-OES).

The results showed that both initial and final setting times of the platinum-bisphosphonate-containing cements increased with increasing amount of drug-loaded HA, while the transformation of α -TCP to hydroxyapatite was delayed by the incorporation of Pt-BP loaded HA nanoparticles. In vitro release tests revealed that Ca release from the set cements increased with increasing PLGA content, but the incorporation of PLGA did not influence the release kinetics of Pt, which indicates that release of Pt-BP complexes from CPCs was enabled by the intrinsic nanoporosity of CPCs. Generally, release rates increased with increasing amount of Pt-BP-loaded HA nanoparticles. CPCs containing amino-free EDPM complexes released Pt at a faster rate compared to cement containing aminated EDPAB complexes, which indicates that the presence of the amino group in EDPAB resulted into a higher binding affinity to hydroxyapatite nanoparticles. . In conclusion, this study demonstrated that Pt-BP complexes can be released in a sustained manner, the rate of which can be controlled by varying the HA-binding affinity of the Pt-BP complexes as well as the amount of drug-loaded HA nanoparticles.

2. Closing remarks and future perspectives

This thesis describes both inorganic and organic approaches to modify the degradation rate of injectable CPCs for bone regeneration. **Chapters 3 and 4** focused on two different strategies to increase the solubility of the ceramic, apatitic cement by incorporation of i) carbonate anions into the apatite phase (**Chapter 3**) or ii) a secondary β -tricalcium phosphate (β -TCP) phase of higher solubility than hydroxyapatite (**Chapter 4**).

All CPC-based approaches resulted into increased degradation rates as compared to unmodified CPCs, but the incorporation of a secondary soluble β -TCP phase was shown to be ~85% more effective than the incorporation of ions that disturb the apatite lattice. In order to increase the solubility of the ceramic cement phase even further, a combination of both strategies would offer new opportunities, for example by the addition of Sr^{2+} ions to biphasic CPCs.

Although modification of the ceramic cement phase was an effective tool to accelerate CPC degradation, the addition of acid-producing organic additives was shown to be more effective. Incorporation of PLGA microspheres into CPCs were shown previously to facilitate the formation of macroporosity and subsequent degradation of CPCs. Still, several challenges need to be overcome before CPC-PLGA composite cements can be translated towards clinical applications in orthopedic and dental surgery. PLGA microspheres compromise the injectability while the mechanical strength of CPCs decreases considerably after PLGA degradation (**chapter 6**). Furthermore, upscaling of the production of PLGA microspheres is time-consuming and thus expensive. This latter drawback can be overcome by production of PLGA microparticles instead of microspheres using cryogenic milling, as shown recently by the Leiden-based company CAM Bioceramics. Still, alternatives to the use of PLGA microspheres or -particles are interesting from a commercial and research perspective. **Chapter 6** describes such an alternative approach by incorporating GDL microparticles that can be used off-the-shelf without the need for additional processing of microspheres. Although the incorporation of up to 10 wt% of GDL microparticles improved the injectability and mechanical strength of the resulting composites, it is not yet clear if GDL microparticles are a suitable replacement for PLGA microspheres. As described in Chapter 6, GDL microparticles reduced the *in vivo* degradation and concomitant ingrowth of new bone tissue, whereas the degradation of CPCs was accelerated *in vitro* after incorporation of GDL microparticles. Therefore, it remains to be elucidated if GDL microparticles mainly act as porogen (by degrading prior to cement degradation but after cement setting) or as acidifier (i.e. by degrading prior to cement setting). Generally, the puzzling results as described in Chapter 6 indicate that the exact degradation mechanism of both porogens should be investigated in more detail in future studies.

Since the degradability of CPCs containing organic additives was unambiguously shown in **chapter 6**, release of drugs from CPCs became feasible which was the topic of investigation in **chapter 7**. Herein, it was

shown that CPC can be used as a drug carrier for chemotherapeutic platinum-bisphosphonate (Pt-BP) complexes. Nevertheless, since the release kinetics of Pt-BP complexes from CPC was not influenced by the presence of PLGA microspheres, it is now possible to locally release chemotherapeutic drugs in a sustained manner from both degradable and non-degradable CPCs. To translate this proof-of-principle towards pre-clinical and clinical studies, several challenges remain to be overcome. First of all, dosing and specificity of the Pt-BP complexes should be optimized after loading into CPCs by using tumor cell lines. Furthermore, the loading efficiency of the Pt-BP complexes onto apatitic nanoparticles needs to be improved since the current loading efficiency was low (i.e. 34-43%). Several strategies can be followed to overcome the restricted drug loading rate, for instance by addition of the drugs to the liquid phase of CPC or by loading the drugs wet-chemically to suspensions containing apatite nanoparticles instead adsorbing the drugs to dried, aggregated nanoparticles.

Samenvatting, slotopmerkingen en toekomstperspectief

3. Samenvatting

Calciumfosfaat-gebaseerde apatitische cementen (CPC) zijn veelbelovende materialen voor botregeneratie in de tandheelkunde, orthopedie en reconstructieve chirurgie. CPCs kunnen worden toegepast om complexe botdefecten te vullen met behulp van minimaal invasieve chirurgie. CPCs zijn biocompatibel en osteoconductief, maar hun langzame afbraaksnelheid resulteert vaak in een onvolledig weefselregeneratie. Daarom zijn afbreekbare implantaten meer geschikt om volledige botregeneratie te bewerkstelligen. Het belangrijkste doel van het in dit proefschrift beschreven onderzoek was om CPCs te ontwikkelen die konden worden afgebroken op een gecontroleerde manier zonder de gunstige eigenschappen te verliezen met betrekking tot de klinische hanteerbaarheid en mechanische eigenschappen. Hiertoe zijn twee chemische strategieën onderzocht om de keramische fase van injecteerbare CPCs oplosbaarder te krijgen. Daarnaast werd de invloed van twee soorten organische toevoegsels (nl. polymelkzuur-co-glycolzuur (PLGA) microsferen en glucono-delta-lacton (GDL) microdeeltjes) op de afbraak van CPCs onderzocht.

Hoofdstuk 2 geeft een literatuuroverzicht van de literatuur over calciumfosfaat-gebaseerde botvervangende materialen die momenteel worden gebruikt voor botregeneratie, waarbij met name is gekeken naar de relatie tussen de fysisch-chemische eigenschappen van calciumfosfaat keramiek en hun vermogen om het proces van botregeneratie te bevorderen. Eén van de belangrijkste nadelen van apatitisch calciumfosfaat cement (CPC) is hun langzame afbraaksnelheid, waardoor volledig botherstel beperkt is. Carbonaat (CO_3^{2-}) komt voor in het botmineraal en kan worden gebruikt om de afbreekbaarheid van apatitisch calciumfosfaat cement te verbeteren. In **Hoofdstuk 3** hebben we het effect van de inbouw van calciet (CaCO_3) op de afbraaksnelheid van apatitische CPCs onderzocht. Hiertoe werd de hoeveelheid CaCO_3 (0-4-8-12 gewichtsprocent) en de deeltjesgrootte (12.0 of 2.5 μm) systematisch gevarieerd. In vergelijking

Samenvatting, slotopmerkingen en toekomstperspectief

met calciëtvrij CPC nam de uithardingstijd van CPCs af met toenemende hoeveelheid CaCO_3 . Vermindering van de deeltjesgrootte van CaCO_3 in het oorspronkelijke poeder verhoogde de injecteerbaarheidstijd van de pasta. Tijdens uitharding van het cement was de toename van calciumafgifte omgekeerd evenredig met de mate van CO_3^{2-} opname in het apatietrooster. De morfologie van het carbonaat-vrije cement bestond uit grote naaldachtige kristallen, terwijl kleine plaatvormige kristallen werden waargenomen in carbonaathoudende apatieten. De druksterkte nam af met toenemend CaCO_3 gehalte. In vitro afbraaktesten toonden aan dat de afgifte van calcium en de oplosbaarheid van de cementen toenam met toenemend CO_3^{2-} gehalte, terwijl de verschillen in CaCO_3 deeltjesgrootte geen invloed hadden op de in vitro afbraaksnelheid.

In **Hoofdstuk 4** nagestreefd we nog een tweede anorganische strategie ontwikkeld om het gebrek aan afbreekbaarheid van apatitisch CPC te overwinnen door het ontwikkelen van bifasische CPC (BCPCs) door inbouw van tricalciumfosfaat (TCP) in zowel α - en β - polymorfen. Het doel van deze studie was om de fysisch-chemische eigenschappen van BCPCs op basis van bifasisch α/β -TCP te analyseren die verkregen waren door een warmtebehandeling van α -TCP. De behandeling en mechanische eigenschappen van de monsters en het in vitro degradatiegedrag werden onderzocht en vergeleken met een standaard CPC van monofasisch α -TCP. De resultaten toonden aan dat verschillende warmtebehandelingen van commercieel beschikbaar α -TCP de vorming van bifasisch calciumfosfaat poeder met verschillende α/β -TCP verhoudingen mogelijk maakte. Het gebruik van bifasische poederdeeltjes als reactant voor CPCs resulteerde in een tragere uitharding en injecteerbaarheidstijden van de uiteindelijke bifasische BCPCs. Tijdens uitharding van het cement nam de hoeveelheid apatietvorming af met toenemende β -TCP gehalte in de bifasische precursor poeders. De morfologie van de monofasische CPC bestond uit plaatvormige kristallen, terwijl naaldachtige kristallen werden waargenomen voor bifasische BCPCs. In vitro afbraaktesten toonden aan dat oplosbaarheid en bijbehorende afgiftesnelheid van calcium uit het uitgeharde cement toenam met toenemende β -TCP gehalte, wat suggereert

dat apatitisch CPC afbreekbaar kan worden gemaakt door het gebruik van bifasische α/β -TCP als poederfase.

Porositeit en interconnectiviteit zijn belangrijke eigenschappen van calciumfosfaat cement (CPC) en andere botvervangende materialen. Porositeit in CPCs kan worden verkregen door het innemen van organische porievormende toevoegingen (porogenen). Porositeit beïnvloedt de mechanische eigenschappen van CPCs, wat van groot belang is voor de uiteindelijke klinische toepassing. In **Hoofdstuk 5** hebben we het effect onderzocht van (combinaties van) deze polymere porogenen op de relevante eigenschappen van CPC zoals het specifiek oppervlak, de porositeit en interconnectiviteit alsmede de uiteindelijke druksterkte. Hiertoe werd CPC poeder gemengd met verschillende hoeveelheden PLGA porogenen van verschillende grootte en molecuulgewicht. De belangrijkste factoren die de eigenschappen van de CPC beïnvloedden waren gerelateerd aan de hoeveelheid en grootte van de porogenen, terwijl het molecuulgewicht geen significant effect op deze eigenschappen had. Een minimale poroengrootte van 40 μm bij een gehalte aan polymeer van 30 gewichtsprocent lijkt de CPC de juiste mechanische eigenschappen, porositeit en interconnectiviteit te geven voor toepassing in de kliniek.

In **Hoofdstuk 6** onderzochten we of de afbraak van apatietvormende cementen kan worden ingesteld door het innemen van (mengels van) zuurproducerende, langzaam resorbeerbare PLGA microsferen en snel resorbeerbare GDL microdeeltjes. De fysisch-chemische, mechanische en degradatie eigenschappen van deze CPC formuleringen werden systematisch geanalyseerd na onderdompeling in PBS. Daarnaast werden verschillende CPC formuleringen intramusculair en orthotopisch geïmplantéerd bovenop de processus transversus van geiten gevolgd door analyse van de zachtweefsel reactie en botingroei na 12 weken. In vitro degradatie van GDL was vrijwel volledig na twee weken zoals bleek uit karakterisering van de afgiftesnelheid van gluconzuur, terwijl PLGA-houdend CPC gedurende de gehele onderzoeksperiode van 12 weken glycolzuur afgaf, wat resulteerde in een verminderde druksterkte. Aanzienlijke in vitro degradatie van de CPC-matrix werd waargenomen bij

Samenvatting, slotopmerkingen en toekomstperspectief

inmenging van mengels van 30% PLGA en 10% GDL. Uit histomorfometrische evaluatie van intramusculair geïmplanteerde monsters bleek dat alle CPCs degradeerden wat gepaard ging met een toename van de dikte van het omringend zachtweefsel-kapsel. Inmenging van 43% PLGA en mengsels van 30% PLGA-5% GDL en 30% PLGA-10% GDL in CPC resulteerden in aanzienlijk toegenomen botvorming blijkens een grotere hoeveelheid nieuw gevormd bot en een grotere hoogte van botingroei ten opzichte cementen die ofwel 10% of 20% GDL bevatten. Samengevat kan worden geconcludeerd dat de inbouw van combinaties van GDL microdeeltjes en PLGA microsferen de botingroei in apatitisch calciumfosfaat cement niet bevorderden in het gebruikte diermodel, ondanks dat in vitro onderzoek een versnellende effect op de in vitro afbraak aantoonde.

Aangezien de inbouw van PLGA microsferen in CPC leidde tot een aanzienlijke versnelling van de afbraaksnelheid, was het doel van **Hoofdstuk 7** om CPC op basis van α -tricalciumfosfaat (α -TCP) te beladen met hydroxyapatiet-bindende, cytostatische platina- bisfosfonaat (Pt-BP) complexen om het potentieel van CPCs voor lokale afgifte van chemotherapeutische geneesmiddelen te onderzoeken. Hydroxyapatiet (HA) nanodeeltjes werden gesynthetiseerd bij kamertemperatuur met behulp van een nat-chemische reactie tussen calciumacetaat en fosforzuur. Deze HA nanodeeltjes werden vervolgens beladen met twee Pt-BP complexen met een verschillende affiniteit voor hydroxyapatiet, d.w.z bis-{ethyleendiamineplatinum (II)}-2-amino-1-hydroxy-1,1-diyl-bisfosfonaat (EDPAB) en bis-{ ethyleendiamineplatinum(II)}-medronaat (EPDM). HA nanodeeltjes beladen met Pt-BP complexen werden in verschillende hoeveelheden (variërend van 5 tot 20 gewichtsprocent) toegevoegd aan de poederfase van het cement. PLGA porogenen werden toegevoegd om apatitisch CPC afbreekbaar te maken. De morfologie en kristalstructuur van de met geneesmiddel beladen cementen werden onderzocht met behulp van Scanning Electronen Microscopie (SEM) en Röntgendiffractie (XRD), terwijl de uithardingstijd van het cement werd bestudeerd met behulp van de Gillmore naalden methode. De afgifteprofielen van de Pt-BP complexen

werden middels in vitro onderzoek bepaald door het met Pt-BP beladen cement gedurende 28 dagen onder te dompelen in PBS gevolgd door kwantificatie van de afgifte van zowel Ca en Pt met behulp van inductief gekoppelde plasma-optische emissie spectroscopie (ICP-OES).

De resultaten toonden aan dat zowel de initiële en finale uithardingstijd van de met Pt-BP complexen beladen cementen toenam met toenemende hoeveelheid chemotherapeuticum, terwijl de transformatie van α -TCP tot hydroxyapatiet werd vertraagd door inbouw van met Pt-BP complexen beladen HA nanodeeltjes. Uit de in vitro testen bleek dat de afgifte van Ca uit de cementen toenam met toenemende hoeveelheid PLGA. De afgifte van Pt was daarentegen onafhankelijk van de inbouw van PLGA microsferen, waardoor geconcludeerd kan worden dat de afgifte van Pt-BP complexen uit CPC mogelijk was door de intrinsieke nanoporositeit van de CPCs en niet door de microporositeit zoals gecreëerd door de PLGA microsferen. De afgegeven hoeveelheid Pt-BP complexen hing lineair af van de hoeveelheid toegevoegde Pt-BP-beladen HA nanodeeltjes. CPCs beladen met amino-vrije EPDM complexen gaven een sneller afgiftepatroon te zien dan cementen beladen met amino-houdende EDPAB complexen, wat aangeeft dat de aanwezigheid van de amino groep in EDPAB resulteerde in een hogere bindingsaffiniteit voor HA nanodeeltjes. Samengevat kan worden gesteld dat deze studie aangetoond heeft dat Pt-BP complexen op een gecontroleerde wijze kunnen worden afgegeven uit CPCs met een snelheid die ingesteld kan worden door variatie van de bindingsaffiniteit van BP-Pt complexen met HA nanodeeltjes alsmede de hoeveelheid van met Pt-BP-beladen HA nanodeeltjes.

4. Slotopmerkingen en toekomstperspectief

Dit proefschrift beschrijft zowel anorganische als organische strategieën om de afbraaksnelheid van injecteerbare CPCs voor botherstel te versnellen. **Hoofdstukken 3 en 4** richtten zich op twee verschillende methoden om de oplosbaarheid van de keramische fase van apatitisch CPC te verhogen door inbouw van i) carbonaat anionen in de apatiet fase (**Hoofdstuk 3**), of ii) een tweede β -tricalciumfosfaat (β -TCP) fase met een hogere oplosbaarheid

Samenvatting, slotopmerkingen en toekomstperspectief

dan hydroxyapatiet (**Hoofdstuk 4**). Alle strategieën leidden tot een verhoogde afbraaksnelheid vergeleken met ongemodificeerd CPC, maar de opname van een tweede oplosbare β -TCP fase bleek ~ 85 % effectiever te zijn dan de inbouw van carbonaationen die het apatietrooster verstoorden. Teneinde de oplosbaarheid van het keramische cement fase verder te doen toenemen zou een combinatie van beide strategieën nieuwe mogelijkheden bieden, bijvoorbeeld door toevoeging van Sr^{2+} ionen aan bifasische CPCs. Hoewel modificatie van de keramische cementfase een effectief middel bleek om afbraak van CPCs te versnellen, bleek de toevoeging van zuurproducerende organische additieven uiteindelijk veel effectiever te zijn. Toch moeten nog een aantal uitdagingen worden overwonnen voordat CPC-PLGA composietcementen klinisch toegepast kunnen worden in de orthopedische en tandheelkundige chirurgie. De inbouw van PLGA microsferen bemoeilijkt de injecteerbaarheid en uitharding van CPC, terwijl de mechanische sterkte van de CPCs aanzienlijk afneemt na afbraak van PLGA (**Hoofdstuk 6**). Bovendien is opschaling van de productie van PLGA microsferen tijdrovend en dus duur. Dit laatste nadeel kan worden ondervangen door productie van PLGA microdeeltjes in plaats van microsferen door middel van cryogeen vermaling, zoals recentelijk is aangetoond door het Leidse bedrijf CAM Bioceramics. Toch blijft de zoektocht naar alternatieven voor het gebruik van PLGA microsferen of -deeltjes commercieel en onderzoeksmatig gezien interessant. **Hoofdstuk 6** beschrijft bijvoorbeeld een alternatieve benadering door het inbouwen van GDL microdeeltjes die off-the-shelf kunnen worden gebruikt zonder dat ze tot microsferen dienen te worden verwerkt. Hoewel het inbouwen van GDL micropartikels (tot 10 gewichtsprocent) de injecteerbaarheid en mechanische sterkte van de resulterende composieten verbeterden, is het nog onduidelijk of GDL microdeeltjes een geschikte vervanging voor PLGA microsferen kunnen zijn aangezien de GDL microdeeltjes de in vivo degradatie en gelijktijdige ingroei van nieuw botweefsel belemmerden, terwijl de in vitro afbraaksnelheid van CPC werd versneld na inbouw van GDL microdeeltjes. Daarom moet nog worden opgehelderd of GDL microdeeltjes voornamelijk fungeren als porogeen (door te degraderen

voorafgaand aan degradatie van de keramische cementmatrix) of als verzuurder (d.w.z door degradatie voorafgaand aan uitharding van het cement). In het algemeen tonen de merkwaardige resultaten zoals beschreven in **Hoofdstuk 6** aan dat het exacte degradatiemechanisme van beide porogenen in meer detail onderzocht dient te worden.

Aangezien de afbreekbaarheid van CPCs met organische toevoegingen overtuigend werd aangetoond in **Hoofdstuk 6**, werd dit materiaal daarmee tevens een interessante kandidaat als dragermateriaal voor lokale afgifte van geneesmiddelen uit CPCs, wat het onderwerp van onderzoek in **Hoofdstuk 7** was. Hierin werd aangetoond dat CPC kan worden gebruikt als een dragermateriaal voor lokale afgifte van het chemotherapeutische platinum-bisfosfonaat (Pt-BP) complexen. Omdat de afgiftekinetiek van deze complexen echter niet bleek af te hangen van de aanwezigheid van PLGA microsferen, kan worden geconcludeerd dat chemotherapeutica op gecontroleerde wijze vanuit zowel afbreekbare als niet-afbreekbare CPCs afgegeven kan worden. Om dit “proof-of-principle” verder te ontwikkelen via pre-klinische en klinische studies moeten echter nog diverse uitdagingen worden overwonnen. Allereerst moet de dosering en specificiteit van de Pt-BP complexen verder worden onderzocht en geoptimaliseerd door gebruikmaking van tumor cellijnen. Bovendien moet het beladingsrendement van de Pt-BP complexen op HA nanodeeltjes worden verbeterd, aangezien het huidige beladingsrendement van 34-43 gewichtsprocent te laag was. Hiertoe kunnen verschillende strategieën gevolgd worden, bijvoorbeeld door toevoeging van de geneesmiddelen aan de vloeibare fase van het cement of door de chemotherapeutica nat-chemisch te beladen aan suspensies van HA nanodeeltjes in plaats van belading aan gedroogde aggregaten van HA nanodeeltjes.



Chapter 9

**ACKNOWLEDGEMENTS, CURRICULUM VITAE, LIST OF
PUBLICATIONS**

Acknowledgements

I would like to express my deep gratitude to my promotor Prof. dr. J. Jansen for accepting me as member of his group. Your profound knowledge, scientific management and creative thoughts on biomaterials guided me throughout my PhD.

First and foremost, I am very grateful to my copromoter Dr. Wolke. Thank you for your scientific guidance and constant support during my research and your willingness to discuss the projects. I was full of motivation whenever I left your office after short discussions. You always encouraged me to find appropriate solutions to build up my dissertation.

Dr. Leeuwenburgh, I would like to express you my sincere appreciation and gratitude for spending me your endless hours proofreading my papers and giving me intellegent suggestions. You improved my vision and encouraged me to find appropriate solution to organize research findings. You showed me how to be a researcher and how to achieve goals. I do not think this dissertation would have been possible without your guidance.

Thanks to our main collaborators Prof. Dr. Yubao and Prof. Dr. Zuo at the research center for Nano-Biomaterials, Sichuan University in Chengdu for sharing your knowledge in the polymer science for the fruitful discussions during my stay in your lab. Thank you for your kindless and help. Working with you was a great pleasure for me.

I express my sincere appreciation and thanks to Biomaterials group, Dr. Walboomers, Dr. van den Beucken, Dr. Yang, for making my PhD easier. Thank you for your help, support and valuable hints.

Dear Dr. Marco Lopez-Heredia, thank you for your all contribution to my extensive Biomaterials knowledge. It was great pleasure for me meeting with you. I hope we always continue our collaborations in the near future.

I would like to thank all my colleagues; Mani, Kambiz, Xiangzhen, Rania, Bart, Daniel, Jingling, Na, Hamdan, Astghik, Rosa, Manuela, Jie, Huanan, Reza, Jiankang, Ljupcho. Many of you are more than just colleagues to me. We all dealt with similar difficulties and dissapointments but also went

through the same happiness and joy of achievements. Thank you creating such a friendly environment.

I would like to thank to Kim, Vincent, Martijn, Henriette and Natasja for assisting me with the technical issues.

Dr. Fang, thank you for helping me to improve my Chinese language. You are very kind and positive colleague of mine. It was pleasure for me to be beaten at table tennis.

Dear Alexy, thank you for your enjoyable working atmosphere. It was great pleasure for me to fit into the same office with you. I will never forget crying some Turkish words “Alo annecim, nasilsin, iyiyim”. I hope in the future we could communicate in Turkish☺.

Dr. Nijhuis, and Wanxun, dear friends, you are much more than a colleague to me. It was difficult to understand you at the beginning, but at the end we build up strong relations. I wish we will continue our connection in the future. I specially thank you both for creating a positive environment, for your excellent hospitality, generosity and good cook.

Last but absolutely not least, I would like to express my love and gratitude for my family: to my dear sister (Selin), father (Yakup) and mother (Tulin), to whom I dedicate this thesis. Sevgili Annem, babam and kardesim, sizin sevginiz ve desteginiz beni bugunlere getirdi. Sizi cok seviyorum.

Teşekkür ederim!

Kemal Sarıbrahimoğlu

Curriculum Vitae

Kemal was born on 22nd March 1982 in Istanbul, Turkey. He graduated from Sisli Terakki High School in September 2000. He obtained his bachelor and master`s degree of Materials Engineering at the University of Kocaeli and Istanbul Technical University in Turkey. In November of 2009 he started his PhD research at the Department of Biomaterials, Radboud



University Medical Center, Nijmegen, the Netherlands, under the supervision of Prof. dr. John A. Jansen. His project was financially supported by KNAW, China-Netherlands Programme Strategic Alliances (PSA). He conducted part of his study at Sichuan University, Chengdu, China in the Nanobiomaterials group of Prof. dr. Yubao Li.

As of 2014, he is working as a postdoc researcher of 3D printing of the biopolymers in the Polymer Technology group of Assoc. dr. Anna F. Wistrand at Royal Institute of Technology (KTH), Chemical Engineering department in Sweden, and he collaborates with a research group of Prof. dr. Kamal Mustafa at the department of Clinical Dentistry, University of Bergen in Norway.

Publications related to this thesis

Sariibrahimoglu K., Leeuwenburgh S.C.G., Wolke J.G.C., Yubao L., Jansen J.A.. Ed. Fisher J.P., Mikos A.G., Bronzino J.D., Peterson D.R. Fundamentals in Tissue Engineering: Calcium Phosphates, Book chapter in handbook of “Tissue Engineering: Principles and Practices”, pg. 3.1-3-22, CRC press, US, Boca Raton, 2012.

Sariibrahimoglu K., Leeuwenburgh S.C.G., Wolke J.G.C., Yubao L., Jansen J.A. 2012. Effect of calcium carbonate on hardening, physicochemical properties, and in vitro degradation of injectable calcium phosphate cements. J Biomed Mater Res A 2012:100A:712–719.

Sariibrahimoglu K., Wolke J.G.C., Leeuwenburgh S.C.G. Yubao L., Jansen J.A. Injectable biphasic calcium phosphate cements as a potential bone substitute. Accepted 2013, J Biomed Mater Res B, DOI: 10.1002/jbm.b.33018.

Heredia L.M.A, Sariibrahimoglu K*, Yang W*, Bohner M., Yamashita D., Kunstar A., van Apeldoorn A.A., Bronckhorst E.M., Lanao F.P.R., Leeuwenburgh S.C.G., Itatani K., Yang F., Salmon P., Wolke J.G.C., Jansen J.A. Influence of pore generator on the evolution of the mechanical properties and the porosity and interconnectivity of a calcium phosphate cement. Acta Biomater 2012;8:404-414. (*Equally contributed)

Sariibrahimoglu K., An J., van Oirschot B., Nijhuis A.W.G., Eman R., Alblas J., Wolke J.G.C., van den Beucken J.J.J.P., Leeuwenburgh S.C.G., Jansen J.A. Tuning the degradation rate of calcium phosphate cements by incorporating mixtures of polylactic-co-glycolic acid microspheres and glucono-delta-lactone microparticles. Submitted: Tissue Eng A.

Sariibrahimoglu K*, Yang W*, Leeuwenburgh S.C.G., Yang F., Wolke J.G.C., Zuo Y., Li Y., Jansen J.A. Development of injectable porous polyurethane/strontium-substituted hydroxyapatite composites for bone regeneration. Submitted: Tissue Eng Regen Med (*Equally contributed)

Sariibrahimoglu K., Iafisco M., Margiotta N., Wolke J.G.C., Jansen J.A., Leeuwenburgh SCG. Controlled release of platinum- bisphosphonate complexes from injectable calcium phosphate cements for treatment of bone tumors. In preparation, 2014.

Lanao F.R.P., Sariibrahimoglu K., Leeuwenburgh S.C.G., Wang H., Wolke J.G.C., Jansen J.A. Accelerated calcium phosphate cement degradation due to incorporation of glucono delta-lactone microparticles. *Tissue Eng A*, DOI: 10.1089/ten.TEA.2012.0427.

Wang H., Boerman O.C., Sariibrahimoglu K., Li Y., Jansen J.A., Leeuwenburgh S.C.G. Comparison of micro- vs nanostructured colloidal gelatin gels for sustained delivery of osteogenic proteins: bone morphogenetic protein-2 and alkaline phosphatase. *Biomaterials* 2012;33:8695-8703.

Sariibrahimoglu K., Wolke J.G.C., Leeuwenburgh S.G.C., Jansen J.A. Characterization of α/β -TCP based injectable calcium phosphate cement as a potential bone substitute. *Key Eng Mater* 2012;529-530,157-160.